

Radio Astronomy

MSc. course

Lecture 4a,4b (of 14):

Basics of radio interferometry & Aperture Synthesis

Prof. Mike Garrett
(ASTRON/Leiden/Swinburne)

Acknowledgements

I've tried to steal the best ideas and bring them together into a coherent picture that broadly covers radio astronomy - the technique and the science.

I acknowledge the following sources of information for this particular (2 x 45 min) lecture:

Publications (in order of usefulness):

Tools of Radio Astronomy (Fourth Revised and Enlarged Edition) Kirsten Rohlfs, Thomas L. Wilson, Publisher: A&A Library/ Springer

Interferometry and Synthesis in Radio Astronomy (Second Edition), A.R. Thompson, J.M. Moran, G.W. Swenson Jr., Publisher: Wiley-VCH.

Very Long Baseline Interferometry Techniques and Applications, Marcello Felli, Ralph E. Spencer, Publisher: Kluwer

Astronomical Society of the Pacific Conference series Volume 180, Synthesis Imaging in Radio Astronomy II, G.B. Taylor, R.A. Perley, Publisher: Astronomical Society of the Pacific Conference

Very Long Baseline Interferometry and the VLBA: Napier, Diamond & Zensus., ASP Conf series, Vol 82, 1995.

An introduction to Radio Astronomy second edition, Bernard F. Burke and Francis Graham-Smith, Publisher: Cambridge University Press

Radio Astronomy (2nd edition), John D. Kraus Publisher: Solutions Manual

Radio telescopes second edition, W.N. Christiansen, J.A. Högbom, Publisher: Cambridge University Press

Presentations in the public domain (some acquired via google):

Interferometry in Radio Astronomy, Tony Wong (ATNF), Interferometry in Radio Astronomy.

“Essential Radio Astronomy,” Condon & Ransom (www.nrao.edu/course/ast534/InterferometersI.html)

Interacademiaal 2006 - Interferometry, Tom Oosterloo & Huib Jan van Langevelde, <http://www.jive.nl/iac06/wiki/>

Interferometry, Richard Porcas, ERIS School 2007.

Array Configurations, Aaron Cohen, 10th NRAO Summer Synthesis Workshop, 2006.

Imaging and deconvolution, Sanjay Bhatnagar, 9th NRAO Summer Synthesis Workshop, 2004.

Fundamental of Radio Interferometry, Rick Perley, 9th NRAO Summer Synthesis Workshop, 2004.

Course overview

Each lecture is 2 x 45 minutes long. 15 minute break between each lecture.

Location: Oort 431

Time: Thursday at 1:45 - 2.30 pm and 2.45-3.30 pm

In February: 5/2, 12/2, 19/2, 26/2

In March: 5/3, 12/3, 19/3, 26/3

N.B. March 12 is the first practical session

In April: 2/4, 9/4, 16/4, 23/4 (N.B. no lectures on 30/4 Konningendag)

In May: 7/5, 14/5, (N.B. 21 May public holiday)

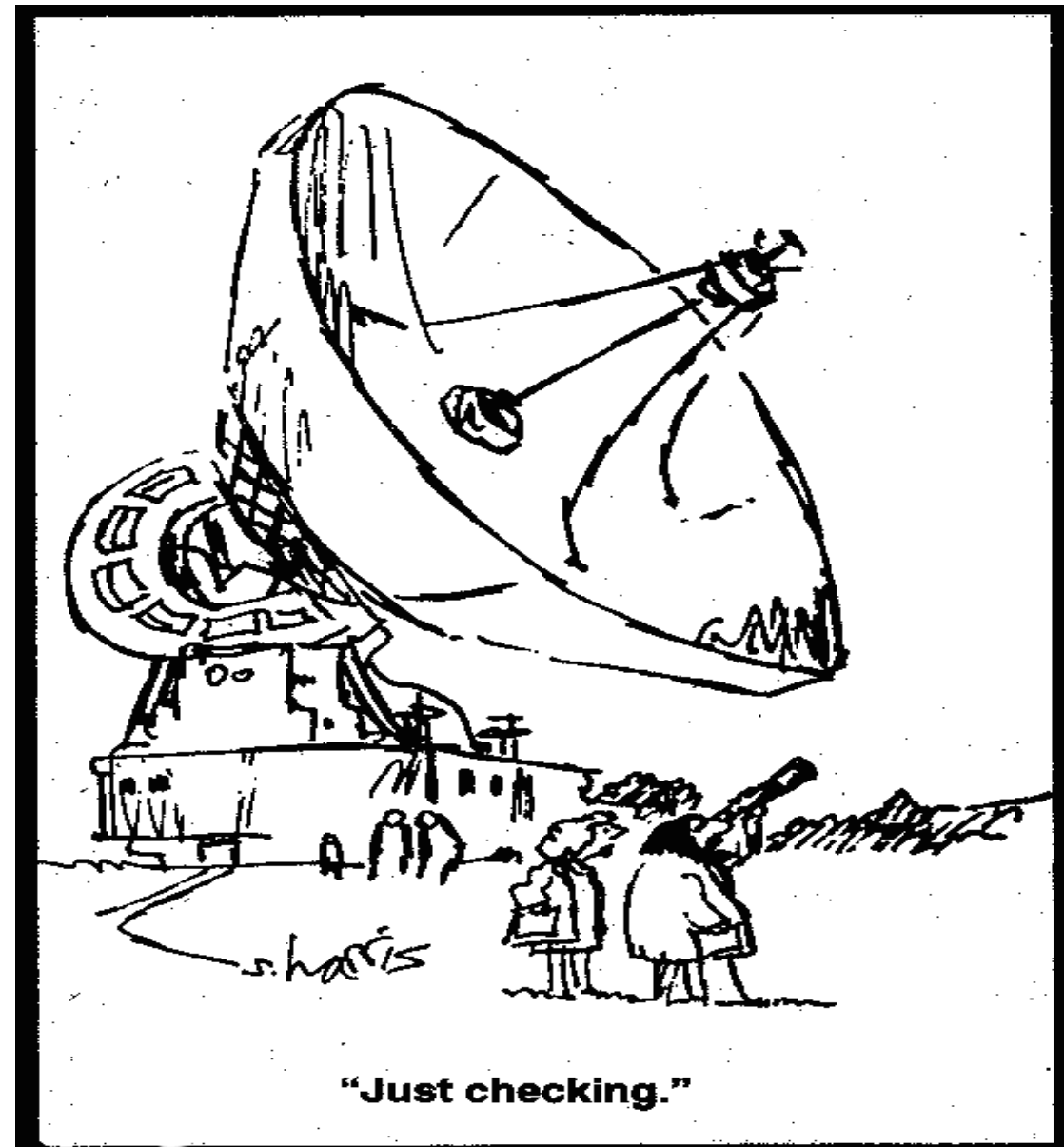
Field trip: visit to ASTRON, Westerbork and Exloo (26 May 2009) - no lecture 28 May.

Exam: by oral examination of the material - details to follow. Possible short presentations.

Radio Imaging

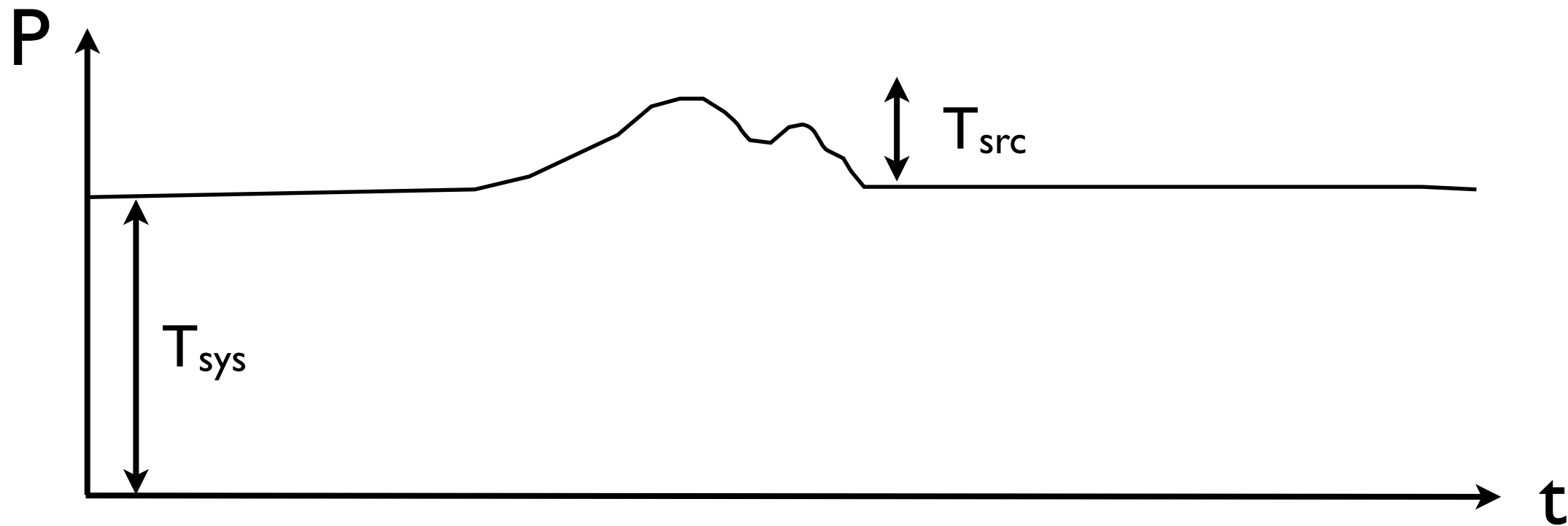
Even the largest single-dish radio telescopes have very limited resolution $\theta \sim \frac{\lambda}{D}$

The resolution of the Effelsberg 100-metre at cm wavelenghts is comparable to the human eye, and much worse than a small optical telescope:



Above: Resolution of the human eye is $\sim 5000\text{E-}9/7\text{E-}3$ rads ~ 2 arcmin, comparable to the resolution of Effelsberg at a wavelength of 6 cm.

Imaging of the sky with a single-dish can be achieved by letting the source drift across the telescope beam and measuring the power received as a function of time. This provides a I-D cut across the source intensity. Usually, the area of interest is measured at least twice, in orthogonal directions (sometimes referred to as “basket weaving”).



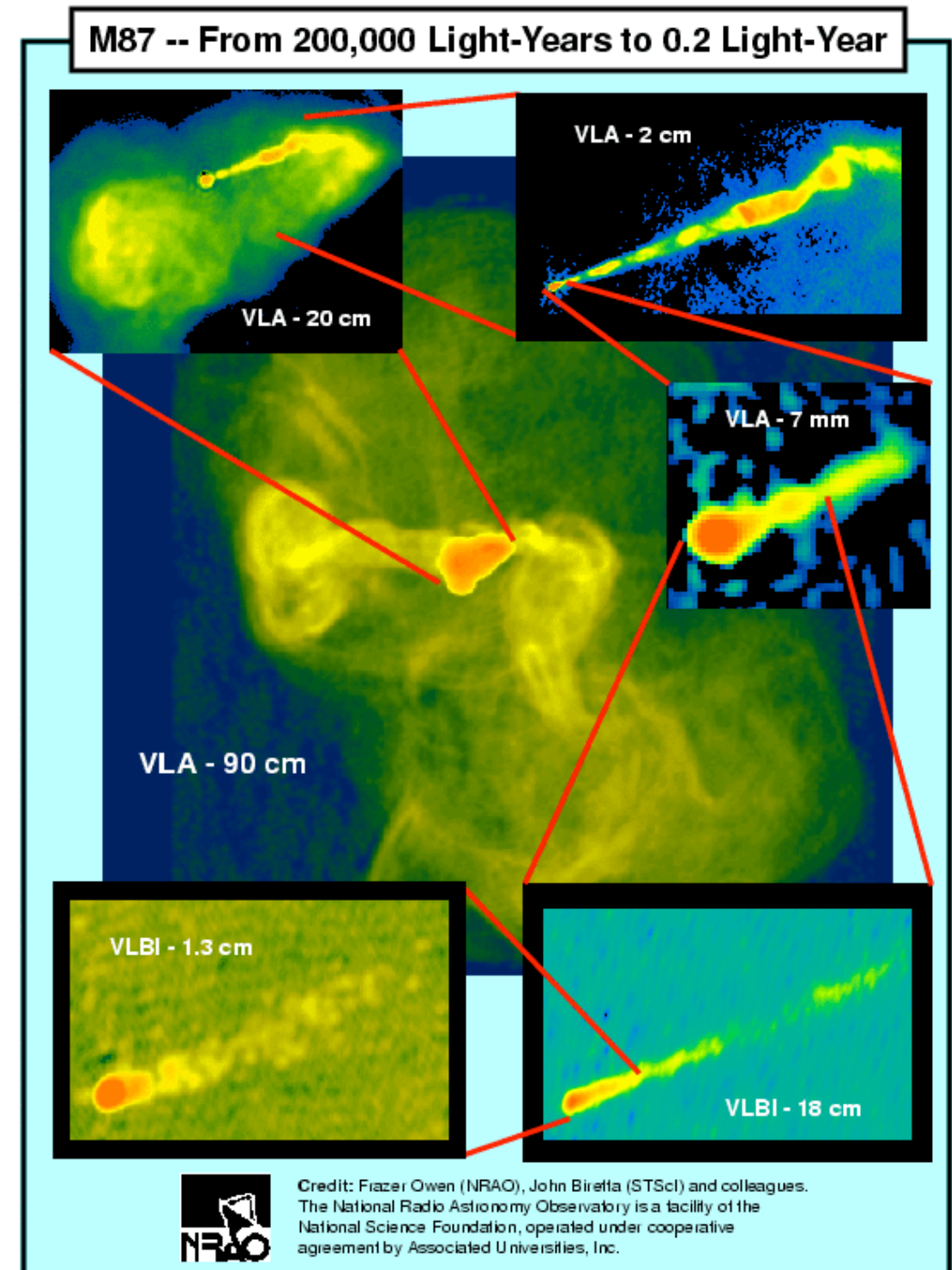
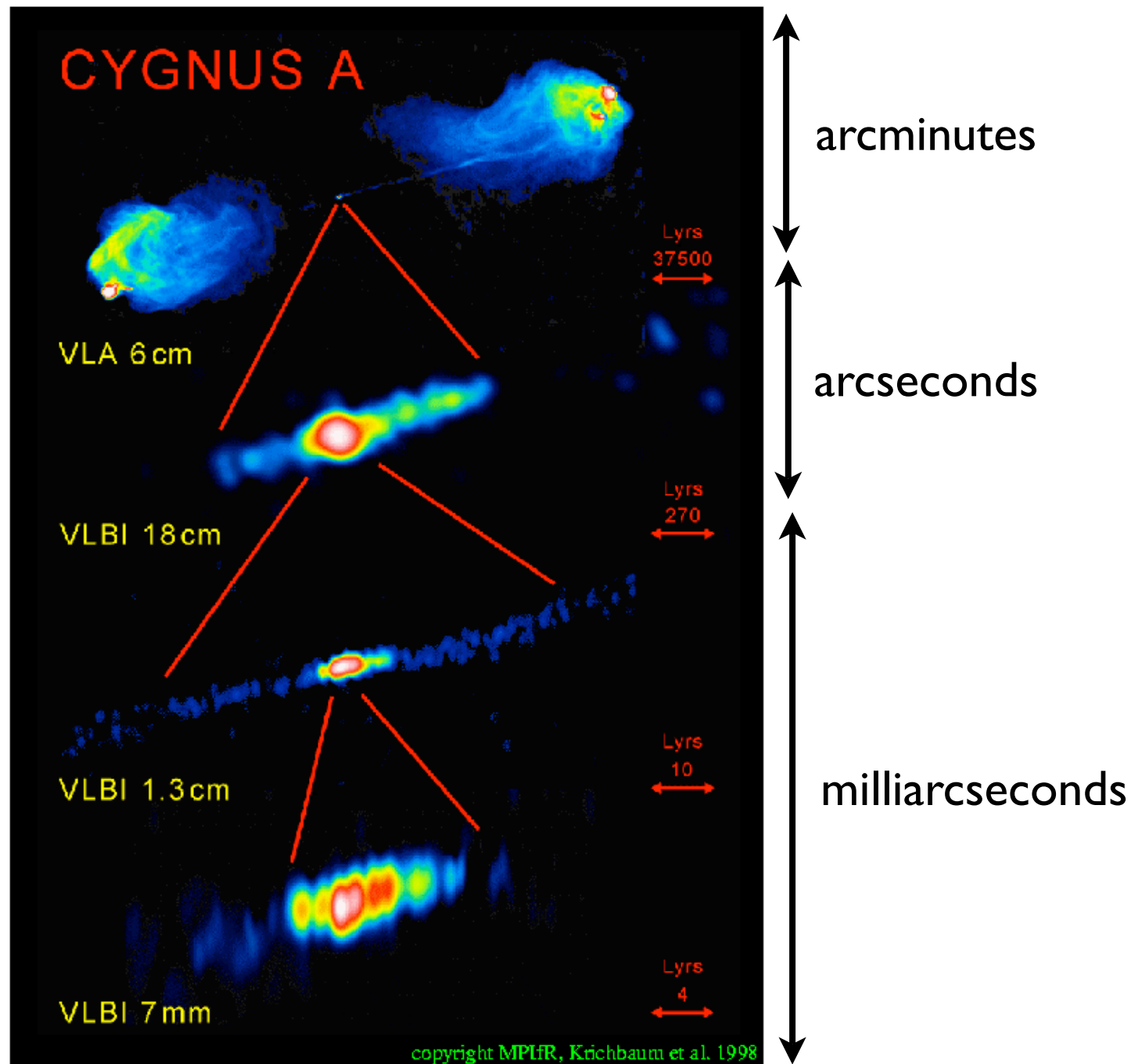
This technique works best for very large and bright sources, it requires stable receivers. The stability can be improved by chopping on and off source - this is a technique that is often used at sub-mm wavelengths.

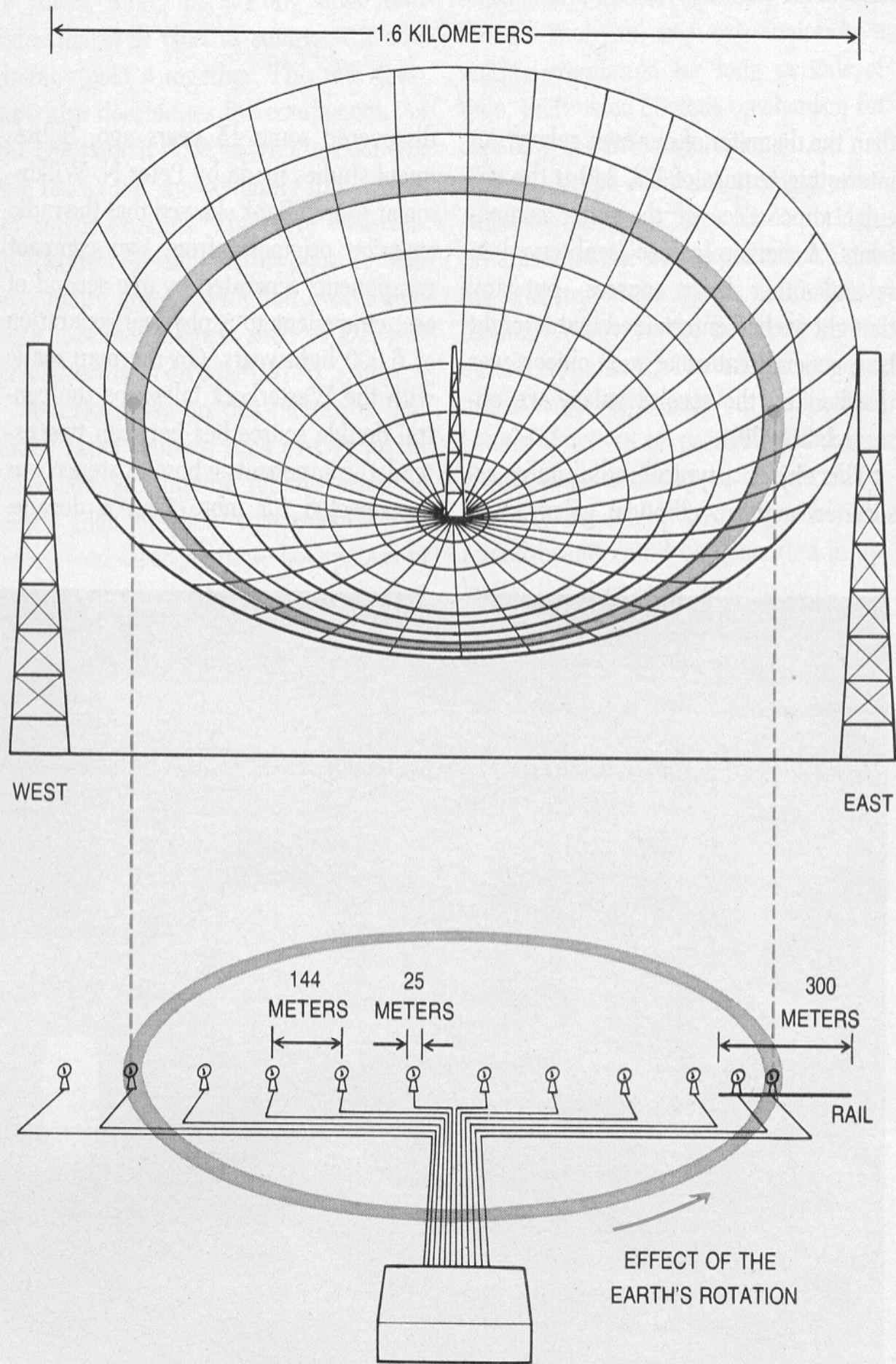
At cm wavelengths almost all imaging is conducted via the technique of interferometry.

Radio Interferometry

Arc-minute resolution is often not good enough to resolve the detailed structure of many astrophysical objects e.g. distant galaxies, quasars etc.

Radio sources can show emission on scales of arcminutes --> arcseconds --> milliarcseconds...






But as we learned in lecture 2, it is impractical to build radio (or indeed optical) telescopes much bigger than 100-metres.

==> The techniques of radio interferometry and aperture synthesis are used to obtain arcsecond, sub-arcsecond and even milliarcsecond resolution from interferometer arrays.

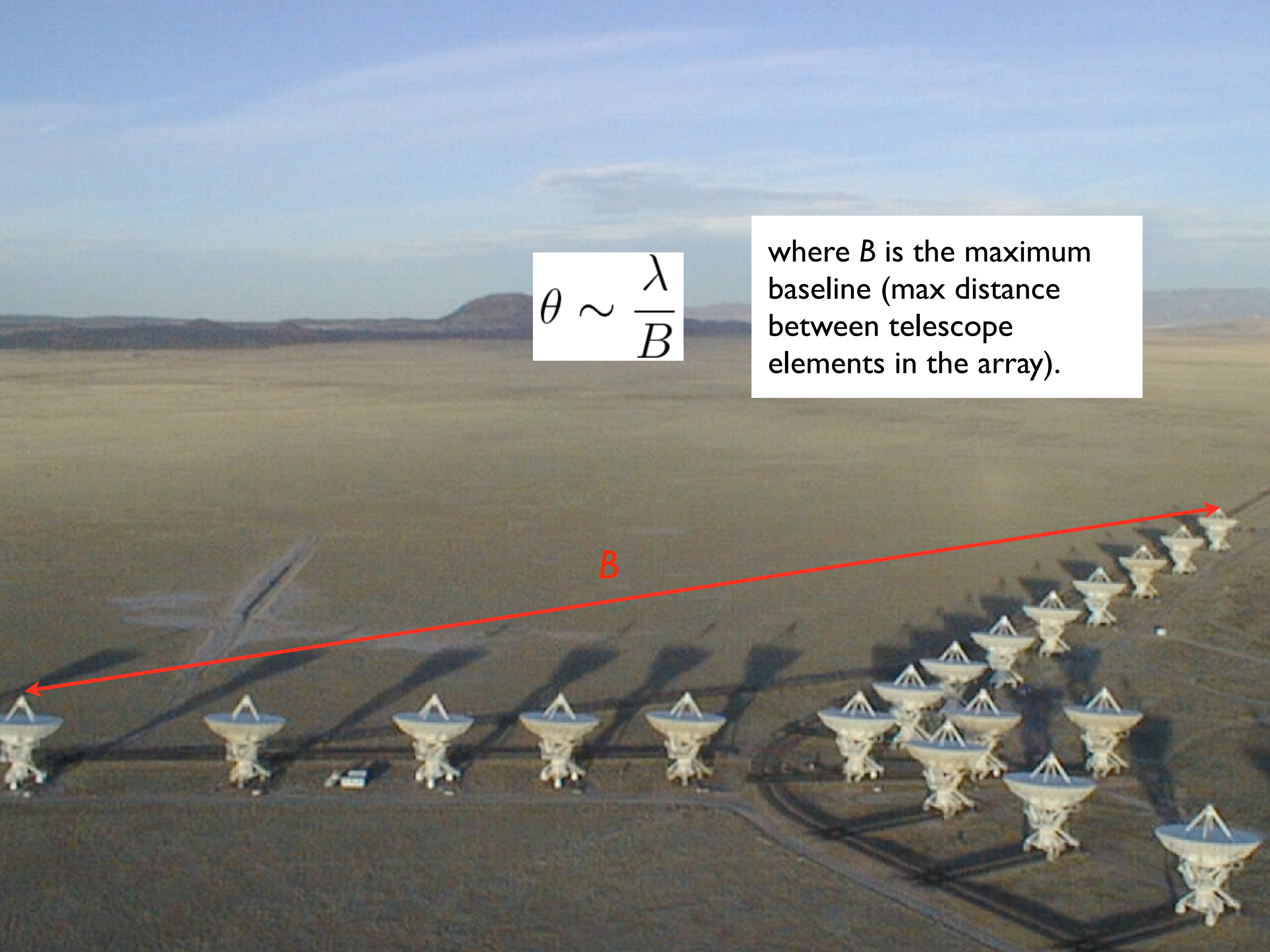
Idea is simple (left): try and synthesize a huge radio telescope - 1-10000 km in extent by combining the signals of many small telescopes together and making use of the rotation of the Earth:

An aerial photograph of a radio telescope array in a desert landscape. The dish antennas are arranged in a grid pattern. A red double-headed arrow labeled 'D' indicates the distance between two adjacent antennas. A white box with a black border contains the mathematical formula $\theta \sim \frac{\lambda}{D}$.
$$\theta \sim \frac{\lambda}{D}$$

D

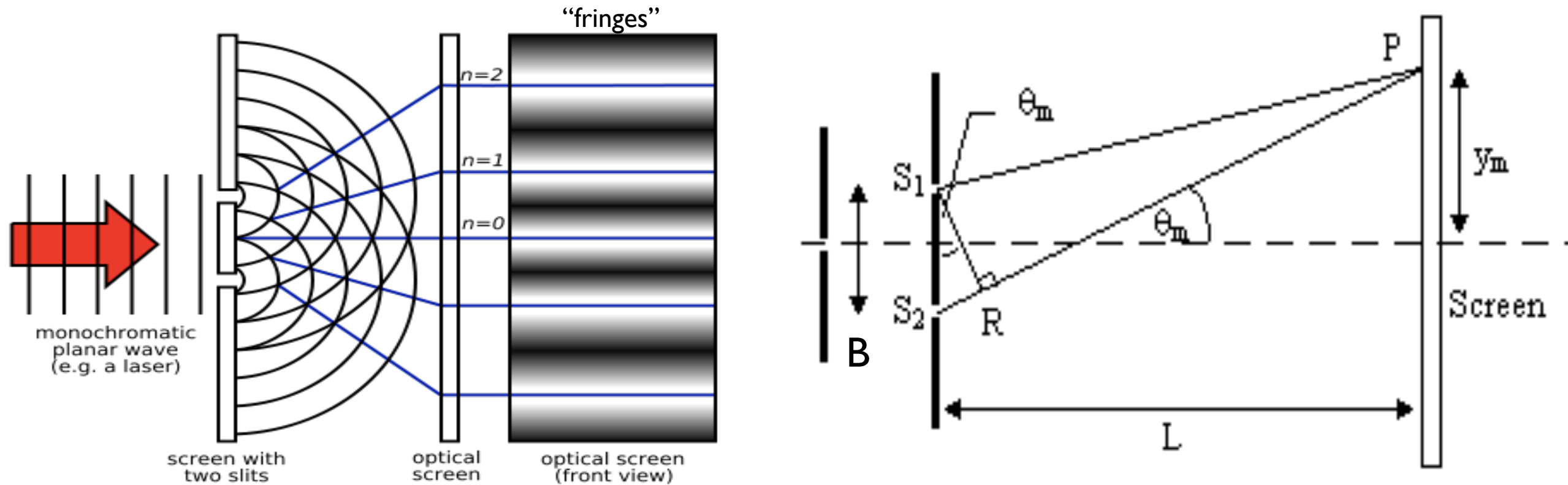
$$\theta \sim \frac{\lambda}{B}$$

where B is the maximum baseline (max distance between telescope elements in the array).



Two-element interferometer

Back to basics... interference fringes and Young's double slit experiment:



Constructive interference "fringes" occurs when the path difference is an integer number of wavelengths. If $d \ll L$ the path difference is just $B \sin(\theta)$ and the condition for maxima is:

$$B \sin(\theta) = m\lambda \quad \text{where } m \text{ is any +ve or -ve integer}$$

Like wise the condition for minima is $B \sin(\theta) = (m + 1/2)\lambda$

In the case that $y \ll L$, one can use the approximate formula:

$$\sin(\theta) = y/L$$

The spatial coordinates of constructive (y_c) and destructive (y_d) interference are then:

$$Y_c = \frac{m\lambda L}{B} \qquad Y_d = \frac{(m + 1/2)\lambda L}{B}$$

The spacing between successive constructive interference is then:

$$\Delta y = \frac{\lambda L}{B}$$

Or as an angular measure the spacing between so-called “fringes” is just:

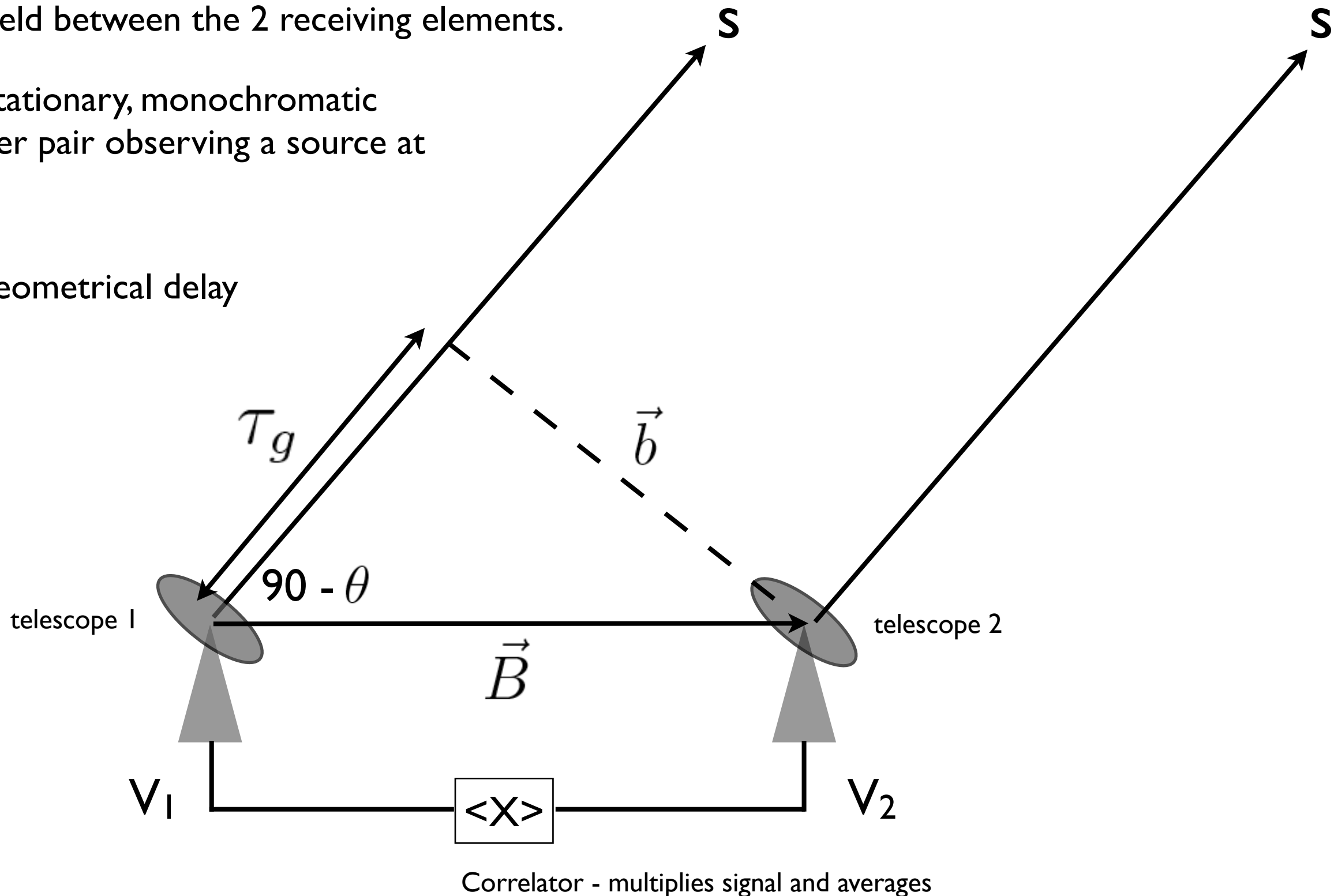
$$\theta \sim \frac{\lambda}{B}$$

Two-element radio interferometer: delay & relative phase

A radio interferometer measures the coherence of the electric field between the 2 receiving elements.

Consider a stationary, monochromatic interferometer pair observing a source at infinity.

τ_g is the geometrical delay



τ_g is the geometrical delay (seconds):

$$\tau_g = \vec{B} \cdot \hat{s} / c \quad [2]$$

where s is a unit vector in the direction of the source, and B is the baseline vector.

b is the projected baseline vector as seen by the source.

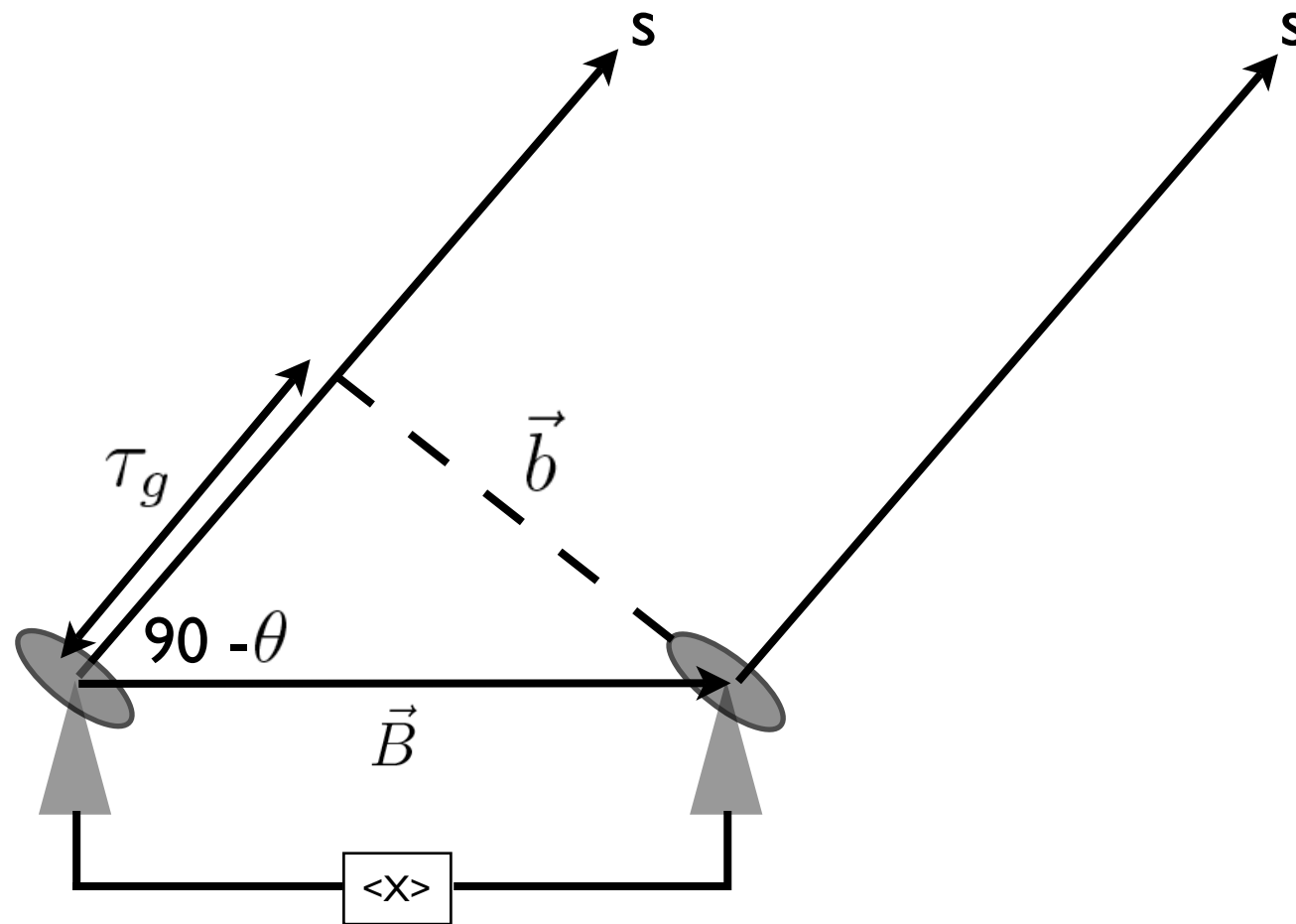
We can also write the mag. of [2] as:

$$|\tau_g| = B \sin(\theta) / c \quad [3]$$

e.g. a geometrical delay of about 1 millisecond is expected for $B \sim 300$ km.

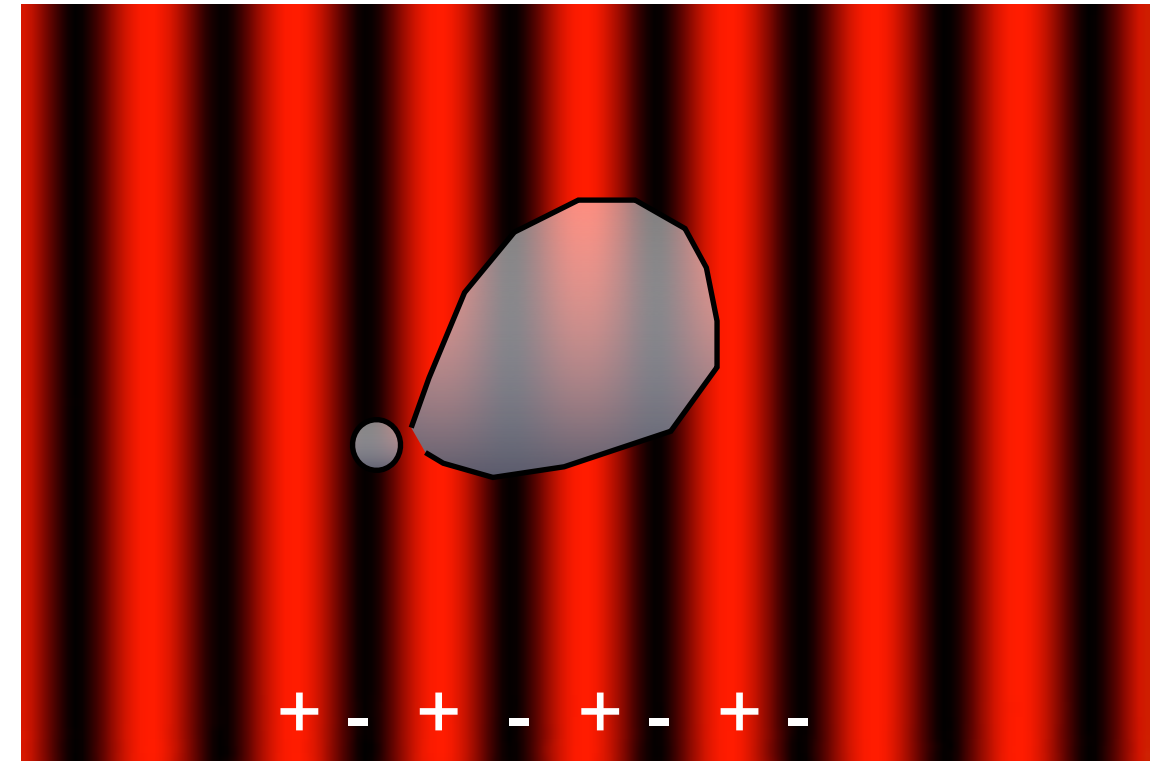
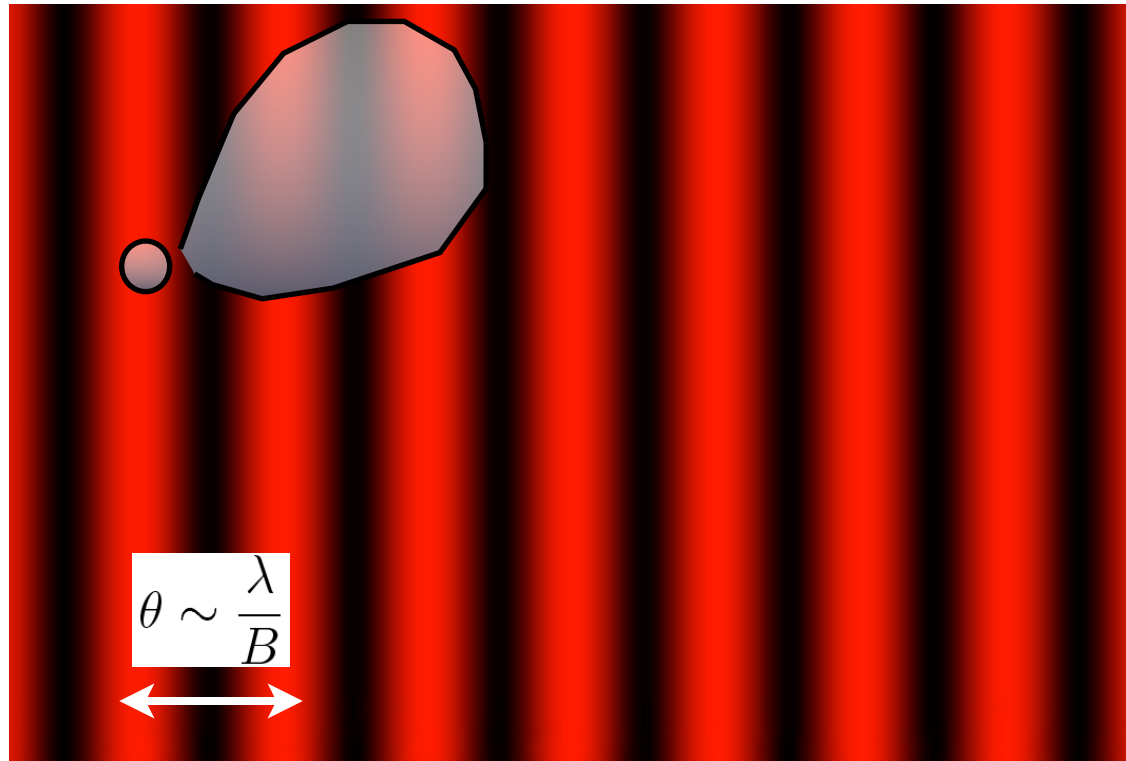
As the telescopes track the source the delay is constantly changing. The maximum in the fringe pattern are measured when $\tau_g c$ is an integral number of wavelengths:

$$m\lambda = B \sin(\theta) \quad \text{where } m \text{ is a +ve or -ve integer:}$$

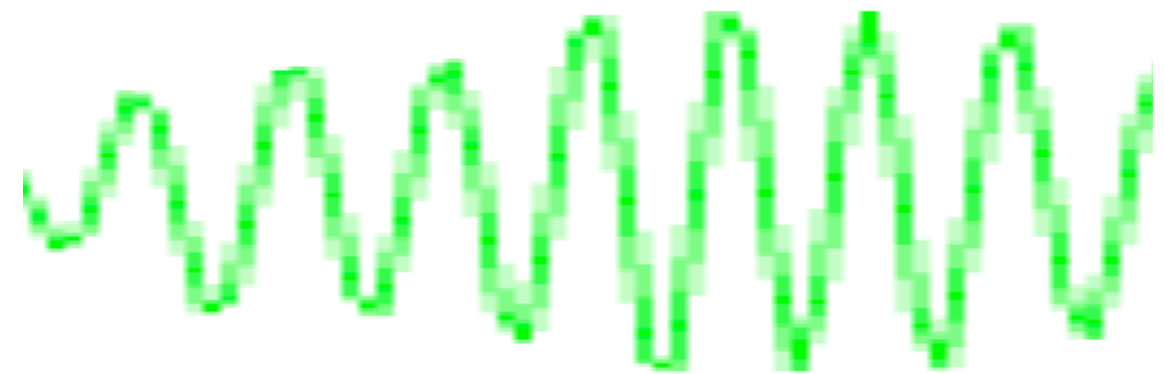


This is directly analogous to Young's slits expt, and in the same way, we can imagine that a radio interferometer casts fringes on the sky.

Consider a *fixed* 2-element interferometer orientated east-west and pointing at one particular position on the sky:

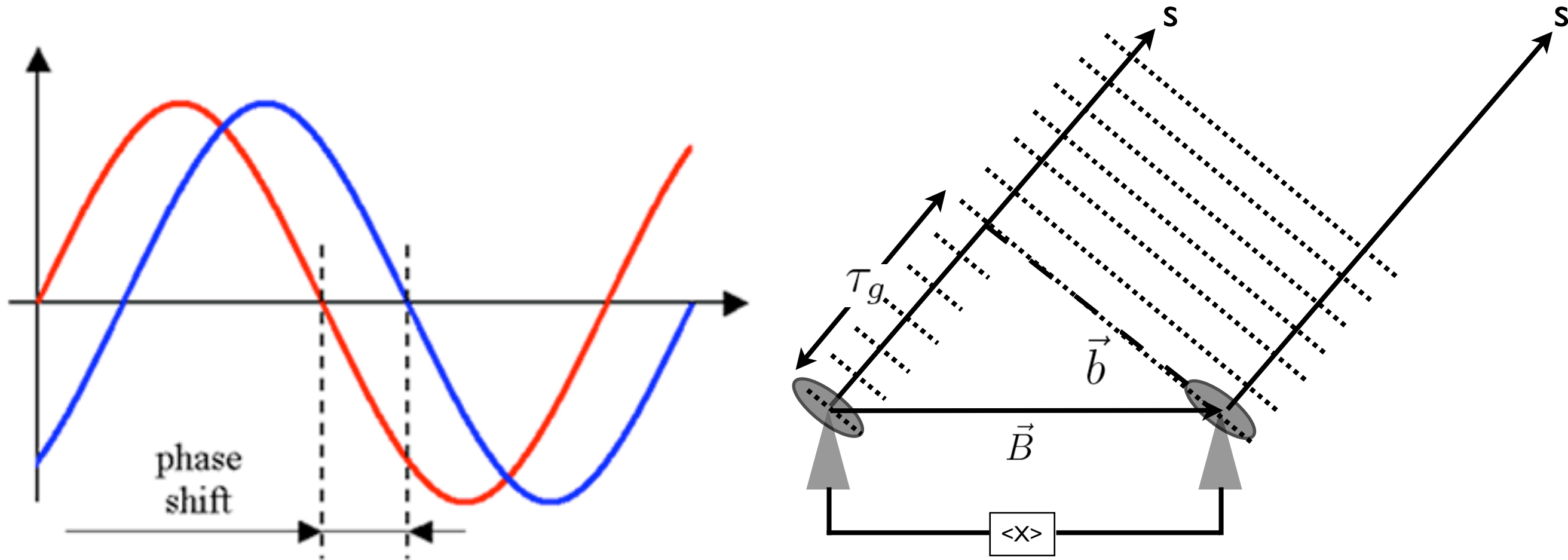


The rotation of the Earth moves the source across the sky with the complex output of the interferometer depending on the alignment between the source structure and the fringes at any given time.



Note that the small source is unresolved by this fringe pattern. The larger source is resolved.

If the angular size of the source is larger than the distance between adjacent positive and negative fringes the source starts to "cancel itself out" (it becomes "resolved").



The relative phase ϕ between the signals received at telescope 1 and 2 is dependent on the geometrical delay and the observing wavelength:

$$\phi/2\pi = \frac{\tau_g c}{\lambda} \quad \text{or:} \quad \phi = 2\pi \nu \tau_g \quad [4]$$

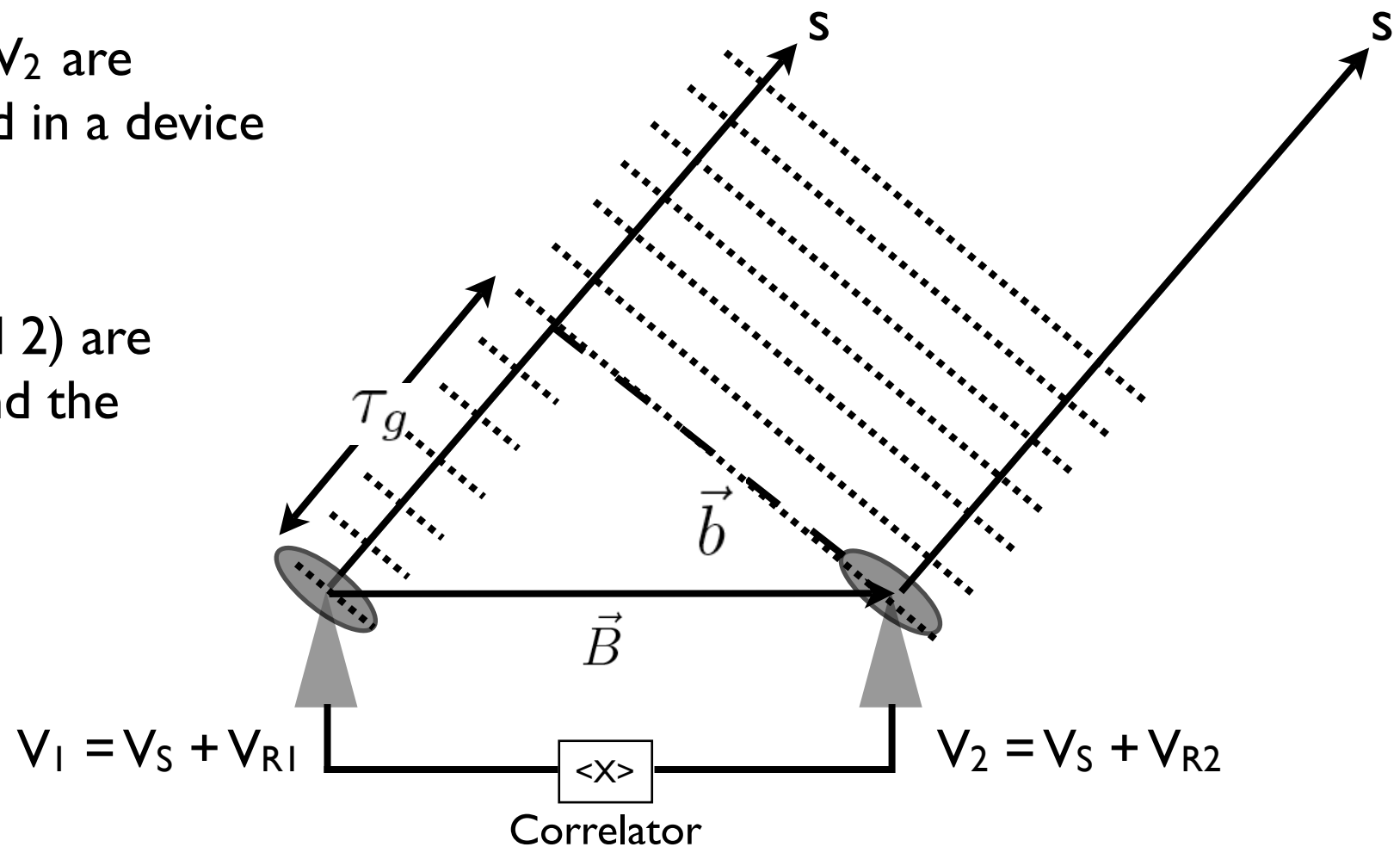
The figure above depicts the case for which the relative phase is an integral number (6) of 2π . Note that the relative phase varies with time, since the delay changes as the interferometer tracks the source on the sky. We'll return to this point later.

Two element radio interferometer: signal multiplication

Input source voltages signals: V_1 and V_2 are combined together and time-averaged in a device called a *correlator*.

The voltages at each telescope (1 and 2) are composed of the source signal (V_S) and the receiver noise (V_R):

$$V_1 = V_S + V_{R1} \quad \text{and} \quad V_2 = V_S + V_{R2}$$



There are several different ways to combine the data:

$$\langle (V_1 + V_2)^2 \rangle = \langle V_{R1}^2 \rangle + \langle V_{R2}^2 \rangle + 4\langle V_S^2 \rangle$$

(Note that products such as $(V_{R1}V_{R2})$ etc do not correlate and can be set to zero).

This is known as an *adding* interferometer (a well-known example is the Michelson interferometer). Note that the output also includes the noise from the 2 receivers. The signal from the source gets buried in the total output.

It can be very difficult to measure the signal from the source if the gains of the receivers fluctuate. For this reason, adding interferometers are not usually used in radio astronomy today.

However, the 2 telescope signals can also be multiplied together:

$$\langle (V_1 \cdot V_2) \rangle = \langle (V_{R1}V_s + V_{R1}V_{R2} + V_sV_{R2} + V_s^2) \rangle = \langle V_s^2 \rangle \quad [5]$$

(Note the possible simplification in the above equation, since terms such as $V_{R1}V_s$ etc are uncorrelated and can be set to zero).

This is known as a *multiplying* interferometer and the correlator is known as a cross-correlator.

Here the output is solely restricted to the source signal.

The receiver noise in each telescope is independent and therefore uncorrelated.

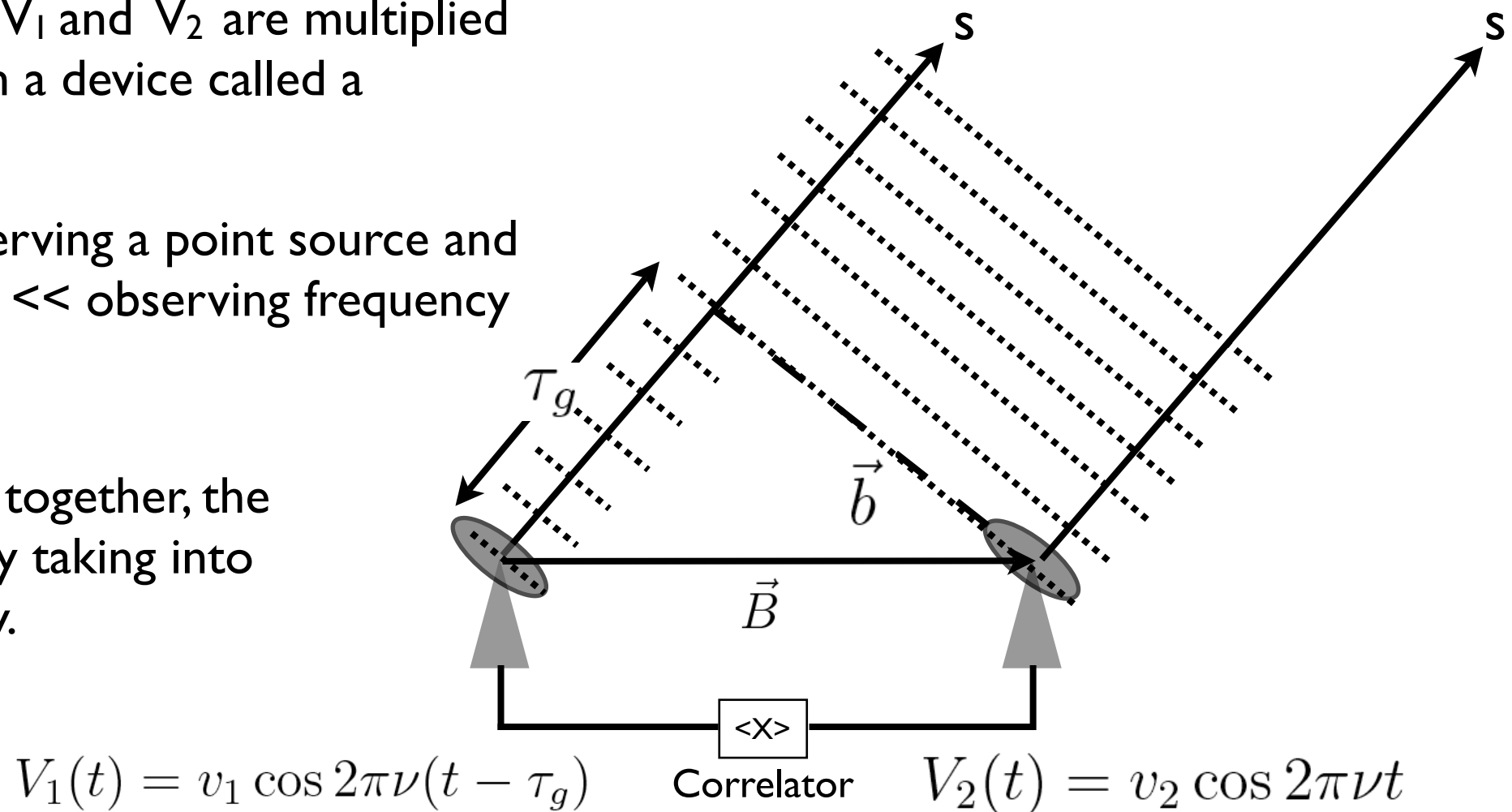
Just about all modern radio interferometers use cross-correlation.

Two element radio interferometer: signal multiplication

Input source voltages signals: V_1 and V_2 are multiplied together and time-averaged in a device called a correlator.

Let's also assume we are observing a point source and that the observing bandwidth \ll observing frequency i.e. $\delta\nu \ll \nu$

Before multiplying the signals together, the correlator aligns the signals by taking into account the geometrical delay.



The output of the correlator is then: $r(\tau_g) = v_1 v_2 \cos 2\pi\nu(t - \tau_g) \cos 2\pi\nu t$

After expanding the first cosine term and multiplying this becomes:

$$V_1 V_2 (\cos^2(2\pi\nu t) \cos(2\pi\nu\tau_g) + \cos(2\pi\nu t) \sin(2\pi\nu t) \sin(2\pi\nu\tau_g))$$

With a little reduction [and remembering the relations: $\cos^2(a) = 1/2(1+\cos(2a))$ and $\sin(2a)=2\cos(a)\sin(a)$] this can be re-written as:

$$\frac{1}{2} V_1 V_2 (\cos(2\pi\nu\tau_g) + \cos(4\pi\nu t) \cos(2\pi\nu\tau_g) + \sin(4\pi\nu t) \sin(2\pi\nu\tau_g))$$

The second and third high frequency terms of this relation vary rapidly (variation of νt is very fast c.f. $\nu\tau_g$) and tend to zero during the period over which the correlator averages the response of the 2 antennas (usually a few seconds).

The correlator response therefore simplifies to:

$$r(\tau_g) = \langle V_1 V_2 \rangle = \frac{1}{2} V_1 V_2 (\cos(2\pi\nu\tau_g)) \quad [6]$$

And for 2 identical antennas: $r(\tau_g) = \langle V_1 V_2 \rangle = \frac{1}{2} V^2 (\cos(2\pi\nu\tau_g))$

The complex correlator response, $V^2/2$, is directly proportional to the spectral power density of the radio source as measured by the interferometer.

i.e. the Flux density of the radio source, S , decreased by a factor $\cos(2\pi \nu \tau_g)$ and multiplied by the effective collecting area of the interferometer $(A_1 A_2)^{1/2}$ or simply: SA for identical antennas.

The correlator response varies sinusoidally as the source moves across the sky i.e. as θ changes. This sinusoidal output is usually referred to as the interferometer “fringes”.

The phase of the fringes (see eqn 4) is given by: $\phi = 2\pi \nu \tau_g$

And from eqn 3 we can write the change in the phase as function of θ :

$$d\phi/d\theta = 2\pi(B \cos \theta / \lambda) \quad [7]$$

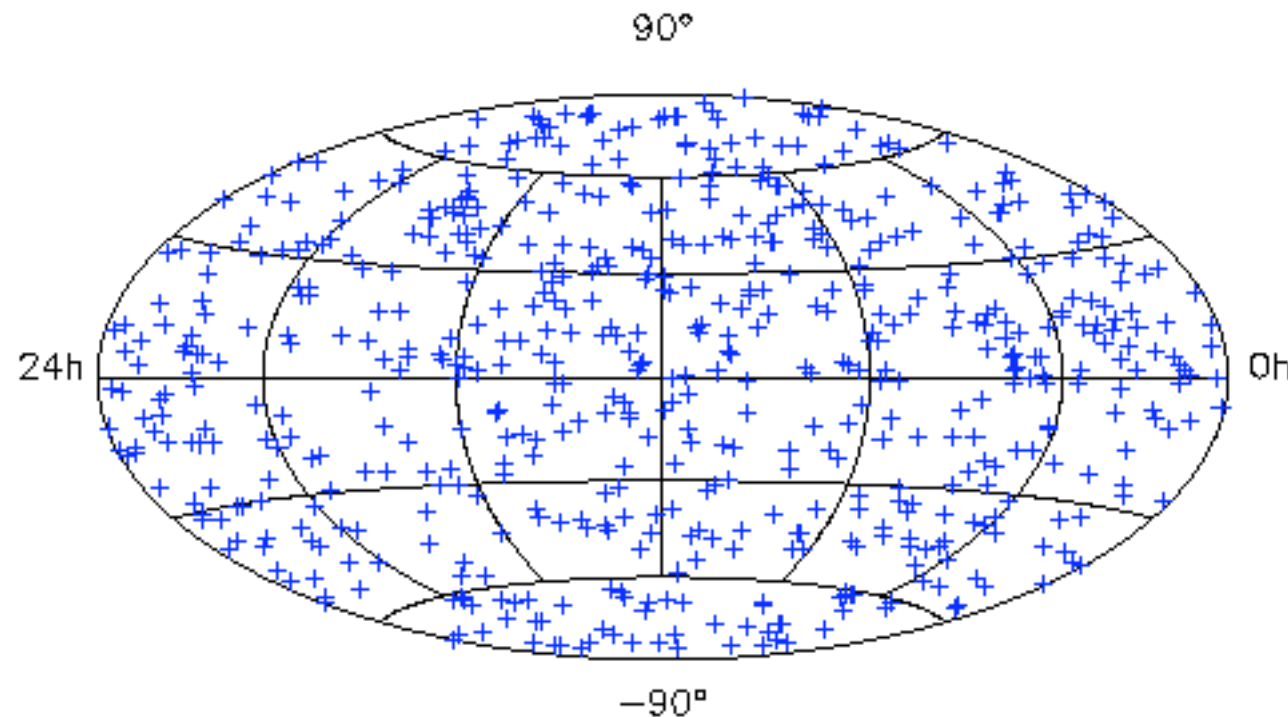
Since the projected baseline $B \cos \theta$ can be very large (thousands of km for VLBI) compared to the observing wavelength, the fringe phase is extremely sensitive to the source position.

For example, a source offset of 1 milliarcsecond corresponds to a change in the fringe phase of a few degrees on a 1000 km baseline.

The VLBI technique provides the most accurate positions (and proper motions) in all of astronomy.

Absolute positions can be measured to better than 1 milliarcsecond (limited by source structure/evolution) and differential positions can be measured at the 10 microarcsecond level.

In particular, VLBI defines the ICRS (the international celestial reference system) which is the fundamental frame in which all celestial bodies are measured.



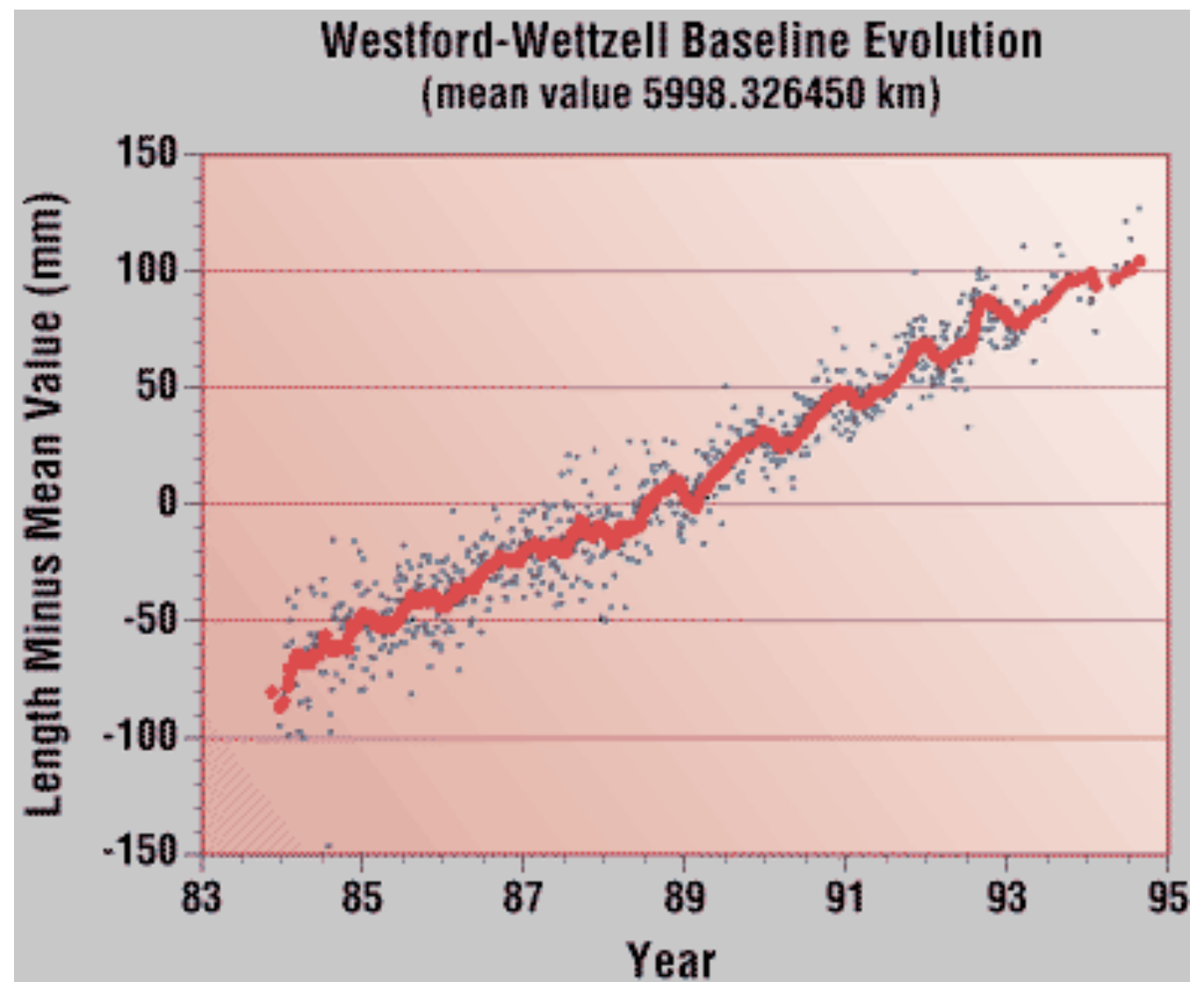
Right: Around 700 bright, compact radio sources with positions measured by VLBI in the J2000 coordinate system are used to define the ICRS.

These radio sources (often quasars) are also relatively bright at optical wavelengths. A few of the radio sources are flare stars with positions that were also measured by the Hipparchos mission. This permits optical observations (and observations at other wavelengths) to be consistently tied together via the ICRS.

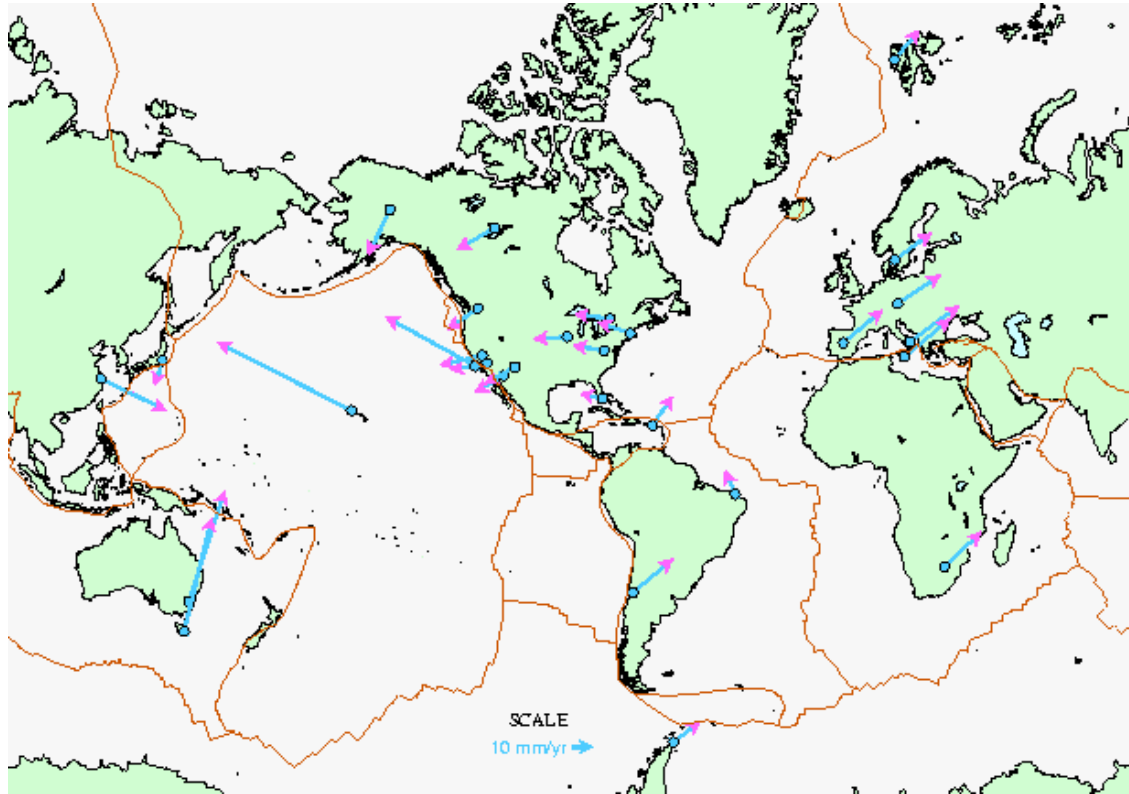
In addition to astrometry, interferometry (specifically VLBI) has other applications, including some that lie outside of astronomy and astrophysics.

In particular, since extragalactic sources are extremely distant, they act as “fixed” beacons that can be used to establish a terrestrial reference frame. By observing many sources with accurate positions, geodetic VLBI turns equation [7] on its head, and solves for the interferometer baseline length (antenna positions).

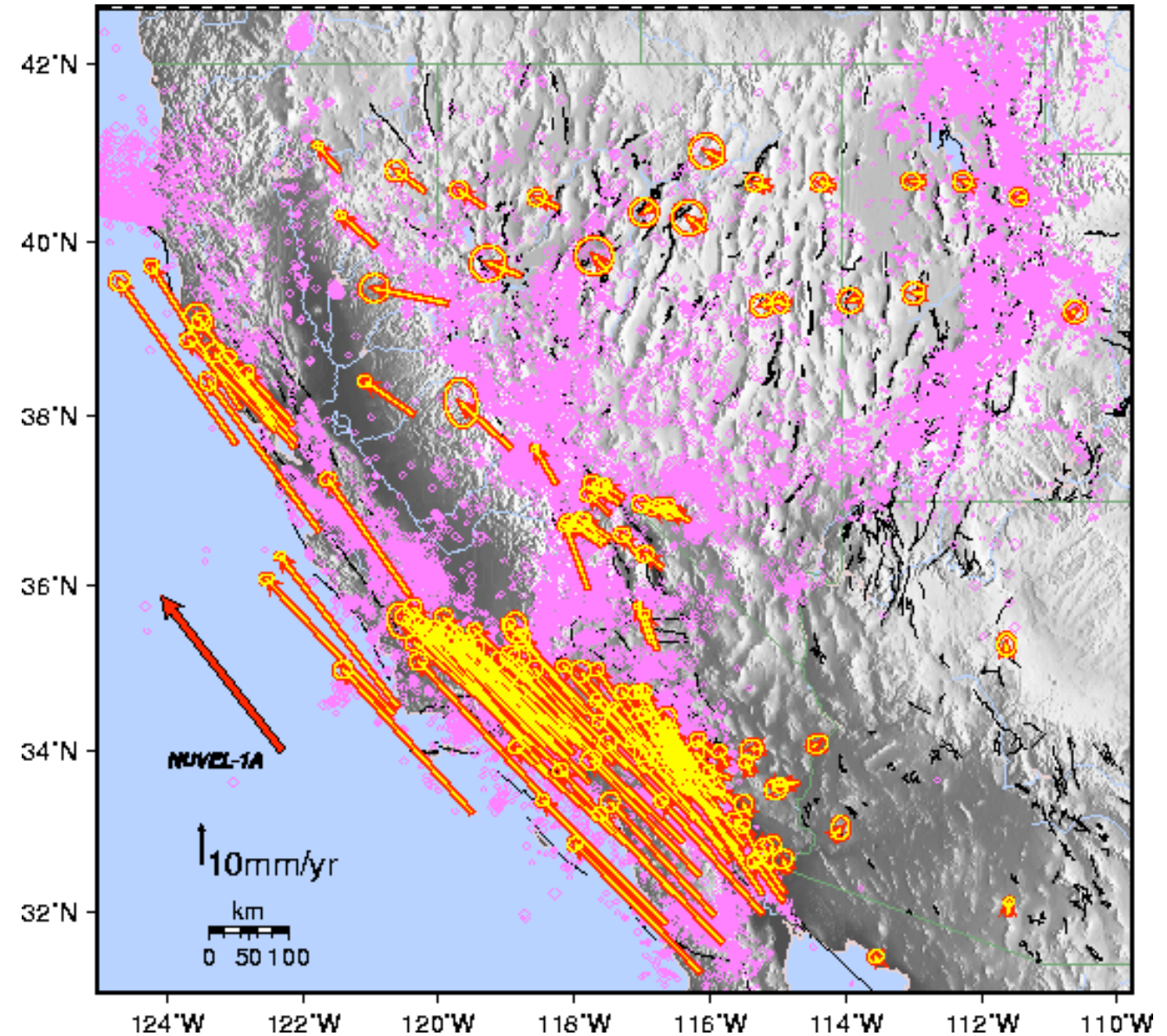
VLBI can measure the position of participating antennas separated across continents (right) to mm precision!



Geodetic VLBI measures continental and regional plate motion:



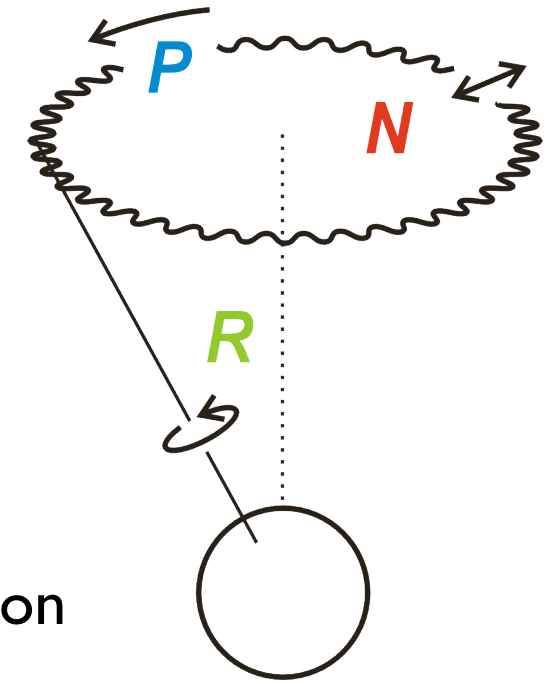
Together GPS and VLBI techniques can measure local plate motions in unstable regions e.g. California (right):



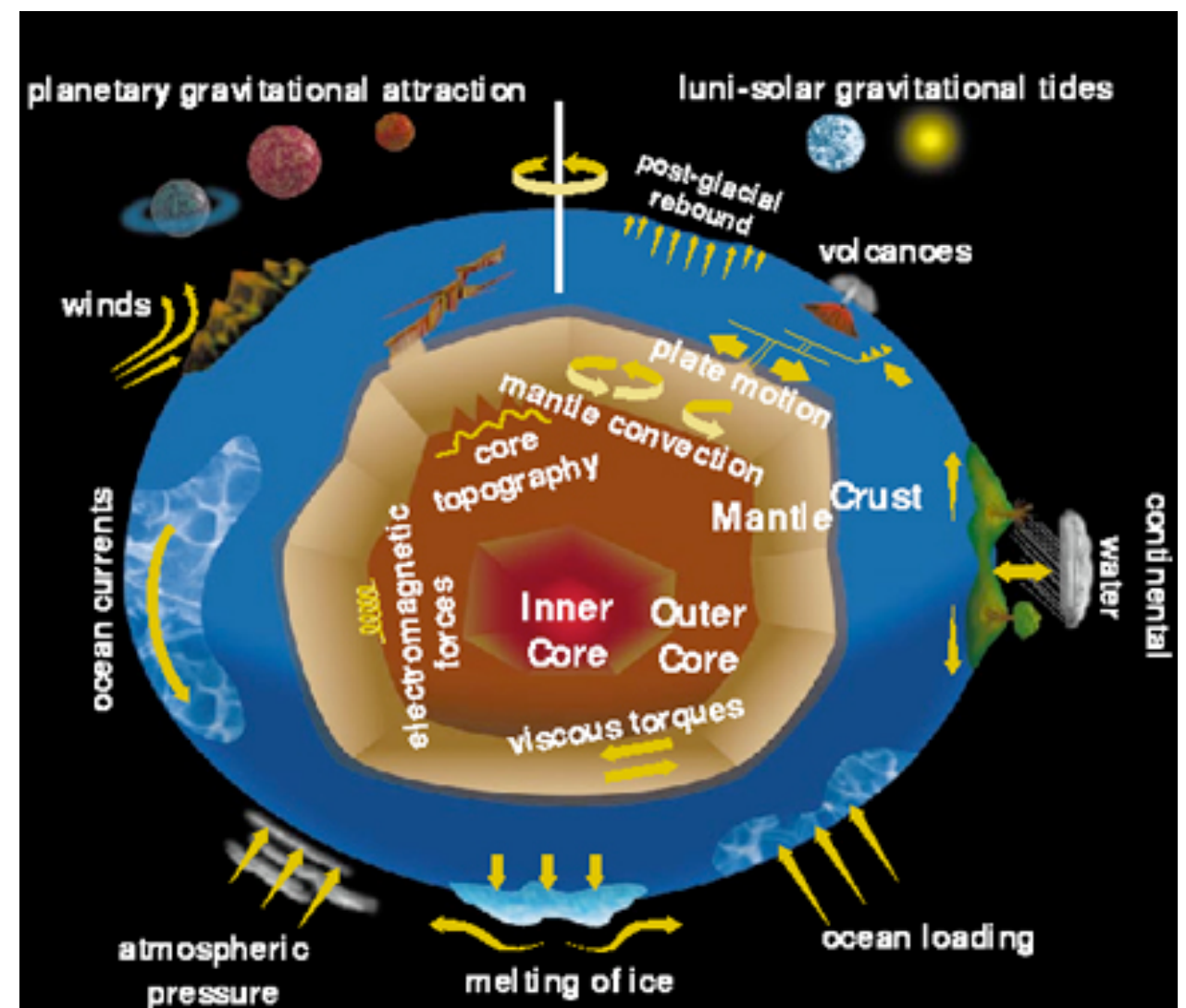
Precise VLBI measurements also permit the orientation of the Earth to be determined.

Nutation (N) and Precession (P) can be measured by VLBI as well as changes in the Earth's rotation rate (length of the day also referred to as "UTI").

A detailed description of the causes for variations on the Earth's Orientation and rotation rate are beyond the scope of this course but include:



- * Planetary gravitational attraction
- * Winds
- * Ocean Currents
- * Atmospheric pressure
- * Melting of Ice
- * Ocean Loading
- * Continental Water
- * Volcanoes
- * Post glacial rebound
- * Lunar - solar gravitational tides
- * Plate motion
- * Mantle convection
- * Core topography
- * Electromagnetic forces
- * Viscous torques



Returning to equation [7], the “fringe frequency” is given by: $\frac{d\phi}{dt} = \frac{2\pi B \cos \theta}{\lambda} \frac{d\theta}{dt}$

$\frac{d\theta}{dt}$ is just the sidereal rate $\omega_e \sim 7\text{E-}5$ rad/sec ($2\pi/86400$).

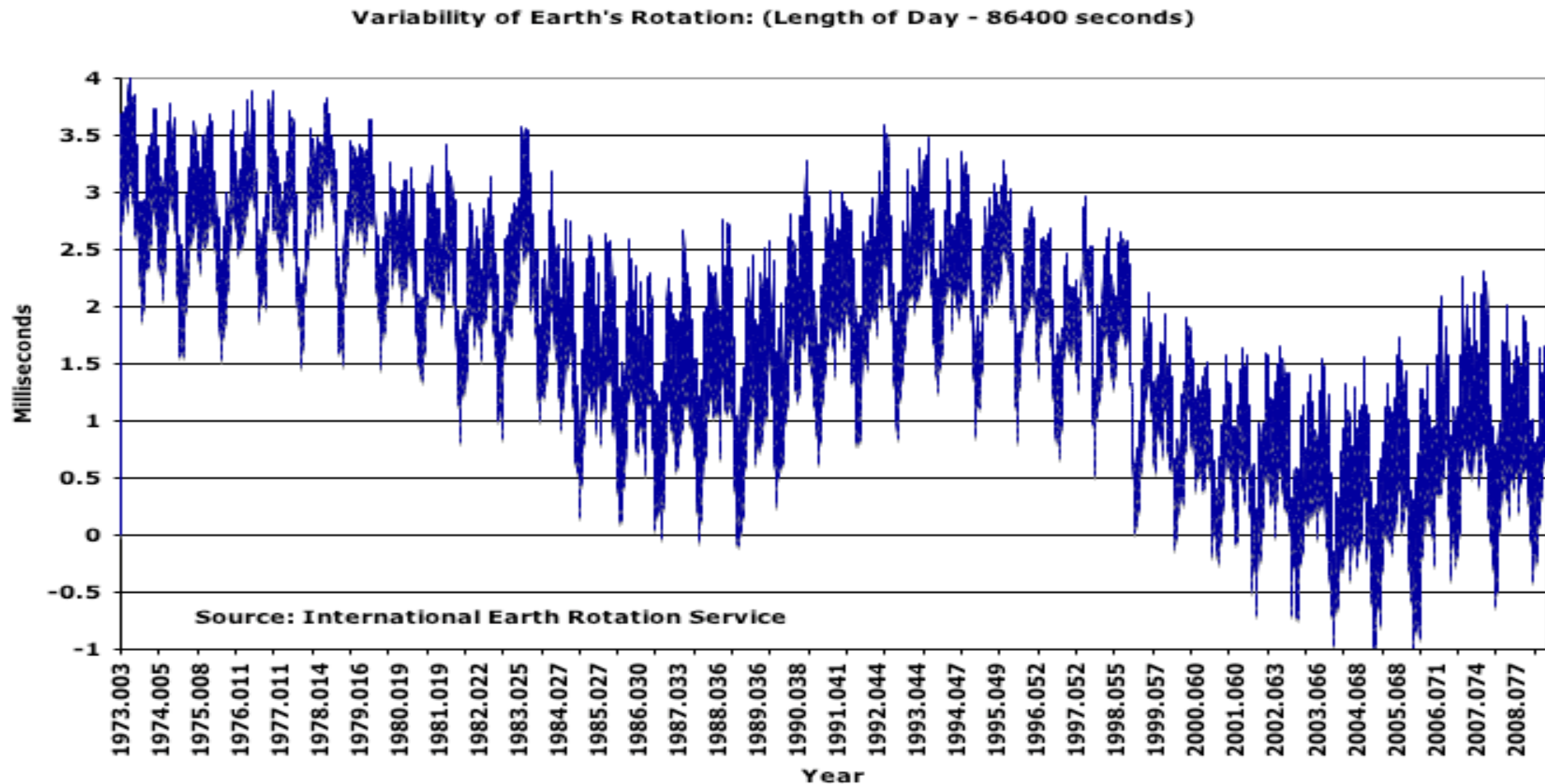
Thus: $\frac{d\phi}{dt} = \frac{2\pi\omega_e}{\lambda/B \cos \theta}$ [8]

From equation [8] the output of the interferometer will be a sinusoid at a frequency that corresponds to the rotation of the Earth divided by the fringe angular spacing.

e.g. $B=100$ km, $\nu=1$ GHz \Rightarrow a fringe frequency of 2kHz.

In practice, the geometric delay of an interferometer must therefore be continuously adjusted by the correlator as the source moves across the sky.

VLBI measurements show that the Earth's rotation rate is slowing, i.e. the length of the day is increasing:



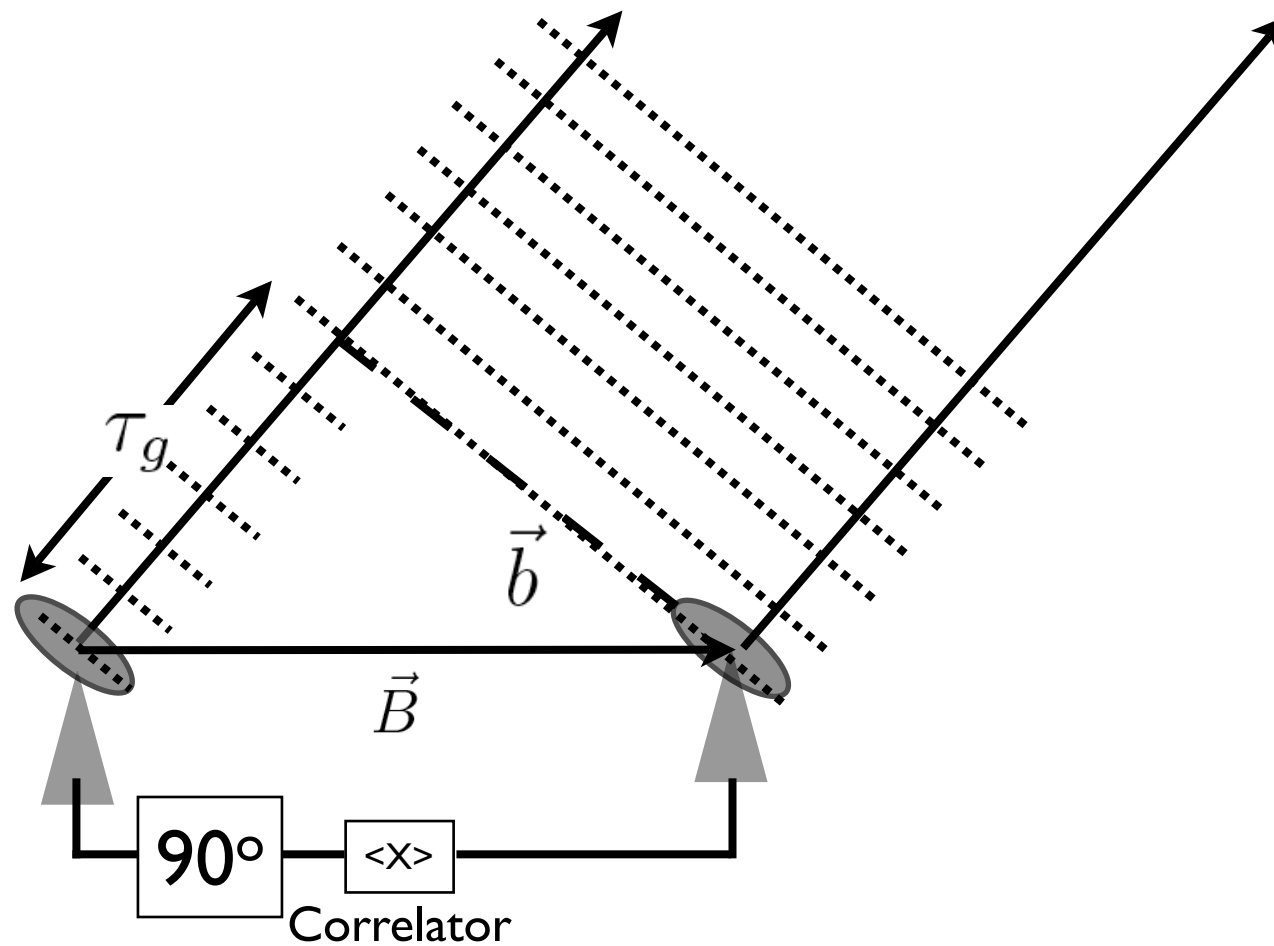
Civil time is defined by atomic clocks known as UTC (Coordinated Universal Time). In order to keep UTC and UTI in step, a leap second is introduced every few years. The last insertion of an extra second was 31 Dec 2008.

The variation of UTI-UTC is difficult to predict ahead of time. Knowledge of the Earth's rotation rate is also required for precision navigation (GPS) and has related military applications.

The voltage term (or correlator output/response), is directly proportional to the Flux density of the radio source, S decreased by $\cos(2\pi \nu \tau_g)$ - see eqn[6]

The signal we have been discussing is called so far is the cosine component of the signal.

To recover the full power of the source, we need to compute both the *cosine* component (see above) and *sine* component. The sine component is computed by applying a phase shift of 90 degrees to the signal from one of the antennas:



$$V_1(t) = v_1 \cos 2\pi\nu(t - \tau_g - \pi/2)$$

$$V_2(t) = v_2 \cos 2\pi\nu t$$

With the 90 degrees phase shift applied to the data, the correlator's sine response (for 2 identical antennas) is:

$$r_{sin}(\tau_g) = \frac{1}{2} V^2 \sin(2\pi\nu\tau_g)$$

Since V^2 is proportional to the flux density of the source, we can write the proportionalities:

$$r_{sin}(\tau_g) \propto \frac{1}{2} S \sin(2\pi\nu\tau_g) \quad r_{cos}(\tau_g) \propto \frac{1}{2} S \cos(2\pi\nu\tau_g)$$

From the 2 components we can recover the full power and characteristics of the signal (its amplitude, a) and phase:

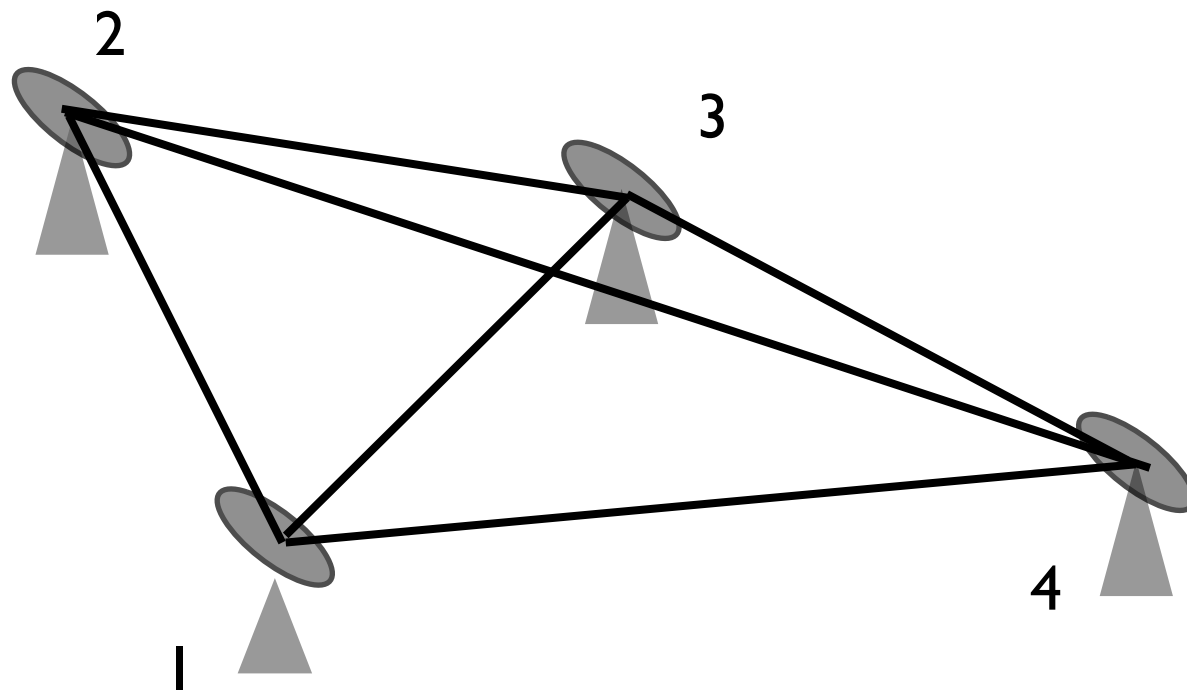
$$a = (r_{cos}^2 + r_{sin}^2)^{1/2} \quad \phi = \tan^{-1}\left(\frac{r_{sin}}{r_{cos}}\right)$$

Since both the sine and cosine components are necessary to fully characterise the signal, correlators compute both the sine and cosine components simultaneously. For this reason, the term “complex” correlator is often used.

Multi-element interferometer

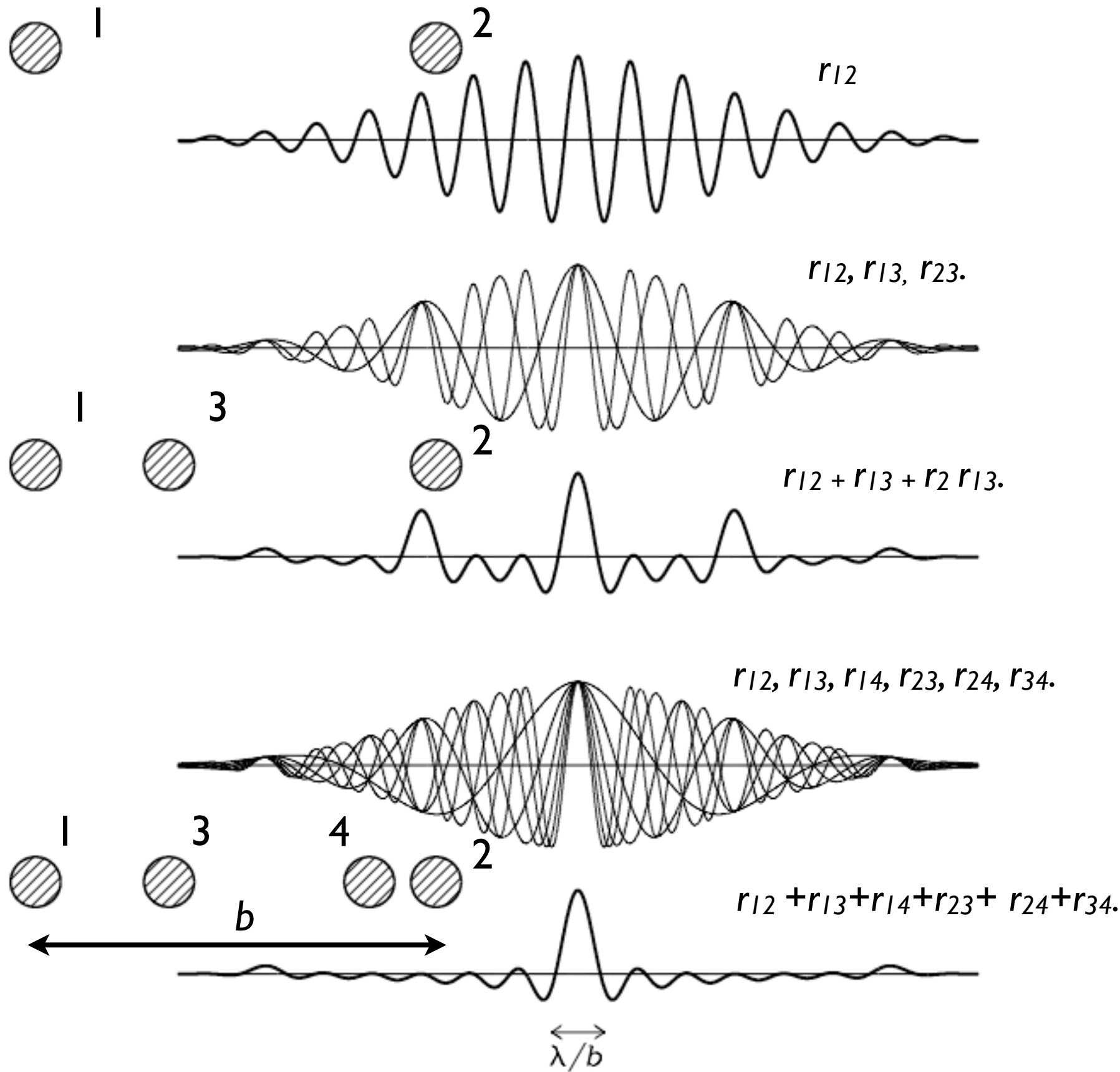
A two element interferometer produces a single response, r_{12} .

A multi-element interferometer (say with N antennas) produces $N(N-1)/2$ unique responses:



For $N=4$, 6 baselines responses are measured:
 $r_{12}, r_{13}, r_{14}, r_{23}, r_{24}, r_{34}$.

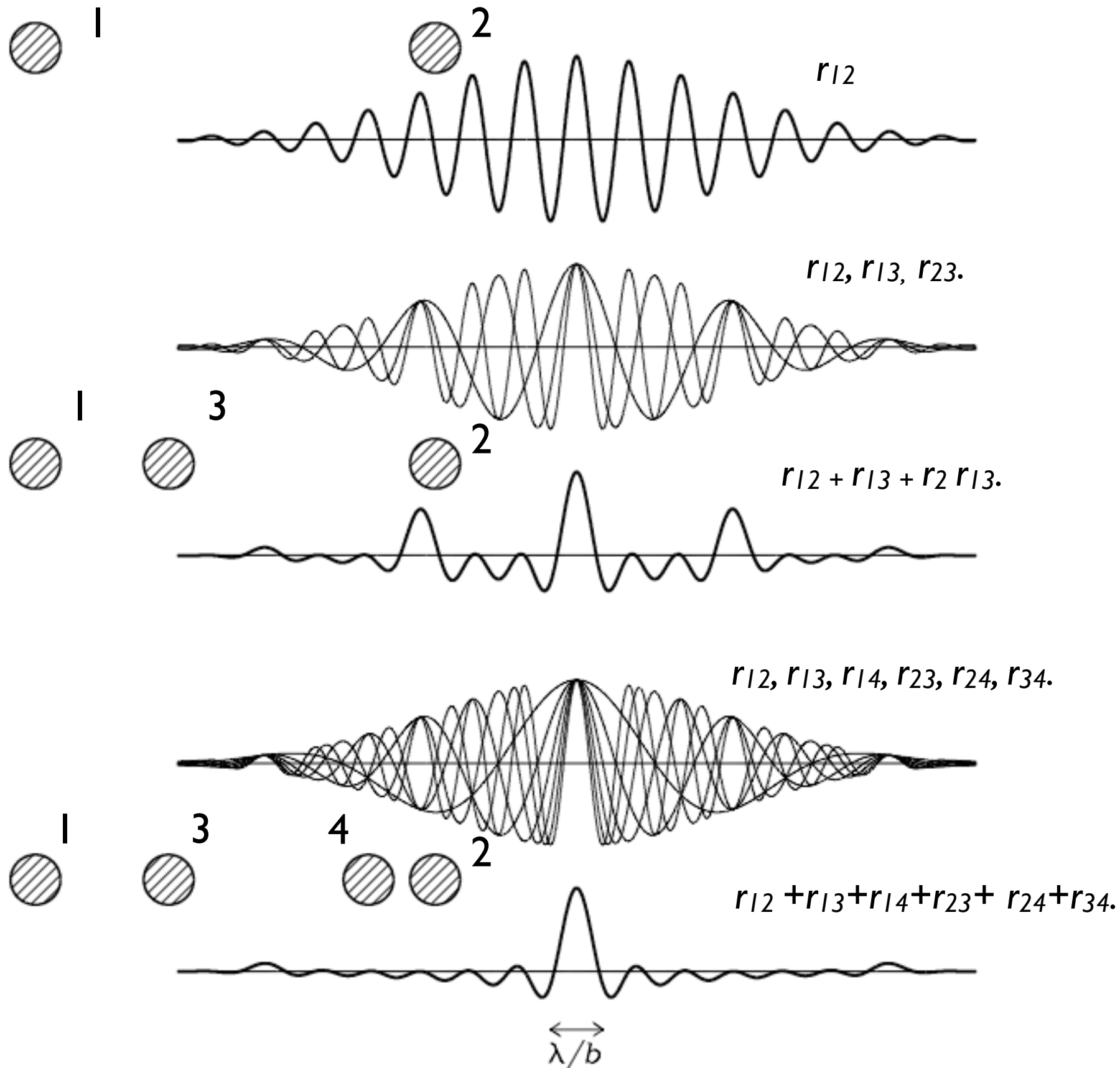
Each interferometer pair presents its own sinusoid at a frequency proportional to the fringe angular spacing (which is usually different for each pair):



An interferometer with N antennas contains $N(N-1)/2$ interferometer pairs.

The instantaneous synthesized beam projected on the sky (the point-source response obtained by averaging the outputs of all pairs - thin curves $r_{12}, r_{13}, r_{14}, r_{23}, r_{24}, r_{34}$.) rapidly approaches a Gaussian (thick curves e.g. $r_{12} + r_{13} + r_{14} + r_{23} + r_{24} + r_{34}$) as N increases.

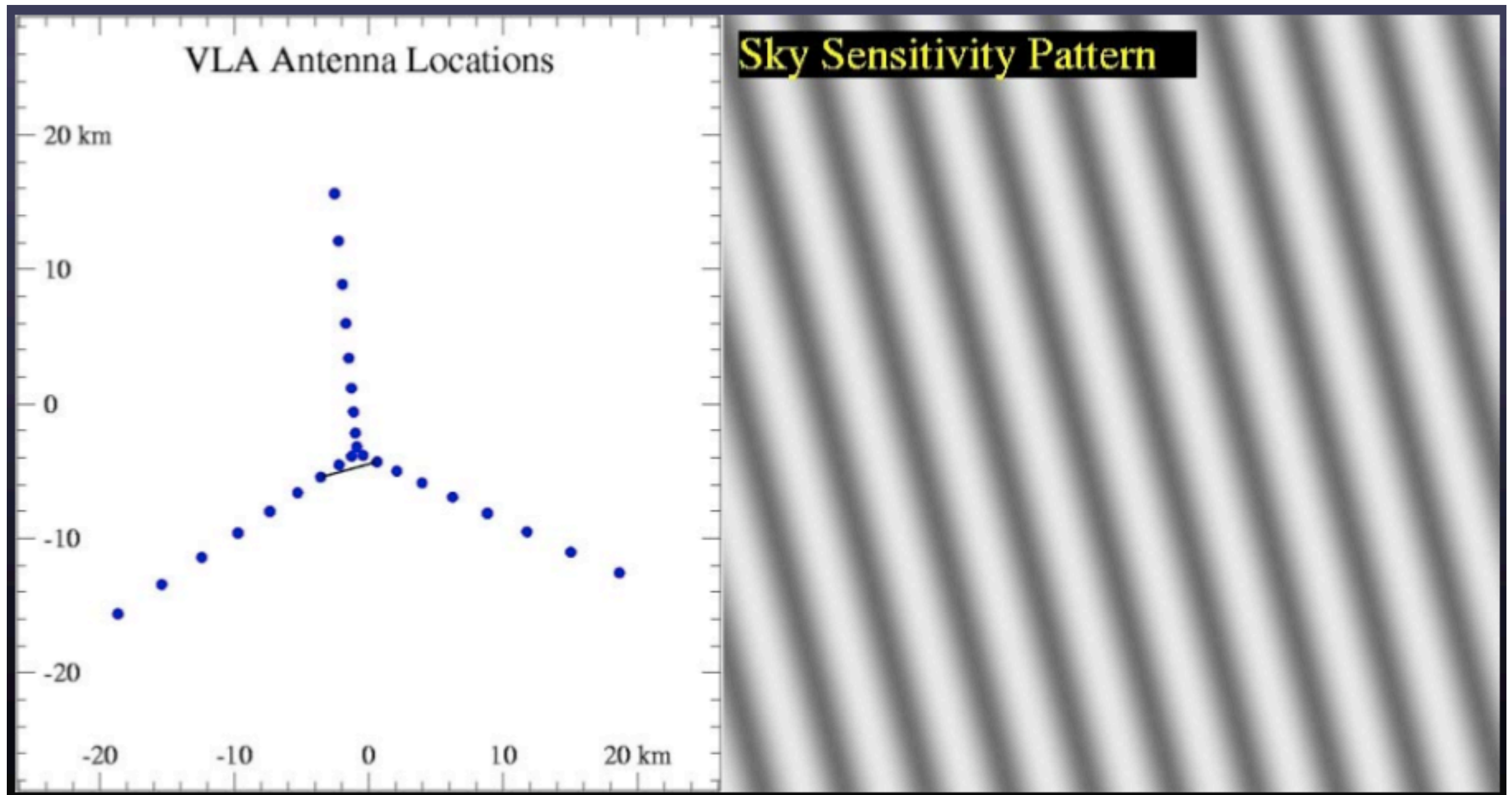
The synthesized main beam of the four-element interferometer (left) is nearly Gaussian with angular resolution $\sim \lambda/b$



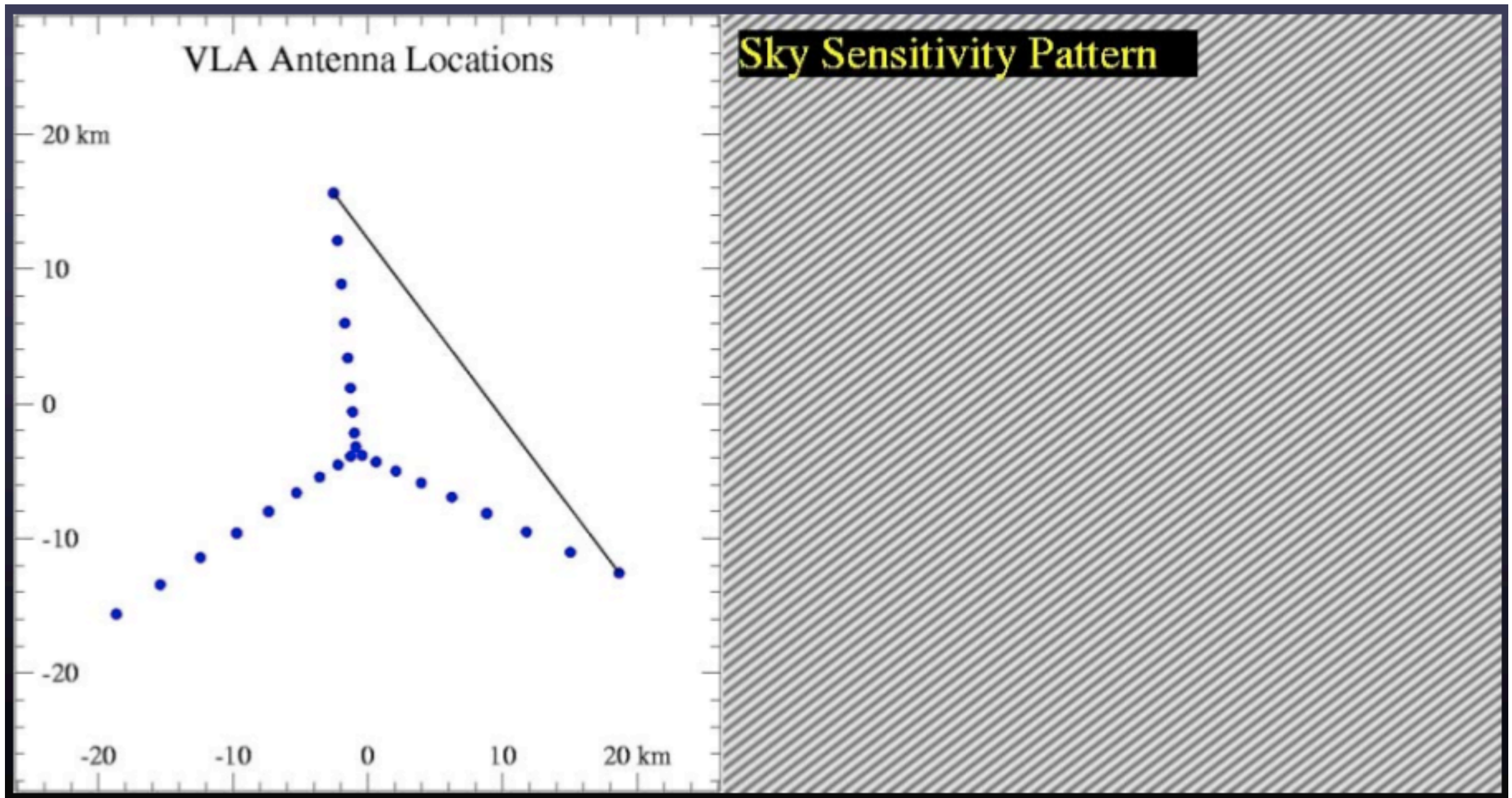
Longer baselines (e.g. r_{12}) have a narrower angular fringe spacing projected on the sky. Their response is sensitive to very compact objects with scales \sim the fringe spacing.

Shorter baselines (e.g. r_{13}) have a larger angular fringe spacing projected on the sky. They are sensitive to extended objects on the same scale as the fringe spacing.

By measuring the response of each interferometer spacing, we can visualise how its possible to build-up an image of the sky!



Fringes projected on to the sky for a short VLA baseline



Fringes projected on to the sky for a long VLA baseline

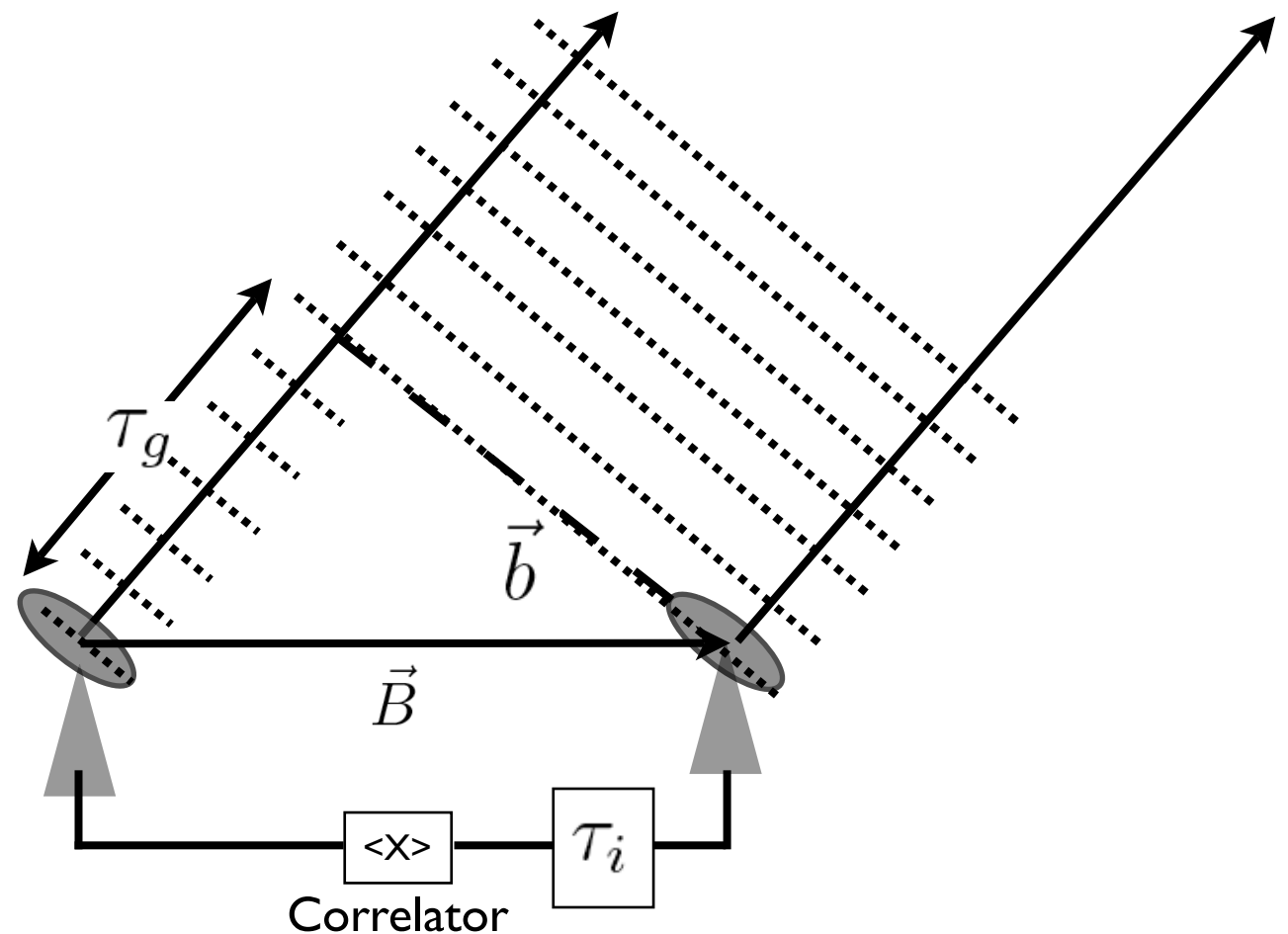
Interferometric imaging

A complex correlator computes the sine and cosine components simultaneously and introduces a compensating instrumental delay τ_i (see figure below) in one of the antennas which is a good (but imperfect) estimate of the true geometrical delay τ_g (the various geophysical effects are hard to predict - see earlier in this lecture).

The difference between the geometrical delay and the instrumental delay is the delay tracking error, τ

$$\tau = \tau_g - \tau_i$$

In a modern interferometer the instrumental delay is introduced via a digital phase shift. In the early days of interferometry.



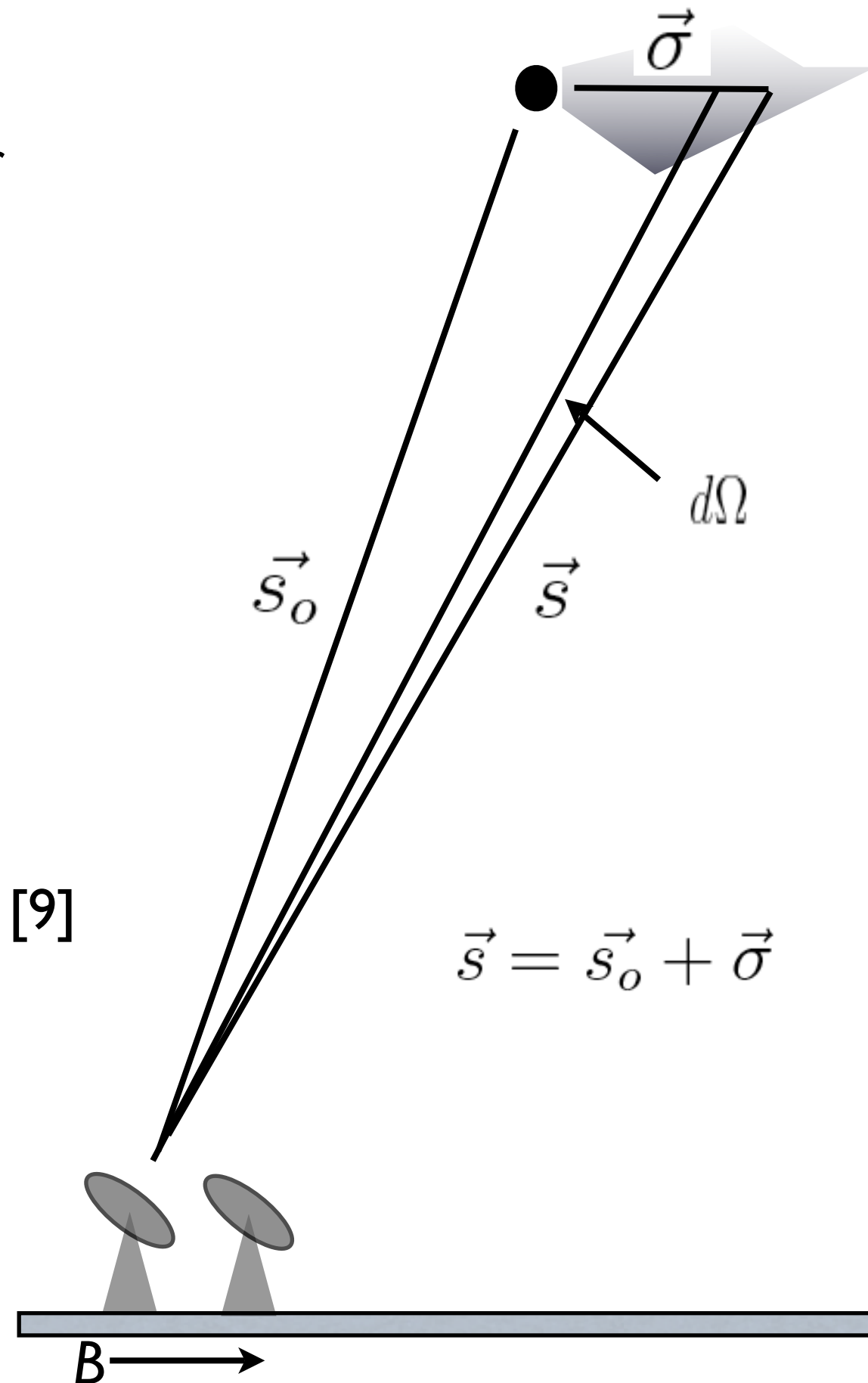
Let us consider a 2-element interferometer observing at frequency, ν , a radio source with a brightness distribution, $I_\nu(s)$, then the output of a complex correlator is the power received per unit bandwidth, $d\nu$, from an element of the radio source, ds is:

$$r_{12} = A(\vec{s}) I_\nu(\vec{s}) e^{i2\pi\nu\tau} ds d\nu$$

The total response is obtained by integrating over the solid angle subtended by the source:

$$R(\vec{B}) = \int \int A(\vec{s}) I_\nu(\vec{s}) e^{i2\pi\nu(\frac{1}{c}(\vec{B}\cdot\vec{s}) - \tau_i)} d\Omega d\nu \quad [9]$$

For parabolic antennas $A(s)$ is usually considered to be zero outside of the fwhm of the antenna primary beam. So in practice the integration is restricted to this area.



For an extended source $\vec{s} = \vec{s}_o + \vec{\sigma}$ and noting that \vec{s}_o and $\vec{\sigma}$ are essentially perpendicular to one another on the celestial sphere, we can write:

$$\vec{B} \cdot (\vec{s}_o + \vec{\sigma}) = \vec{B} \cdot \vec{s}_o + \vec{b} \cdot \vec{\sigma}$$

Substituting this in eqn[9] we can write: $R(\vec{B}) = V(B) A_0 e^{i2\pi\nu(\frac{1}{c}(\vec{B} \cdot \vec{s}_o) - \tau_i)} d\nu$

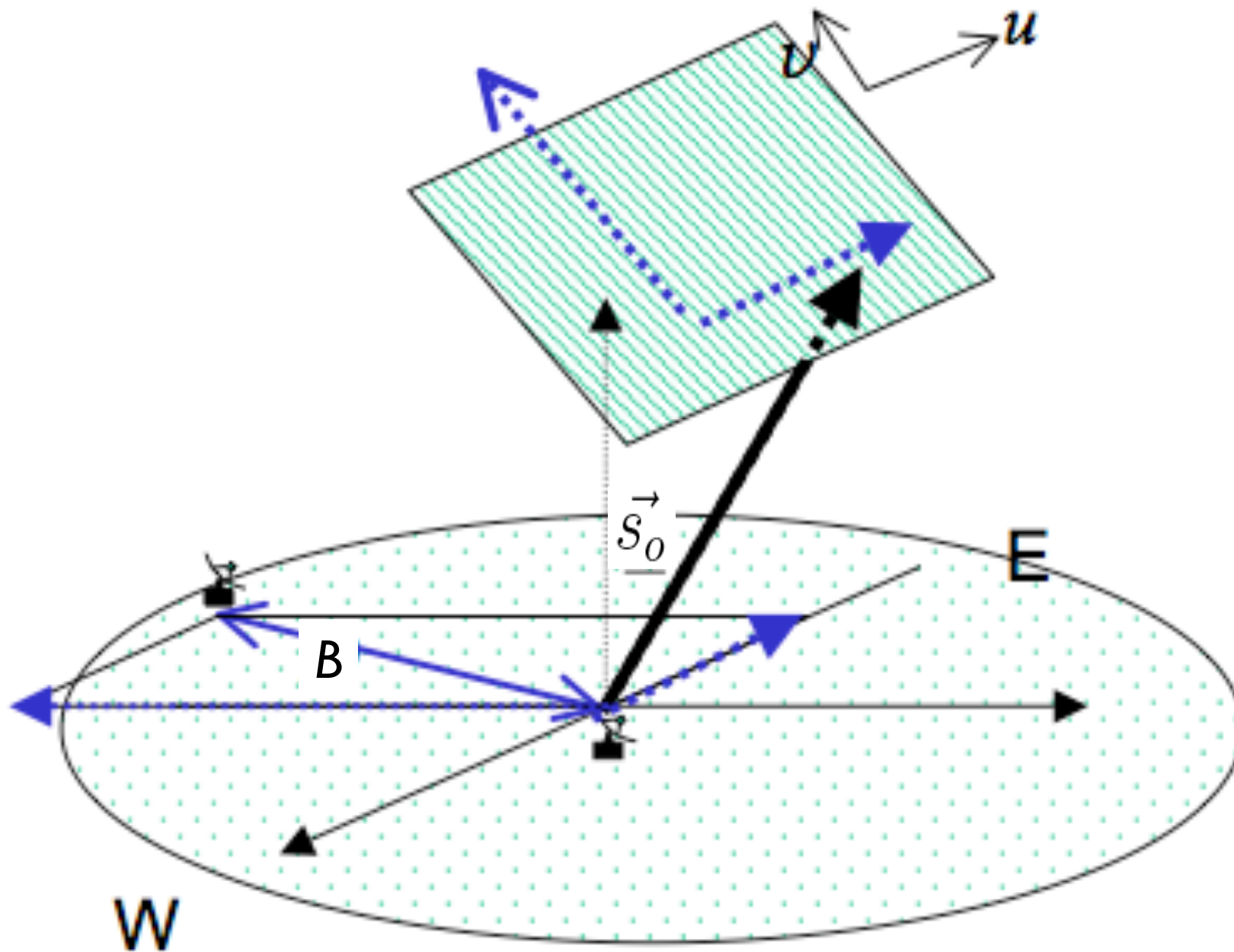
where: $V(\vec{B}) = \int \int A'(\vec{\sigma}) I(\vec{\sigma}) e^{i2\pi(\frac{\vec{B}}{\lambda} \cdot \vec{\sigma})} d\Omega$ [10]

and $A'(\sigma) = A(\sigma)/A_0$

is the normalised beam pattern with A_0 being the response at the beam centre in the direction of \mathbf{s}_o

The integral above, $V(B)$ is the *visibility function* and from its form you can probably see already it is the Fourier Transform (FT) of the source brightness distribution. In principle, we may therefore recover the source brightness distribution by performing the inverse FT on the visibility function.

In order to make use of eqn 10., it is useful to introduce a cartesian coordinate system.



The baseline vector is specified by (u, v, w) where w is chosen to be in the direction of the source direction (known as the phase centre), normal to the u, v plane.

u and v form a plane with u orientated towards the east and v orientated towards the north. This plane, known as the $u-v$ plane is perpendicular to the source direction.

The (u, v, w) coordinates are measured in terms of wavelengths.

Another look at the sky - uv-plane - telescope baseline geometry :

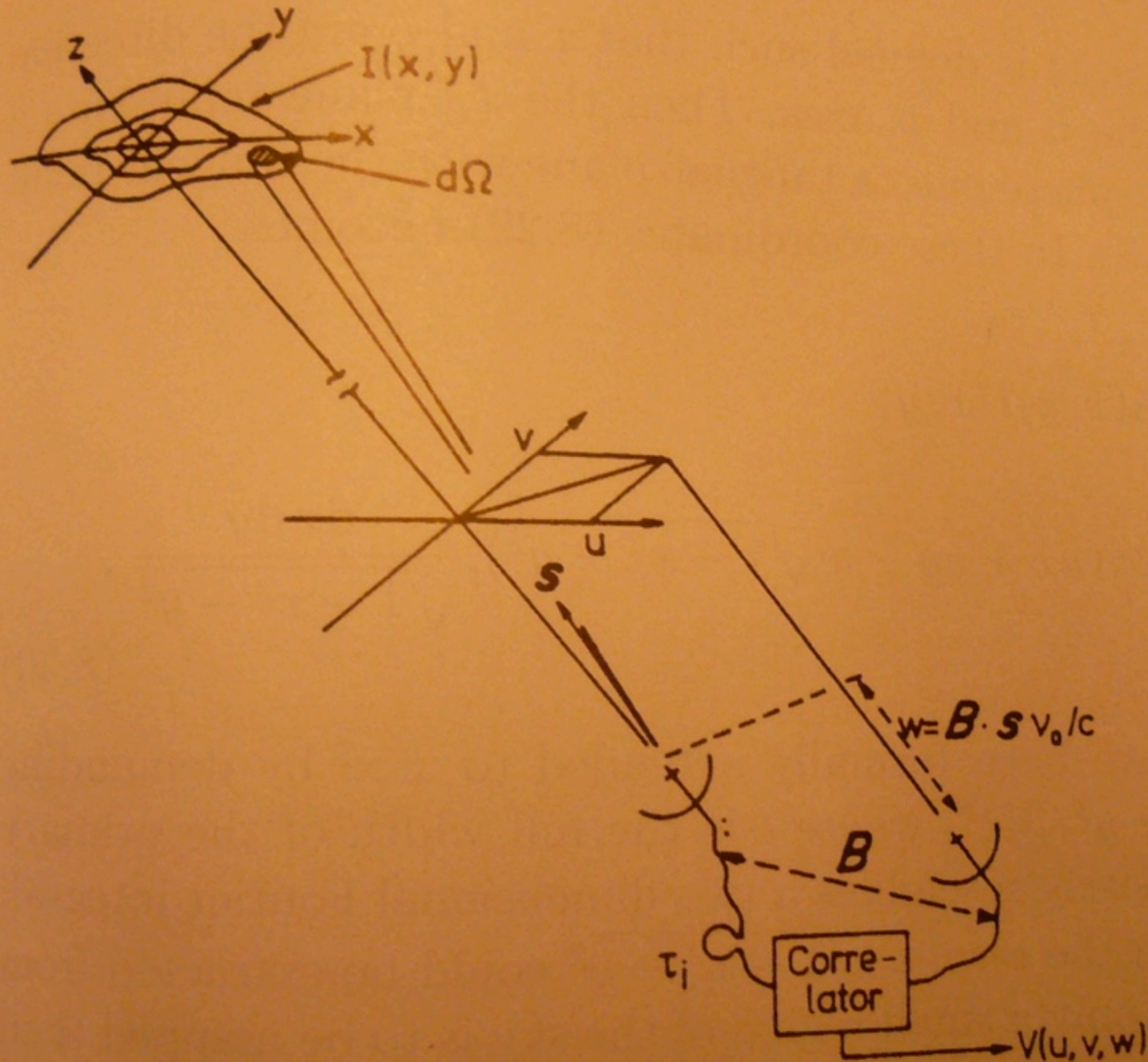


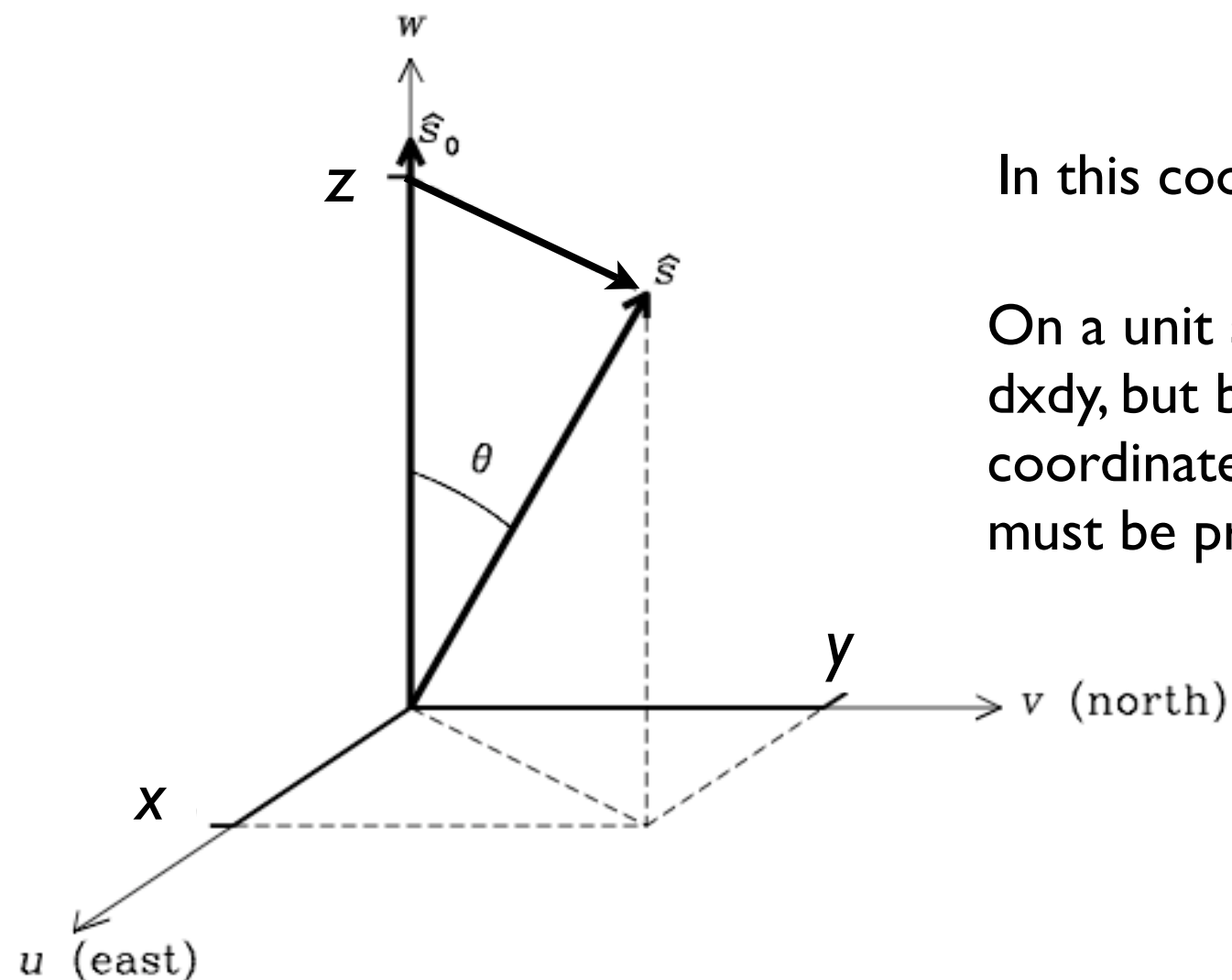
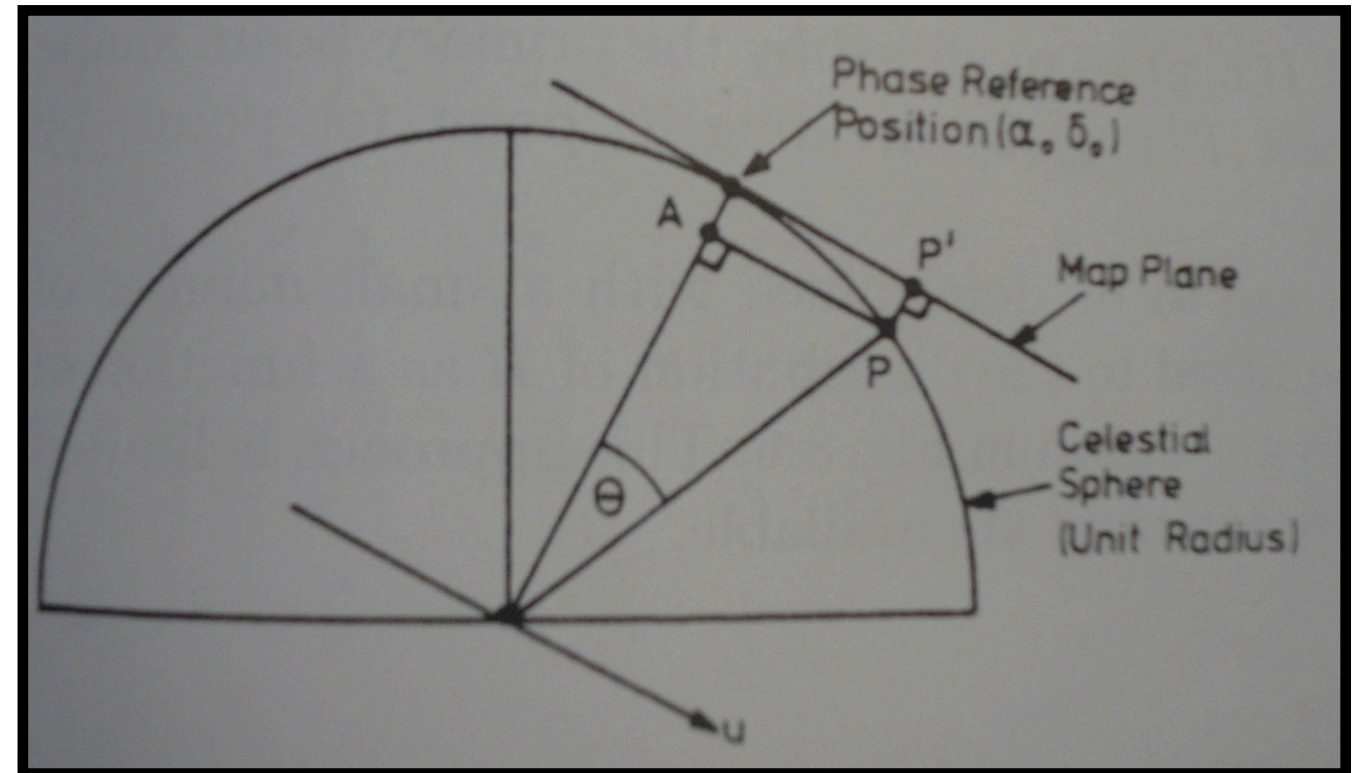
Fig. 8.4.

Geometry and coordinates for a detailed discussion of interferometry, leading to aperture synthesis. Here the coordinates u and v are shown [after Thompson et al. (1986)]

u, v, w coordinates specify the baseline vector.
(in units of wavelength): $B=(u, v, w)$

Positions on the sky, are defined with direction cosines, x and y , and measured w.r.t. the u and v axes (bottom).

The x - y plane is the projection of the celestial sphere onto a plane (right) with a tangent point defined by s_0



In this coordinate system, $\vec{\sigma} = (x, y, z)$ and $z = (1 - x^2 - y^2)^{1/2}$

On a unit sphere the source solid angle is $d\Omega$, but because dx and dy are cartesian coordinates (and the solid angle measured area must be projected on a sphere:

$$d\Omega = dx dy / \cos(\theta)$$

$$= dx dy / z = dx dy / (1 - x^2 - y^2)^{1/2}$$

In this coordinate system we can therefore re-write eqn[10] as:

$$V(u, v, w) = \int_{-\infty}^{+\infty} \int_{-\infty}^{+\infty} A'(x, y) I(x, y) \exp(i2\pi(ux + vy + w(1 - x^2 - y^2)^{1/2})) \frac{dxdy}{(1 - x^2 - y^2)^{1/2}} \quad [11]$$

- noting again that $A'(x,y)=0$ outside of the primary beam of the antennas.

Also note, that for an array of telescopes orientated exactly east-west, the baseline vector always rotates within the uv-plane such that $w=0$. Eqn[11] then reduces to:

$$V(u, v) = \int_{-\infty}^{+\infty} \int_{-\infty}^{+\infty} A'(x, y) I(x, y) \exp(i2\pi(ux + vy)) dxdy \quad [12]$$

i.e. the measured visibility function, $V(u,v)$, is related to the projected brightness on the sky $I(x,y)$ via an exact 2-D Fourier Transform. Eqn[12] is called the van Cittert-Zernike relation after the person that first derived it in the context of physical optics.

More explicitly, we can formulate the inverse FT of [12]:

$$I'(x, y) = A'(x, y)I(x, y) = \int_{-\infty}^{+\infty} \int_{-\infty}^{+\infty} V(u, v) \exp(i2\pi(ux + vy)) dx dy \quad [13]$$

where $I'(x,y)$ is the brightness distribution on the sky modified by the beam shape (primary beam) of the individual antennas. Since the beam shape is well known (and also close to unity in the centre of the field) its effect can easily be removed by applying what is known as a “primary beam correction”.

In any case, the point is that we can make images of the sky by measuring the amplitude and phase of the visibility function at different points in the (u,v) plane. These points in the uv -plane correspond to different projections of the baseline vector, B .

N.B. what we have derived so far, is the special case for arrays that oriented East-West. Westerbork is a good examples of an E-W array:



Aperture synthesis

Not to scale!

As a telescope collects measurements of $V(u,v)$ we talk of “filling in” the uv -plane. In this pursuit, astronomers are greatly aided by the rotation of the Earth!

As the Earth rotates, the projected baseline vector, B changes as seen by the source. In this way we collect many measurements of $V(u,v)$ - these measurements are called “visibilities”.

The visibilities are values for the amplitude and phase of the response of the correlator for each interferometer (baseline) at a given time (equivalent to a measurement in the uv -plane).

Consider a source located at the pole, and a simple 2 telescopes interferometer (see diagram above). As the Earth rotates, the source sees the baseline vector rotating too, tracing a circle in the sky. For a source at the pole, the projection of the baseline length does not change, but its orientation does. In the uv -plane, the baseline traces out a circle:

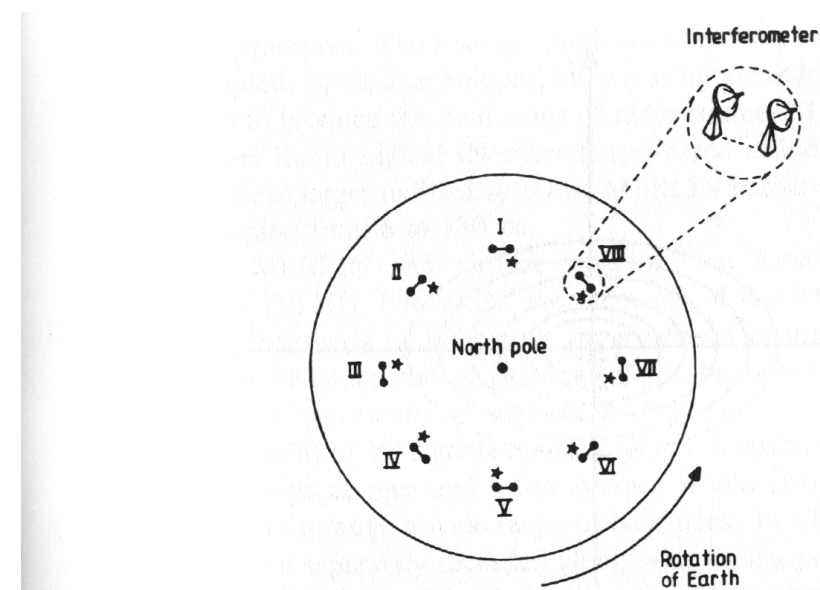
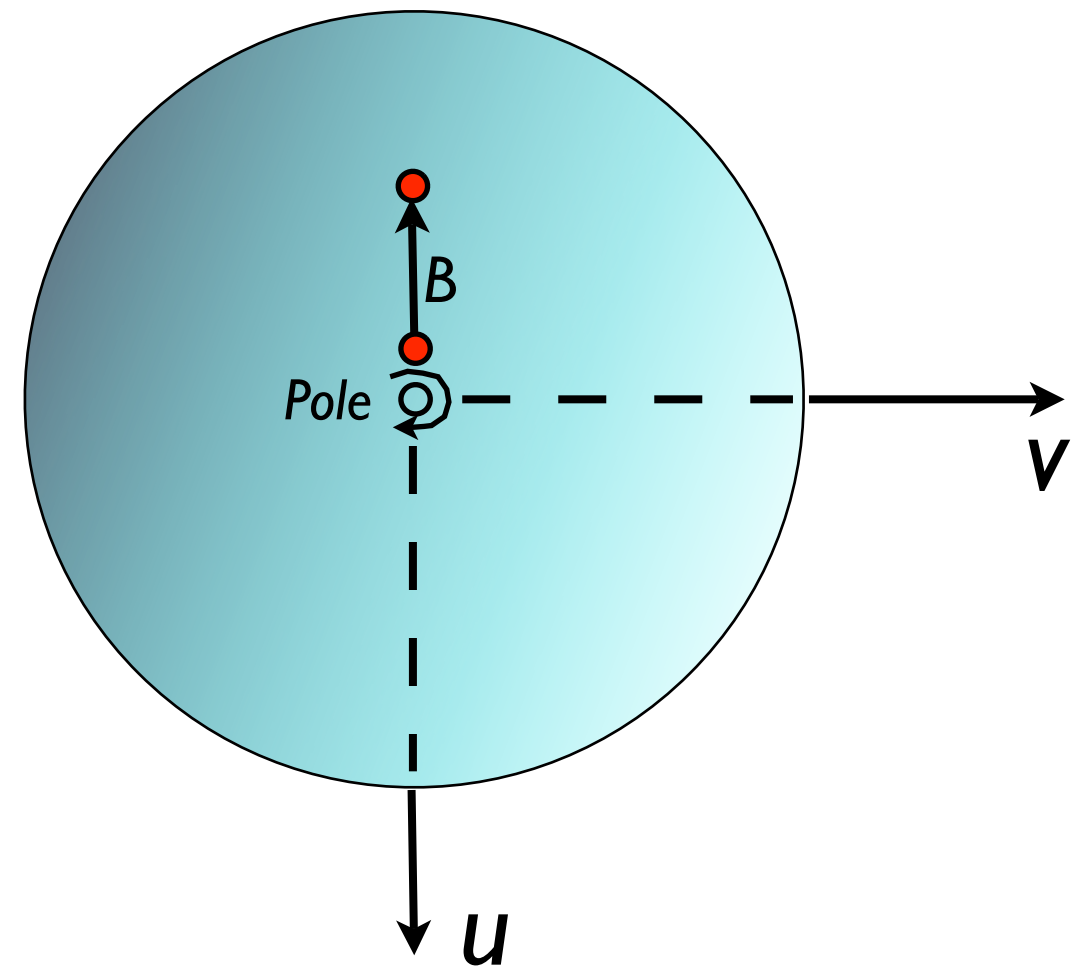
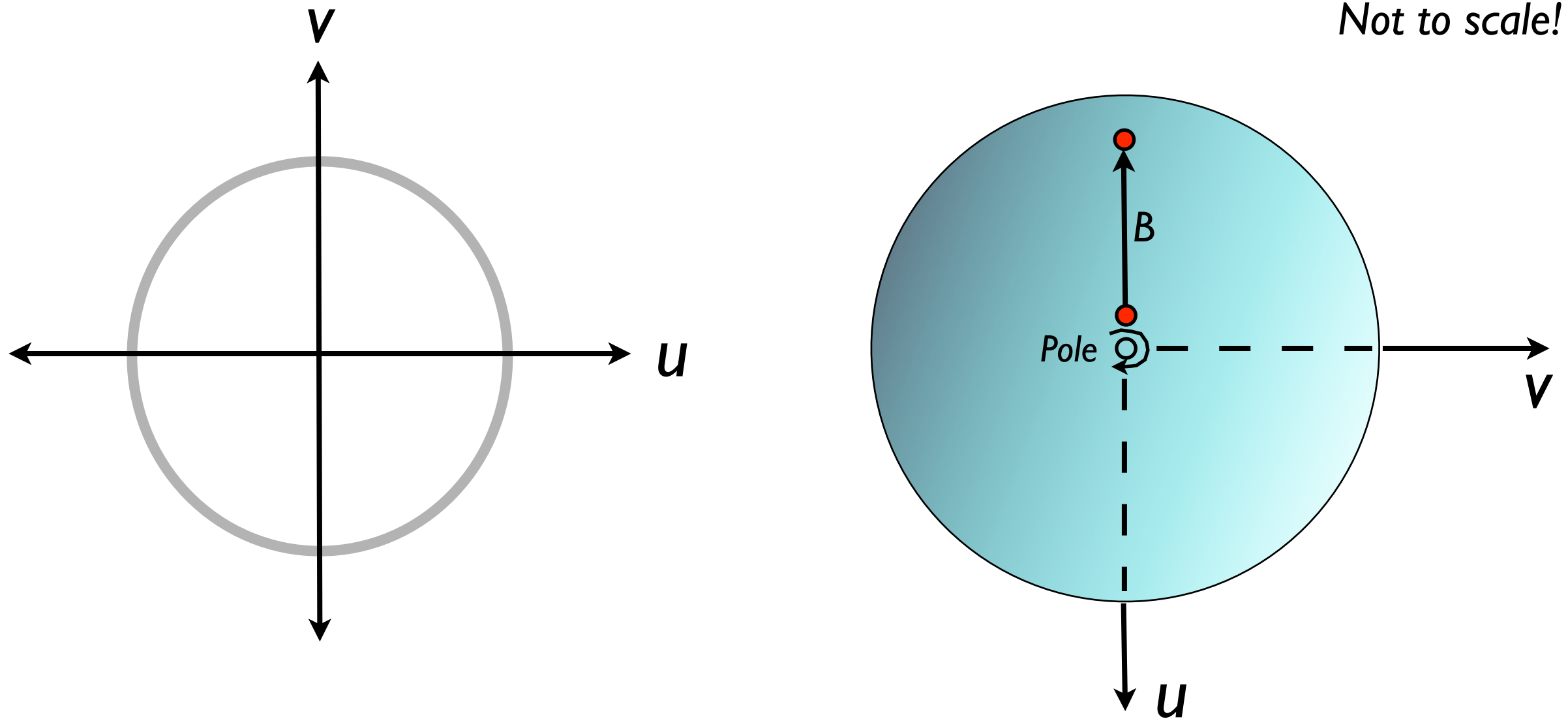


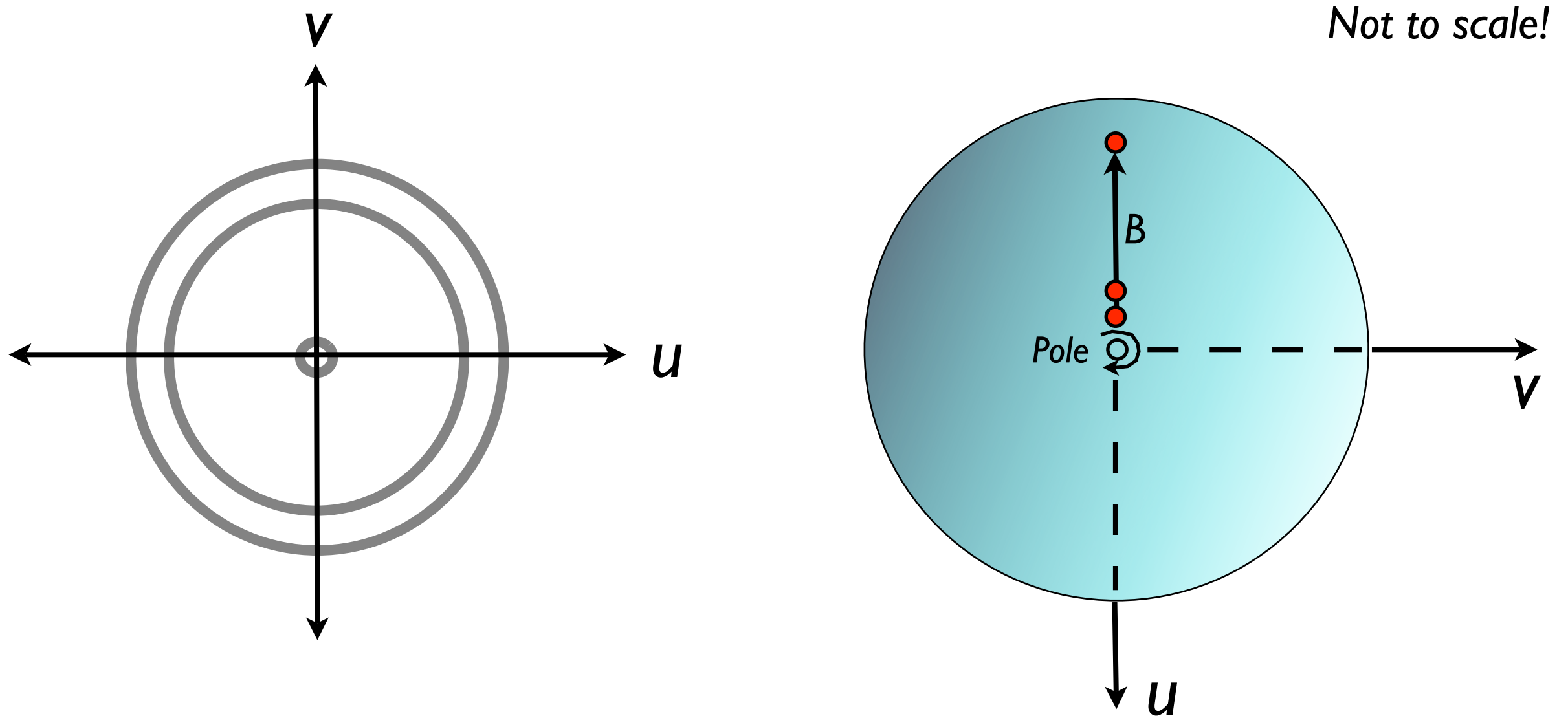
Figure 2.5.17. Changing orientation of an interferometer. The Earth is viewed from above the north pole and successive positions of the interferometer at three hour intervals are shown. Notice how the orientation of the starred aerial changes through 360° with respect to the other aerial during a day.



If we add more antennas, say in between the 2 pictured above (red dots) we begin to fill-in the uv-plane...

The better we fill-in the uv-plane, the higher the quality and fidelity of the images.

After 12 hours, no new information is obtained - this is because $V(u,v)$ is equal to its complex conjugate i.e. $V(u,v) = V^*(u,v)$. You can see this by looking at the figure above. The orientation of the baseline formed by the 2 telescopes clearly repeats (with only the phase reversed) after half a rotation of the Earth.

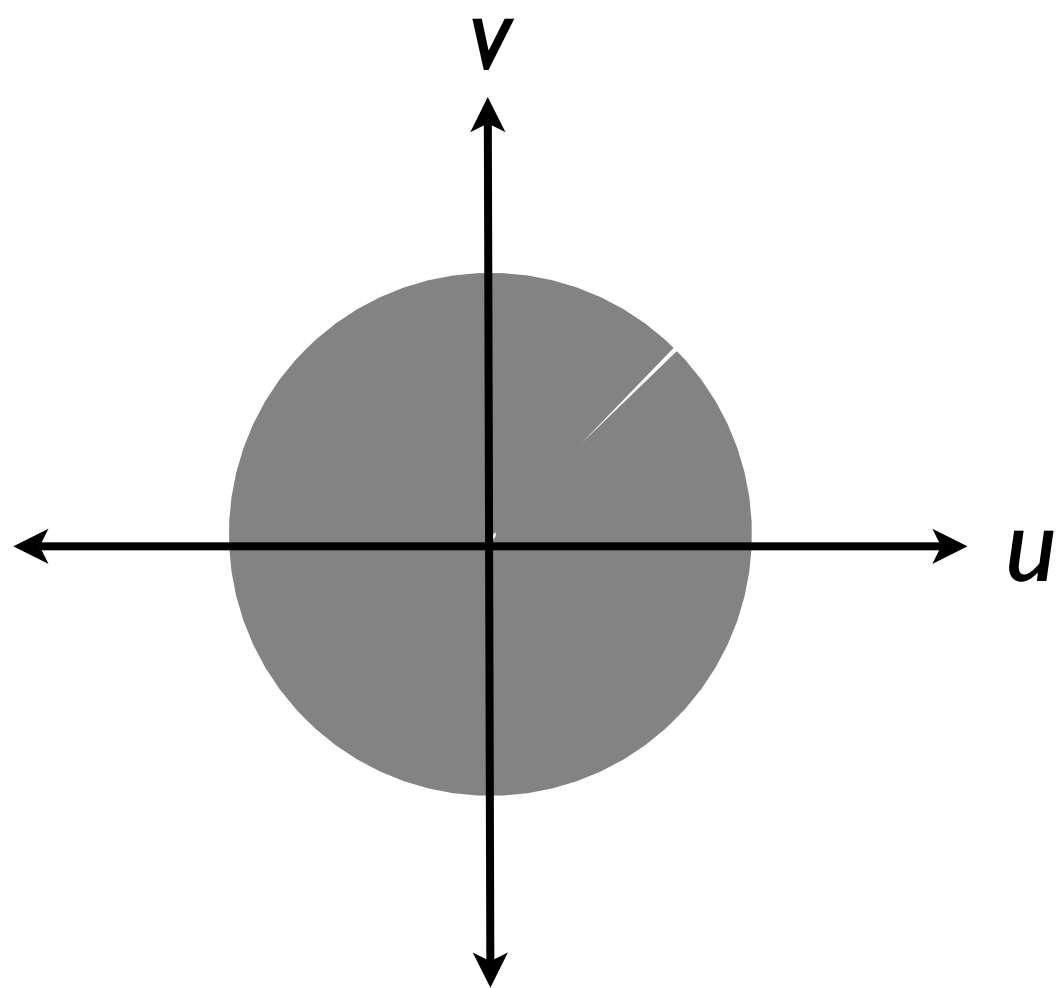


If we add more antennas, say in between the 2 pictured above (red dots) we begin to fill-in the uv-plane...

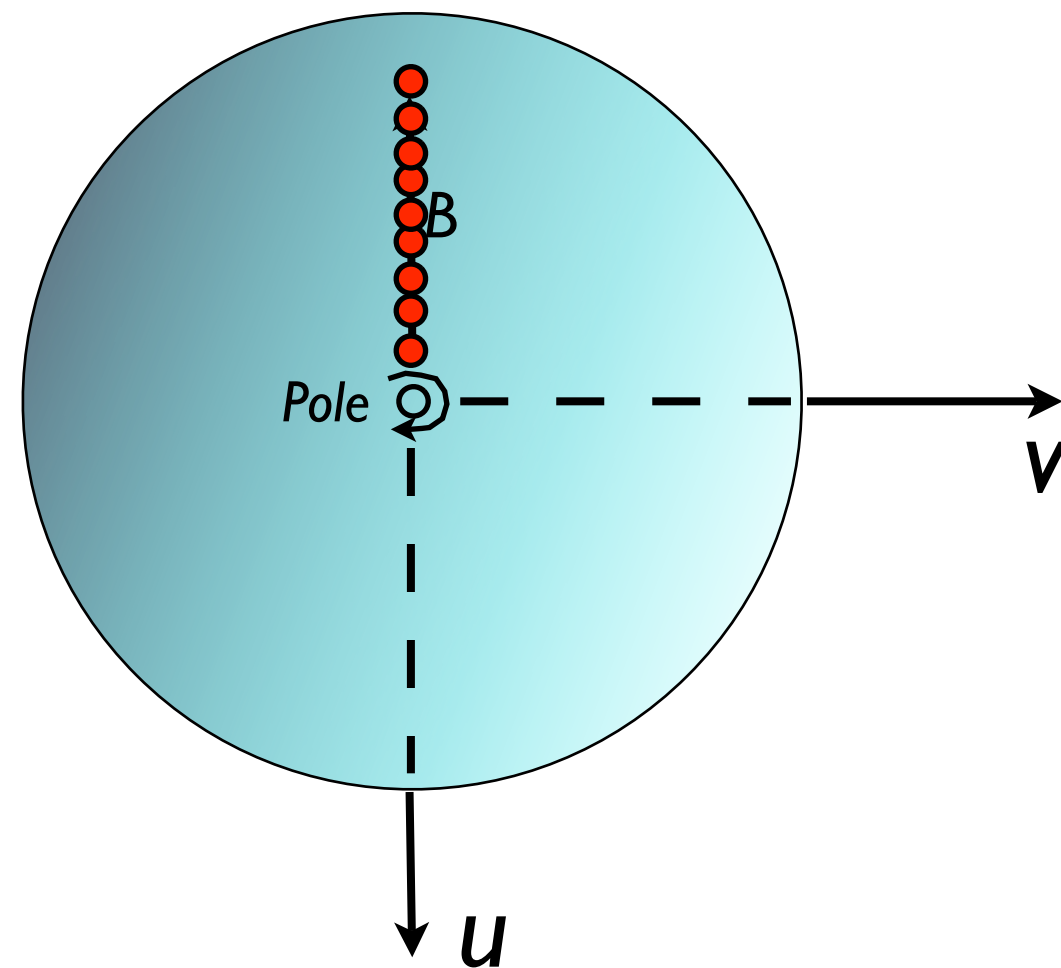
Mathematically we say that each visibility is a Fourier component of the sky brightness.

The better we fill-in the uv-plane, the higher the quality and fidelity of the images.

In the case of Westerbork we have 14 antennas, and we can also move the antennas on rails!



Not to scale!



For Westerbork, a 6 x 12 hour observing run (moving some of the antennas after each 12 hr run) produces almost full uv -coverage (see above).

Westerbork telescope on rails.



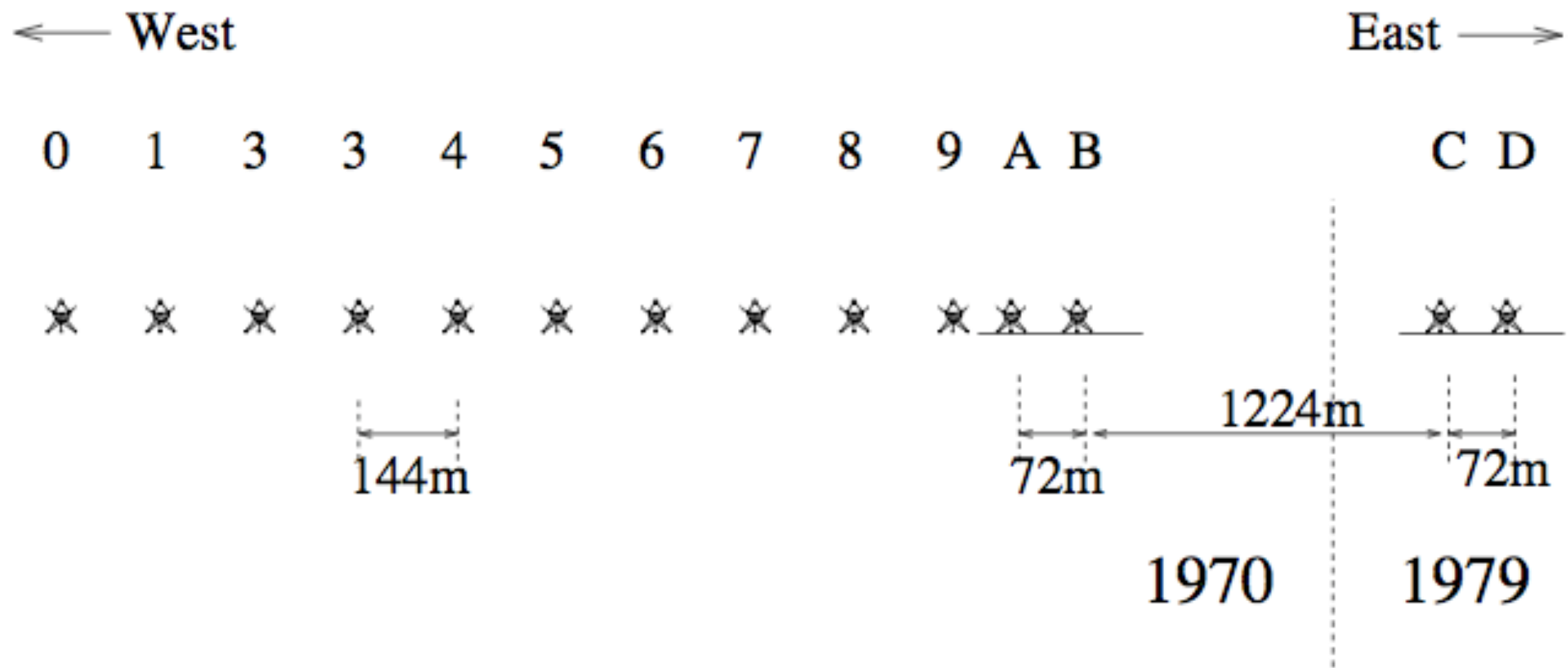


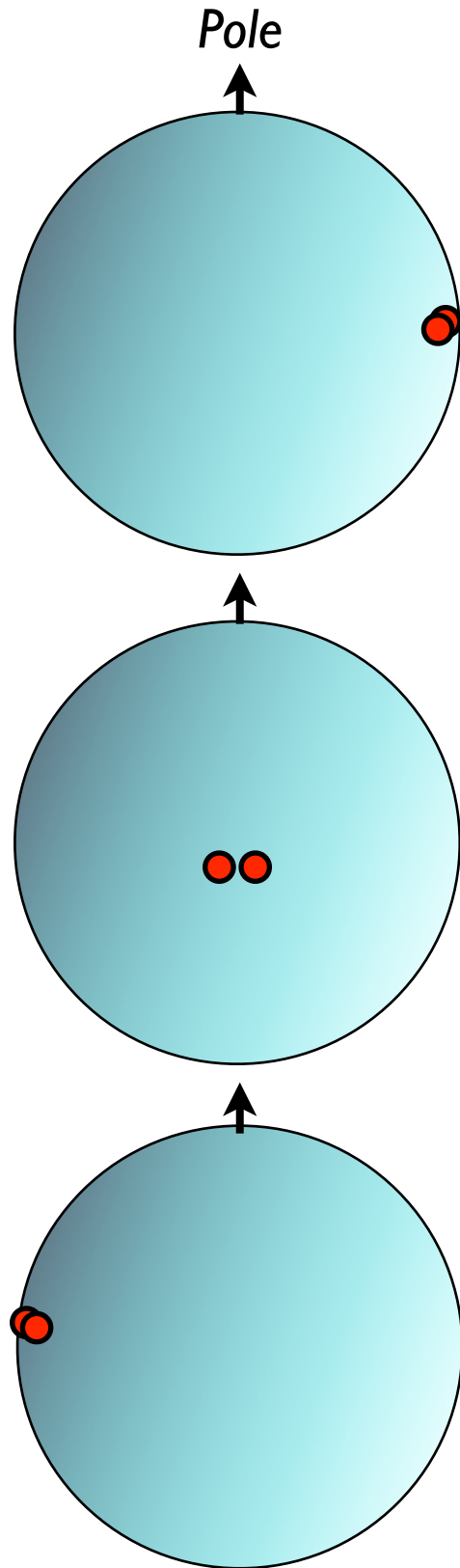
Figure 8.1: *The geometry of the WSRT.*

Telescopes 0-9 have fixed positions, A-D can be moved on rail tracks to a number of positions.

Telescopes C and D were added later, first (1976) next to A and B on the same rails, later (1979) to be moved out to a new rail and thus roughly doubling the total size of the array.

N.B. for the WSRT, there are many identical baselines. When the WSRT was under construction this was considered to be a good idea as it provided redundancy - this was used to help simplify the calibration of the instrument. With new calibration techniques available today, if the WSRT was to be rebuilt, it's unlikely such redundancy would be required - more likely the separation of the telescopes would be less regular, in order to sample as many different parts of the uv-plane simultaneously.

For sources not located at the pole, the projected baseline length appears to change as the Earth rotates. In these figures imagine that YOU are the source!



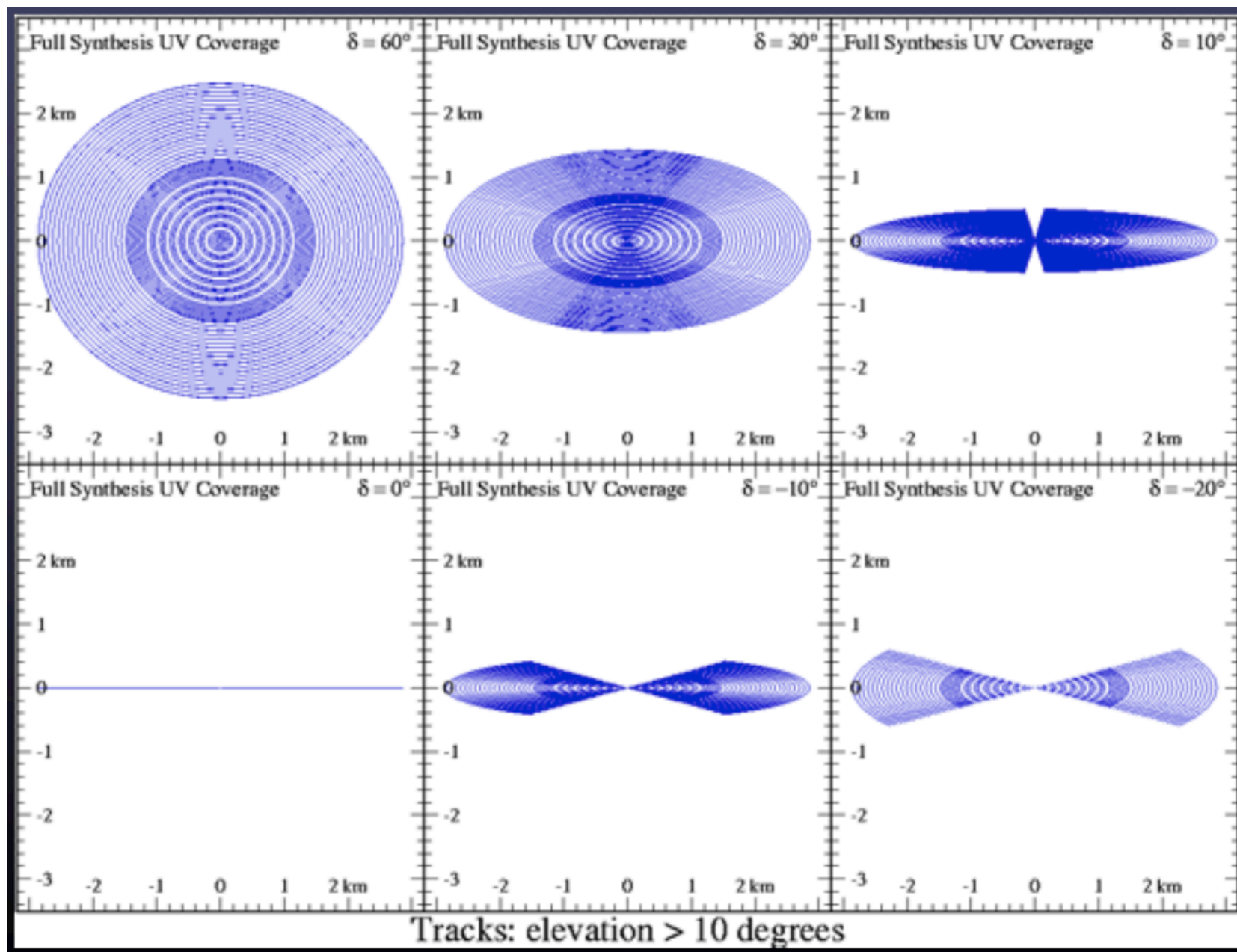
As the source rises for the telescopes at the start of the observation, the projected baseline is greatly foreshortened.

As the earth rotates, and source culminates, the maximum baseline length is achieved.

As the source sets for the telescopes at the end of the observation, the projected baseline is again greatly foreshortened.

Aside: note also, that when the source is rising and setting, there is a greater chance of shadowing of one telescope by another. This is especially a problem for very compact arrays.

So, for sources not located at the pole, the projected baseline length appears to change as the Earth rotates. In particular, for sources at declinations < 90 deg, the uv-tracks become elliptical:



uv-coverage of the WSRT for various source declinations.

The uv-tracks are only plotted when the source is 10 degrees above the local horizon. Below 10 degrees the data are often discarded because they are partially corrupted by the atmosphere at low elevations.

The maximum value of u equals the antenna separation in wavelengths. For an E-W array, the maximum value of v is smaller by the projection factor: i.e. $v_{max} = u_{max} \cos(90 - \delta_s) = u_{max} \sin(\delta_s)$ where δ_s is the source declination. If the interferometer has more than two elements, or if the spacing of the two elements is changed via rail tracks, the (uv) coverage will become a number of concentric ellipses.

Note that the uv-coverage becomes poorer for low-declination sources and becomes 1-dimensional for source located at zero declination. It is very difficult for the WSRT to make good images of low-declination sources (dec < 20 deg) even after a 12 hour observing run.



WSRT neutral hydrogen aperture synthesis image (orange colours) of nearby galaxies, Dwingeloo 1 and 2 - courtesy Tom Oosterloo (ASTRON). This image was obtained after a full 12hr synthesis. The sources are located at declination ~ 60 degrees; excellent u-v coverage is therefore obtained in a single full-track.

The poor uv-coverage that east-west arrays produce instantaneously is a serious problem. Non-coplanar, 2-dimensional arrays produce much better “snapshot” coverage, especially for sources at low-declinations.

Current and future telescopes like the VLA, MERLIN, VLBI, ALMA and SKA are non-coplanar arrays i.e. the antennas are not restricted to lie along the east-west direction and therefore they do not perfectly lie in a single plane (the u-v plane), i.e. we cannot simply set $w=0$!

Recall eqn[11]:

$$V(u, v, w) = \int_{-\infty}^{+\infty} \int_{-\infty}^{+\infty} A(x, y) I(x, y) \exp(i2\pi(ux + vy + w(1 - x^2 - y^2)^{1/2})) \frac{dxdy}{(1 - x^2 - y^2)^{1/2}}$$

If we assume that only a small region of sky is to be imaged, then we can make the approximation* that: $(1-x^2-y^2)^{1/2} \sim 1 - 1/2(x^2+y^2) + \dots \sim 1$ where $x, y \ll 1$.

We can also divide both sides of the eqn by $e^{i2\pi w}$. This permits us to cheat, and to write eqn[11] as a 2-D Fourier integral:

$$V(u, v, w)e^{-i2\pi w} = \int_{-\infty}^{+\infty} \int_{-\infty}^{+\infty} A'(x, y) I(x, y) e^{i2\pi(ux+vy)} dxdy \quad [14]$$

*Footnote: we'll return this assumption when we consider wide-field imaging.

The factor, $e^{i2\pi w}$ in [14] is the (approximate) conversion factor to rotate the visibility to the value that would have been measured in the (u,v) plane with $w=0$, i.e.

$$V(u, v, w)e^{-i2\pi w} = V(u, v, 0)$$

Substituting this into [14] and taking the Fourier transform, we can write:

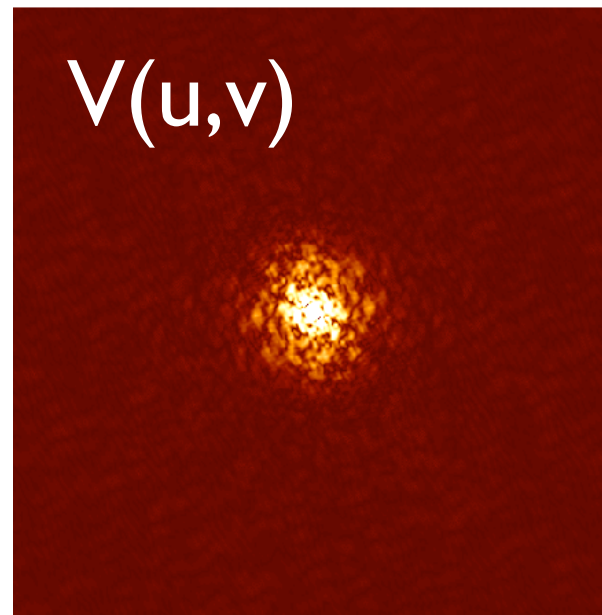
$$I'(x, y) = I(x, y)A'(x, y) = \int_{-\infty}^{+\infty} V(u, v, 0)e^{-i2\pi(ux+vy)}dudv \quad [15]$$

One can correct $I'(x,y)$ by making a primary beam correction across the image, i.e. pixel-by-pixel.

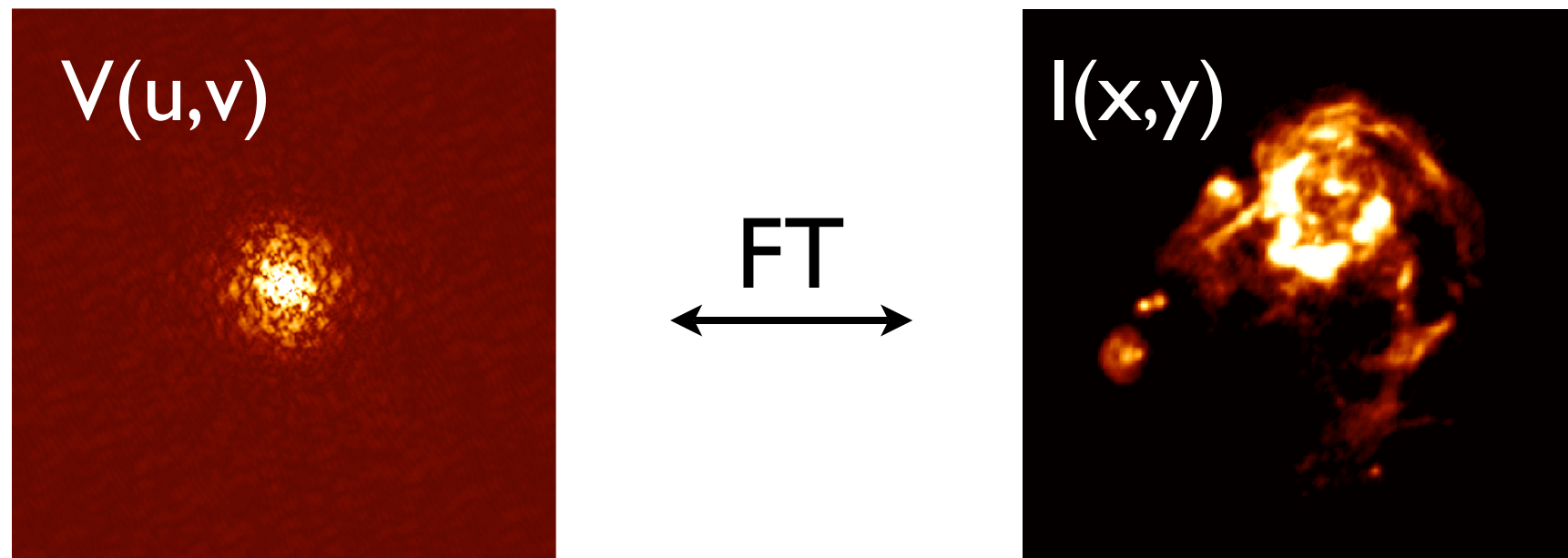
Eqn[15] assumes knowledge of all $V(u,v)$ for all values of u and v . As we shall see later, sufficient (but incomplete) knowledge of the visibility function permits us to make a reasonable estimate of the source brightness distribution (see lecture 6).

Aside: In practice, we therefore have only a finite number of measurements of V (say N_v), to make an image with N_m cells. The number of calculations scales as $N_v N_m$ which can easily exceed 10^{12} . Aperture synthesis is often compute-bound limited, and future radio telescopes push computing to the edge of Moore's law and perhaps beyond. For example, the SKA demands petaflop computing capabilities.

In the *ideal* case we measure the visibilities, $V(u,v)$ over the entire uv -plane:



And the FT of the visibilities produces an image of the source:

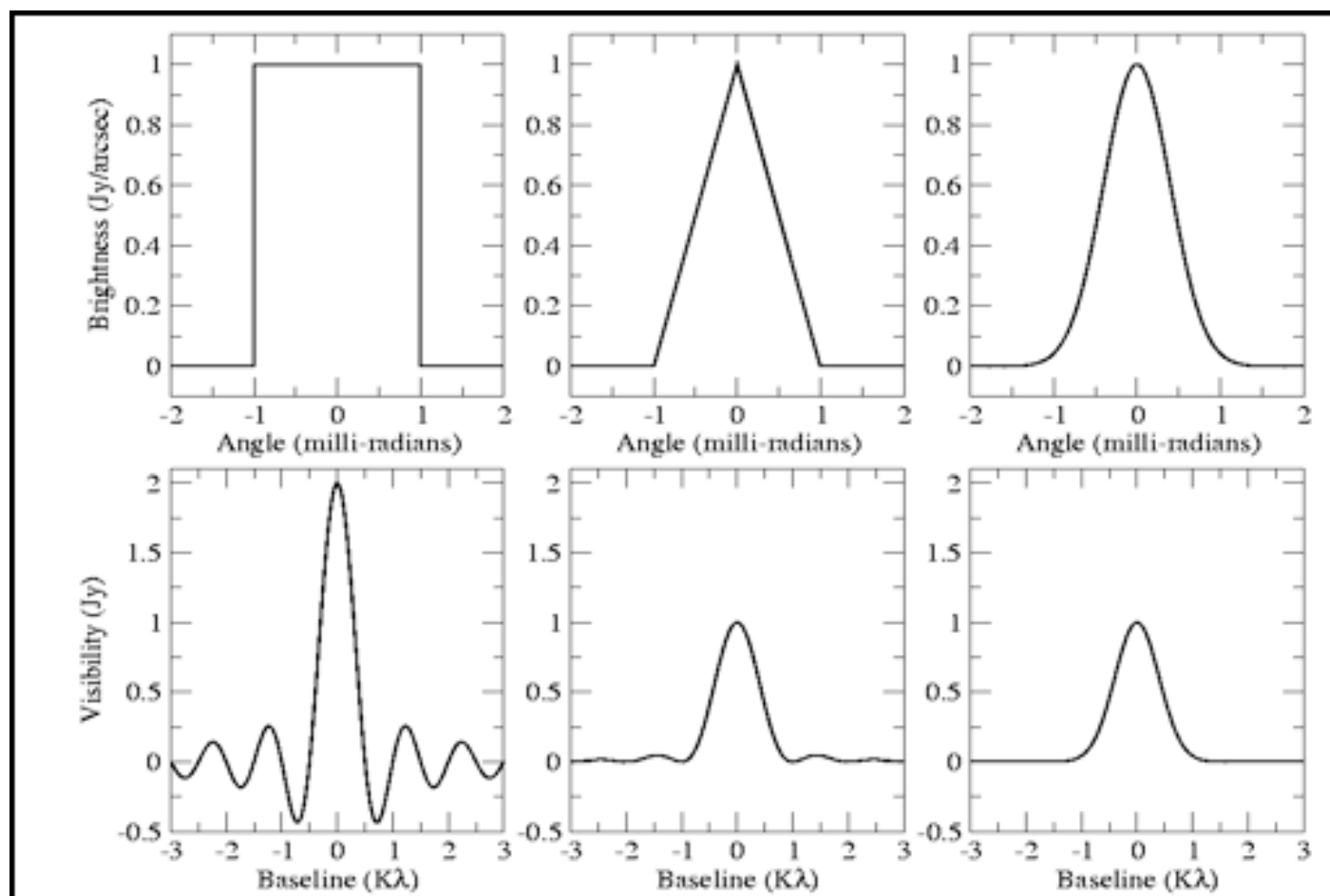


Real life is different - sampling of the uv -plane is often incomplete - we will discuss the various imaging algorithms developed to ease this problem in a subsequent lectures.

Source models & visibility functions

Radio sources can have very complex brightness distributions. However, they can always be decomposed into many simple components.

The figure below shows some simple source brightness distributions and their visibility functions. They are complex valued functions with amplitude and phase - only the amplitude is shown here. Note that sharp features in a source always lead to 'ringing' in the FT of that source that spread across the uv-plane. This is understandable, because characterising a sharp feature in an image requires very high spatial resolution which you obtain through acquiring large Fourier components.

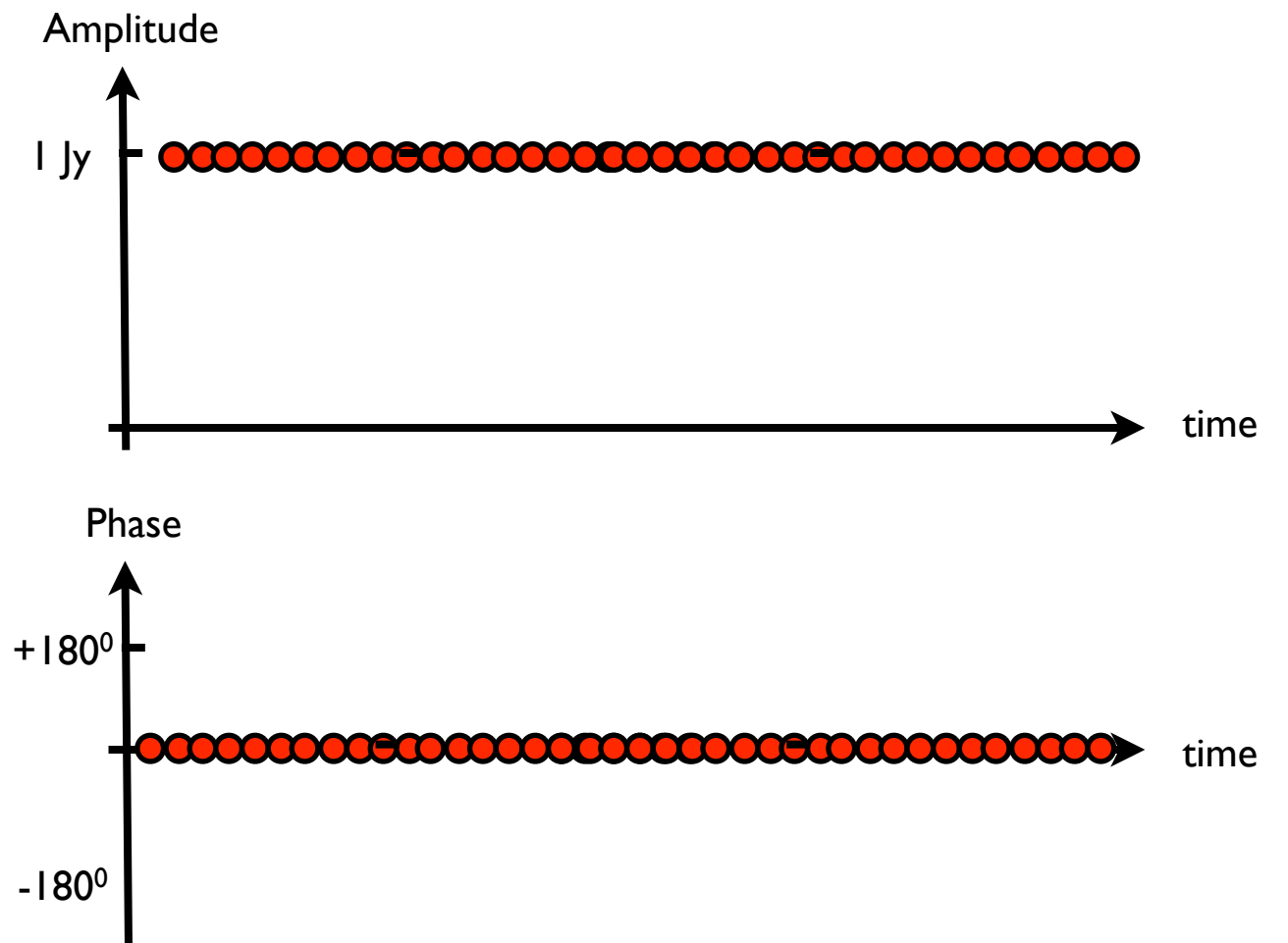


← source model

← Visibility function

Source models & visibility functions (cont)

A single, unresolved 1 Jy point source at the origin produces the following visibilities (data):



Extended or multi-component sources (left) produce more complicated functions e.g. Fomalont & Wright (1974)

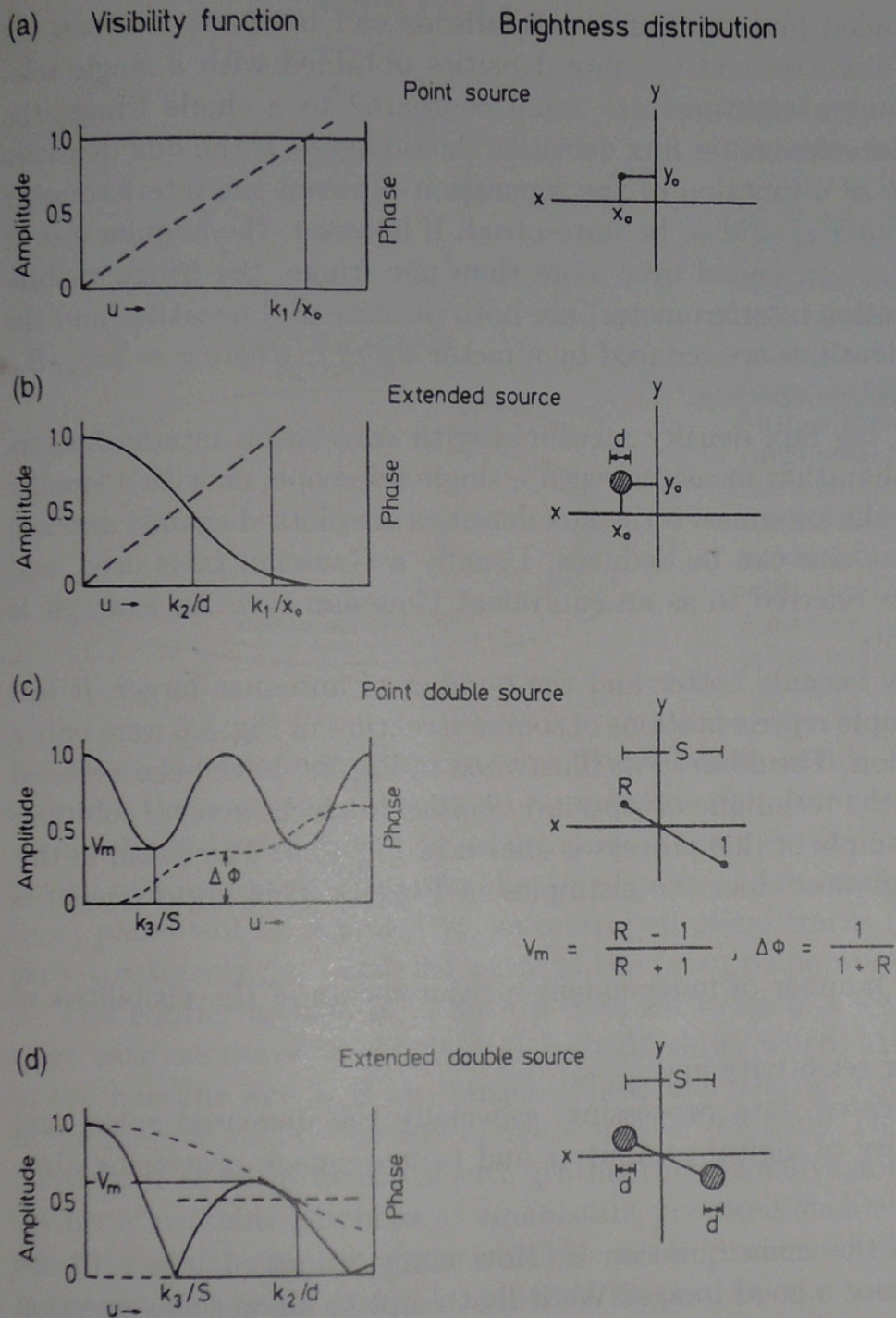
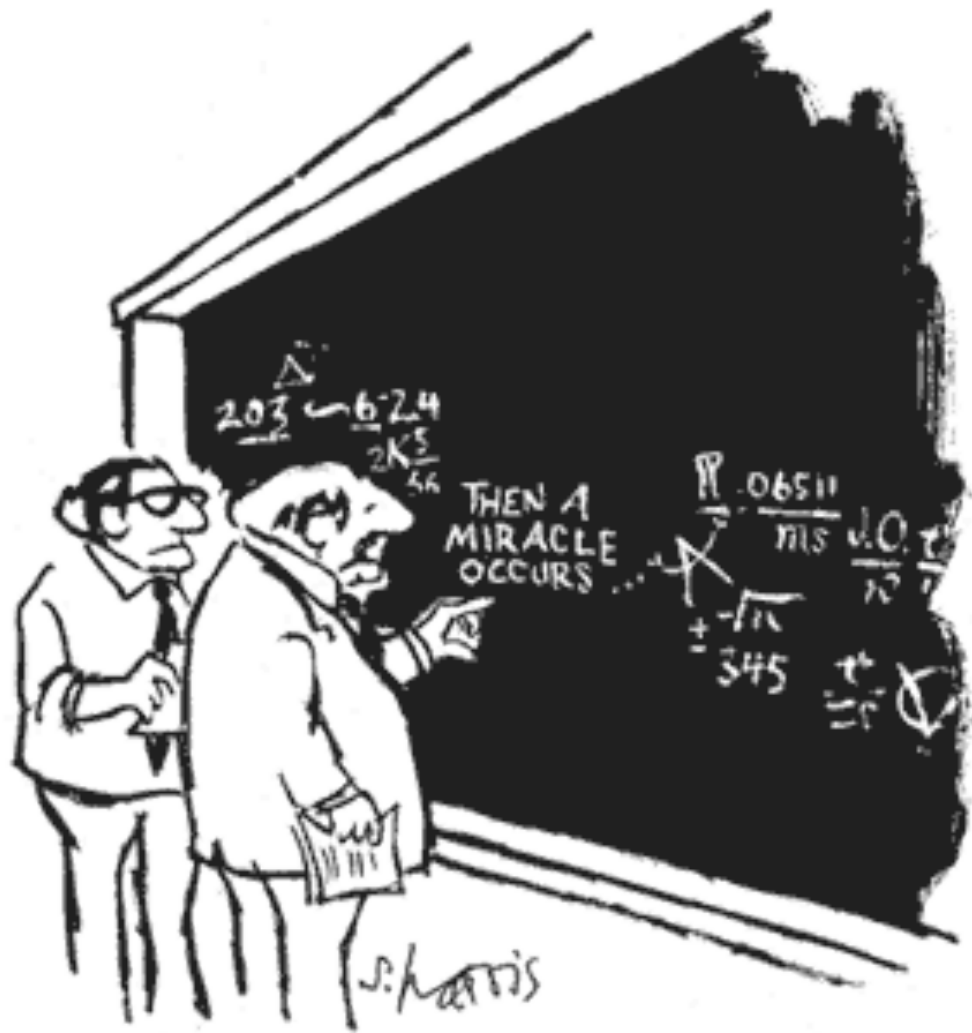


Fig. 8.6. The visibility function for various brightness distribution models. The solid lines are amplitudes, the dashed lines are phases. (a) A point source displaced from the phase center; a displacement of $x_0 = 1''$ shifts phase by one fringe for a $k_1 = 206265$ wavelength baseline. (b) A displaced Gaussian shaped extended source of FWHP $1''$; the amplitude reaches a value of 0.5 at $d = 91000$ wavelengths. (c) Two point sources with an intensity ratio R ; the period of amplitude and phase depends on the separation. If the centroid of the double is the phase center, the sign of phase gives the direction of the more intense components, with positive to the east. (d) Two extended double sources; this has been obtained from the response to a pair of point sources by multiplying the visibility amplitude by the envelope shown in (b). The numerical values are $k_3 = 103000$ if $s = 1''$ and $k_2 = 91000$ if $d = 1''$ [after Fomalont and Wright (1974)]

uv-coverage: the general 2-D array case

For 2-Dimensional radio telescope arrays with interferometer baselines with a significant E-W and N-S baseline component, the uv-tracks are ellipses displaced along the v-axis. The equations describing the u and v as a function of source HA, declination and the geocentric telescope coordinates (X,Y,Z) on earth, require a bit of spherical trigonometry (see TMS Ch4). It is an exercise for the student to show:



"I THINK YOU SHOULD BE MORE EXPLICIT HERE IN STEP TWO."

Exploit earth rotation to sample uv plane

u, v, w coordinates:

X pointing to $ha = 0h, \delta = 0^\circ$
 Y pointing to $ha = -6h, \delta = 0^\circ$
 Z pointing to $\delta = 90^\circ$

L_x, L_y and L_z are coordinate differences of 2 antennae, h is hourangle and δ declination

$$\begin{pmatrix} u \\ v \\ w \end{pmatrix} = \frac{1}{\lambda} \begin{pmatrix} \sin h & \cos h & 0 \\ -\sin \delta \cos h & \sin \delta \sin h & \cos \delta \\ \cos \delta \cos h & -\cos \delta \sin h & \sin \delta \end{pmatrix} \begin{pmatrix} L_x \\ L_y \\ L_z \end{pmatrix}$$

\Rightarrow

$$u^2 + \left(\frac{v - (L_z / \lambda) \cos \delta}{\sin \delta} \right)^2 = \frac{L_x^2 + L_y^2}{\lambda^2}$$

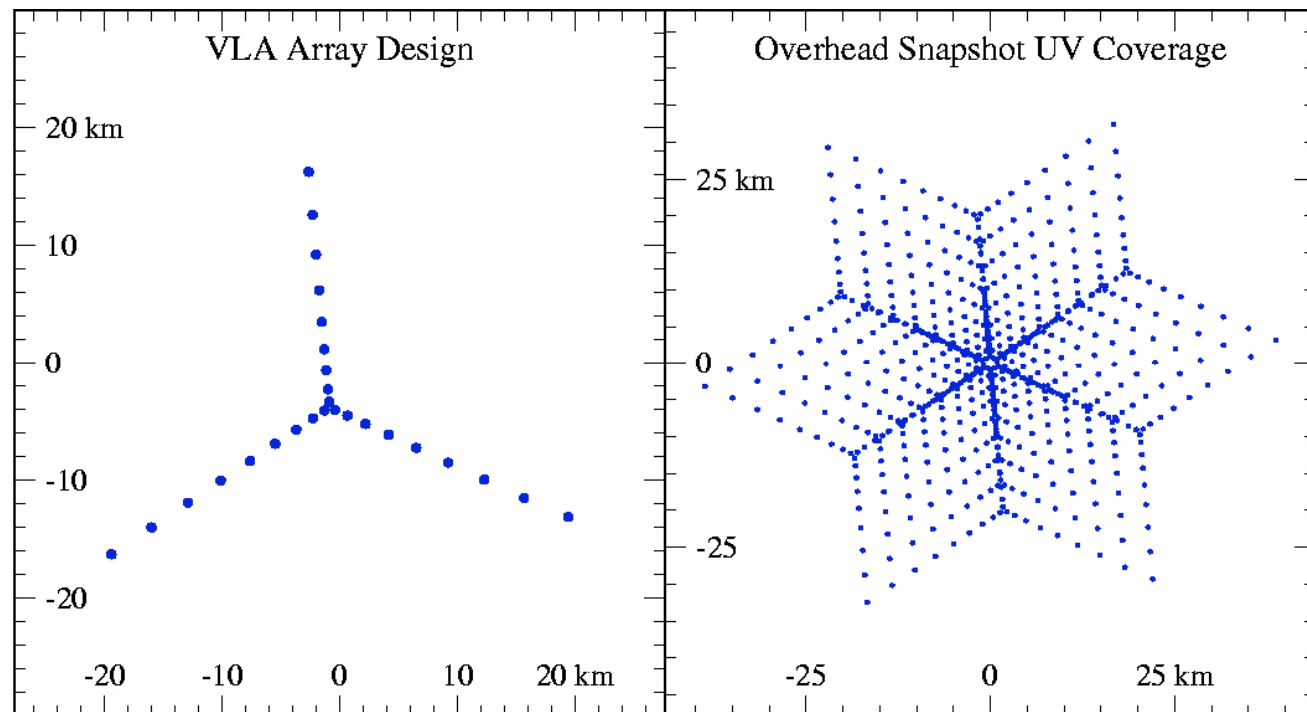
\rightarrow as earth rotates, baselines describes an ellipse.

For EW baselines: $L_z = L_x = 0$, i.e. concentric, coplanar ellipses

Various interferometer arrays and their uv-coverage

The VLA: 27 telescopes located in New Mexico. Reconfigurable from A-array (max baseline 36 km; min baseline 0.68km) to D-Array (max baseline 1km, min baseline 35m!). Configuration changes take place every 4 months or so.

The antennas are arrayed along the three arms of a Y-shape (max arm length 21 km).



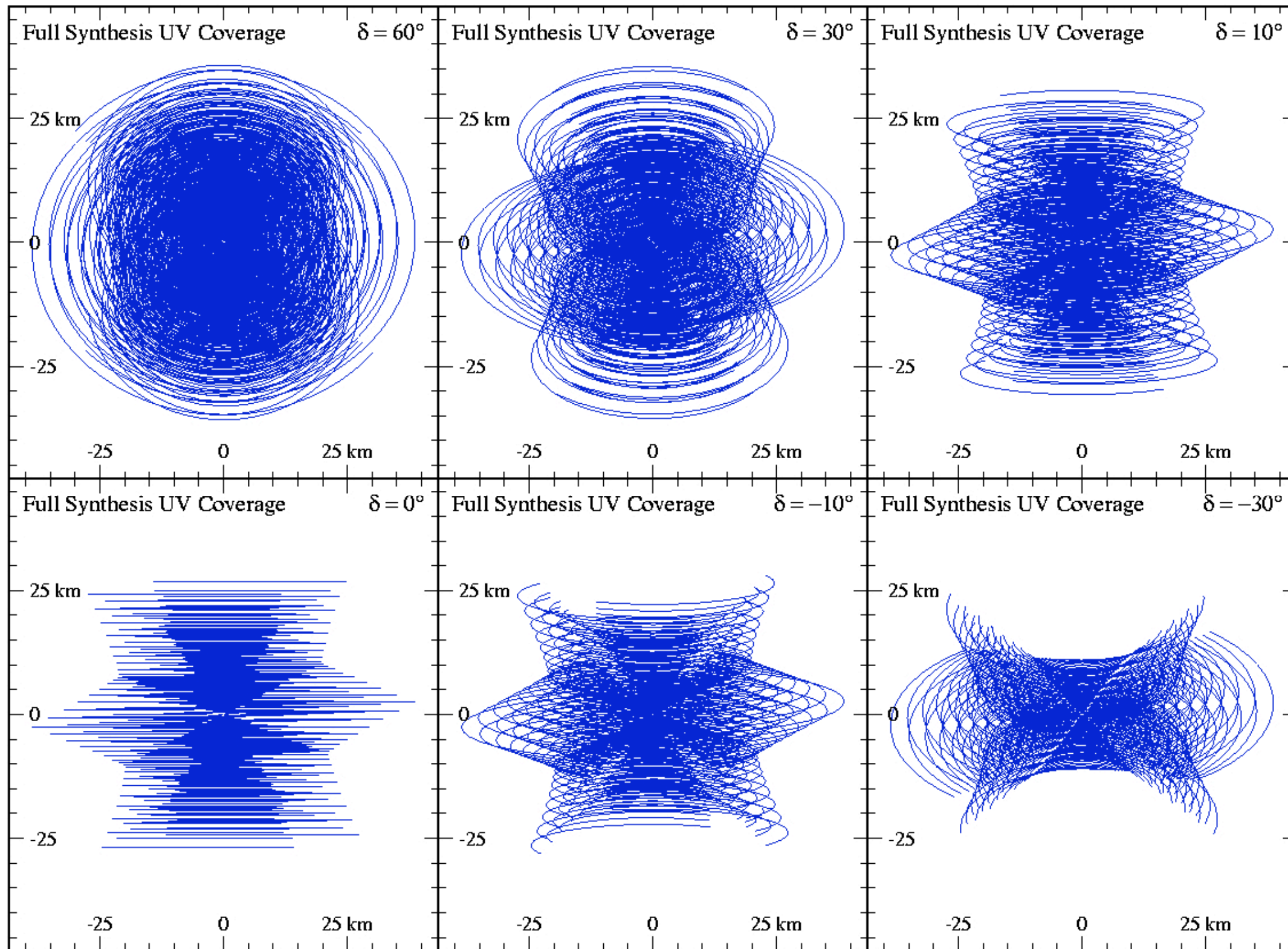
Above: u - v coverage of A-array



Photo of the VLA in compact D-array

The longer we observe the better the uv-coverage gets. "Snapshot" observations refer to short observations lasting a few minutes.

Full synthesis (sometimes referred to as “full track”) VLA observations of sources at different declinations (c.f. WSRT previous slides):



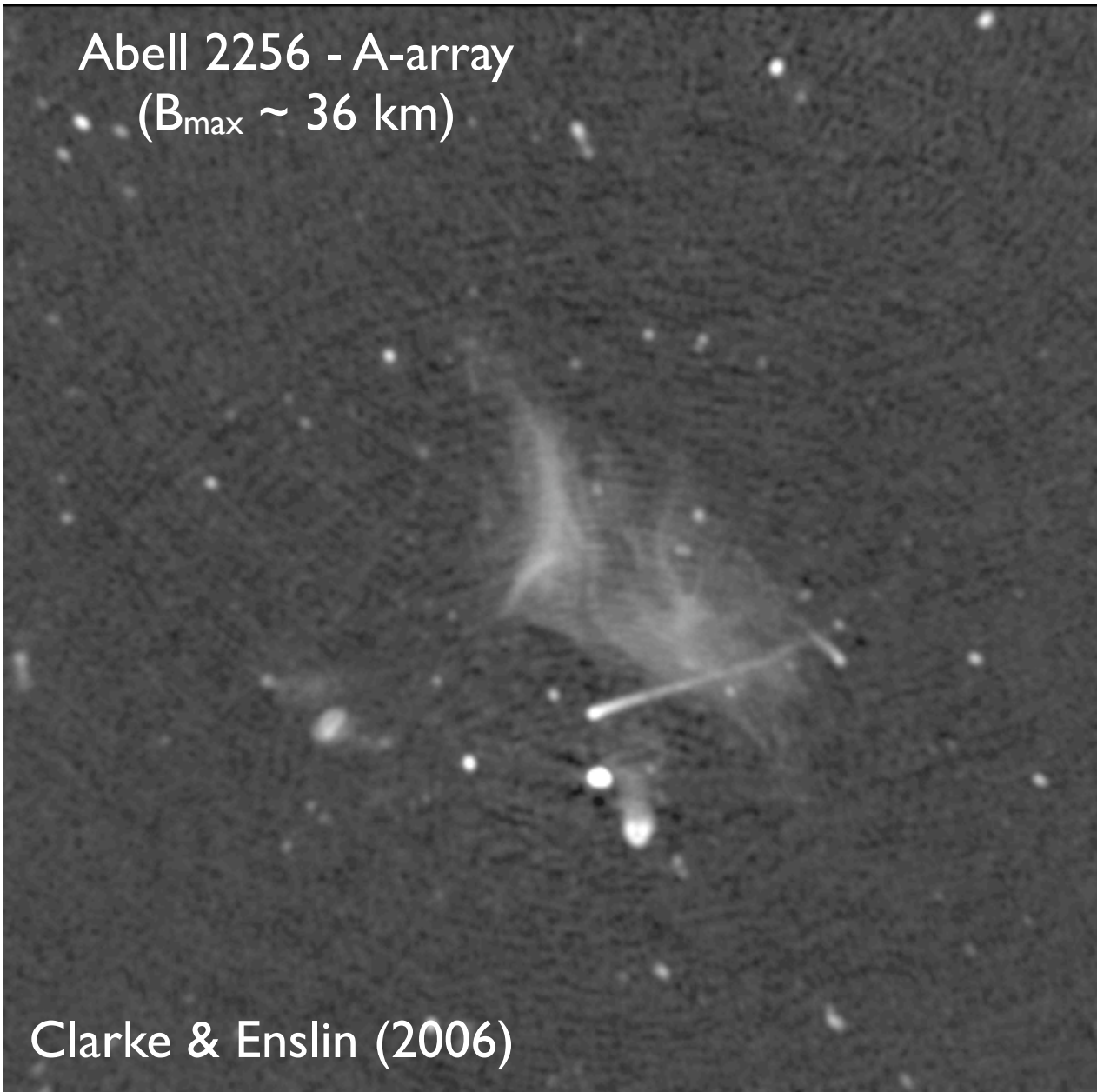
Tracks: elevation > 10 degrees

Different VLA array configurations produce different images of the source.

Long baselines detect the most compact, unresolved structures (e.g. A-array).

Short baselines detect extended, low-surface brightness, large-scale structure (e.g. D-array)

Abell 2256 - A-array
($B_{\max} \sim 36$ km)



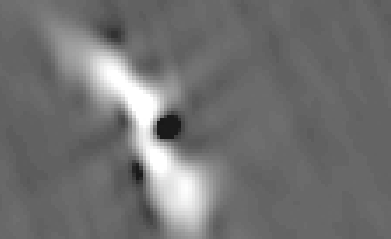
Abell 2256 - D-array
($B_{\max} \sim 1$ km)



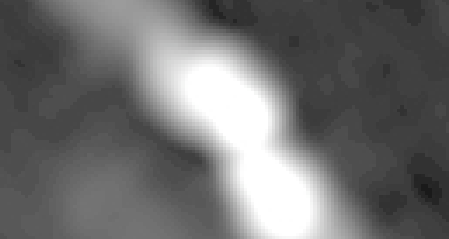
Note that some of the extended sources detected in D-array are not present in the A-array image. However, the A-array provides more detail on some of the features - not seen in D-array.

For many complex sources, all VLA configurations (i.e. as many baseline lengths as available) are required in order to get a good “picture” or to properly understand the source:

Hydra-A in A-array



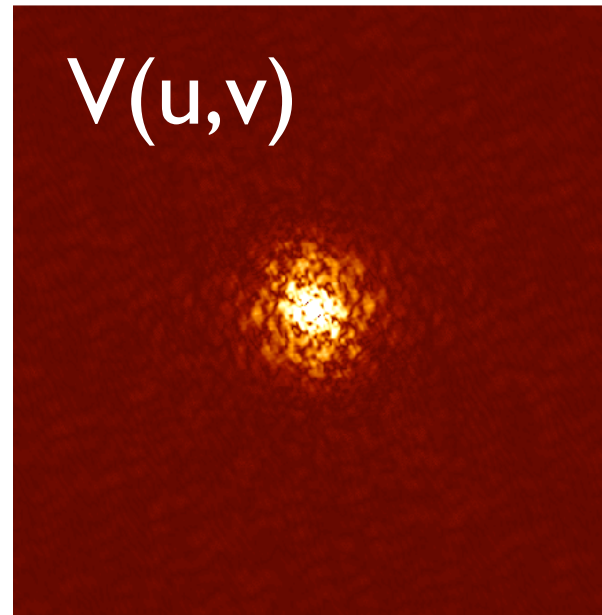
Hydra-A - A+B+C+D-array



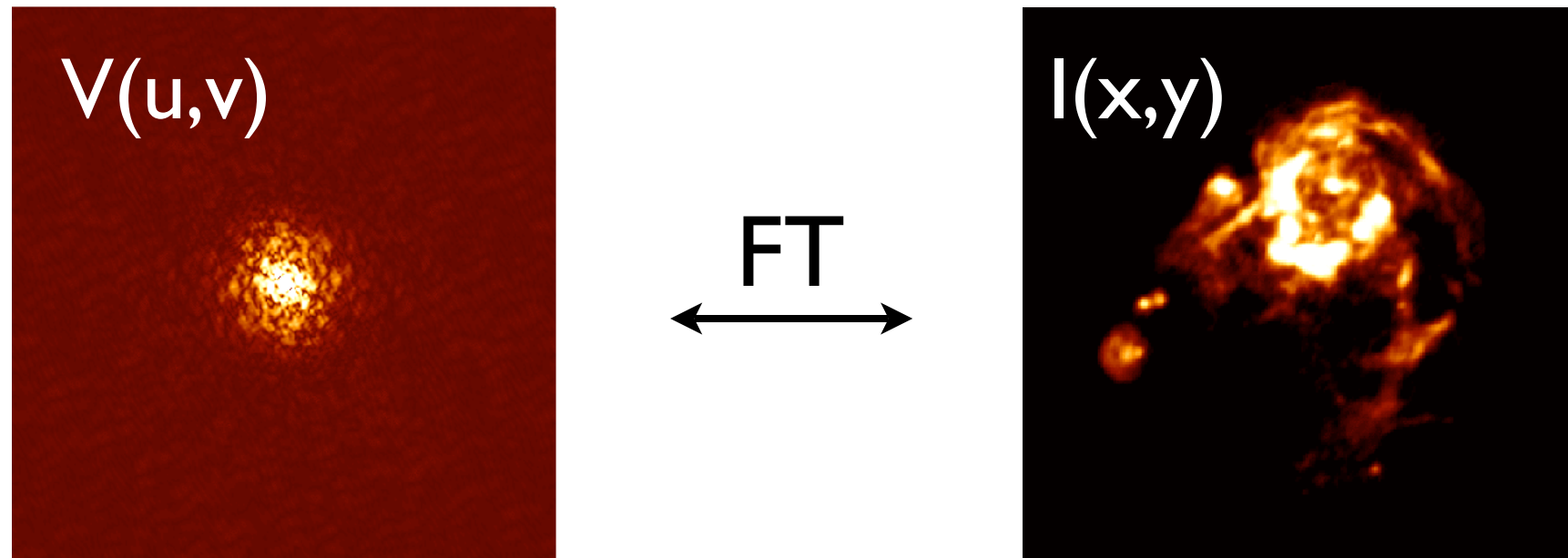
Images: W.M. Lane

Since the configurations of the VLA are separated by many months (even years), care must be taken in combining data from different configurations - potential problems include source variability and a stable calibration from one configuration to another.

In the *ideal* case we measure the visibilities, $V(u,v)$ over the entire uv -plane:

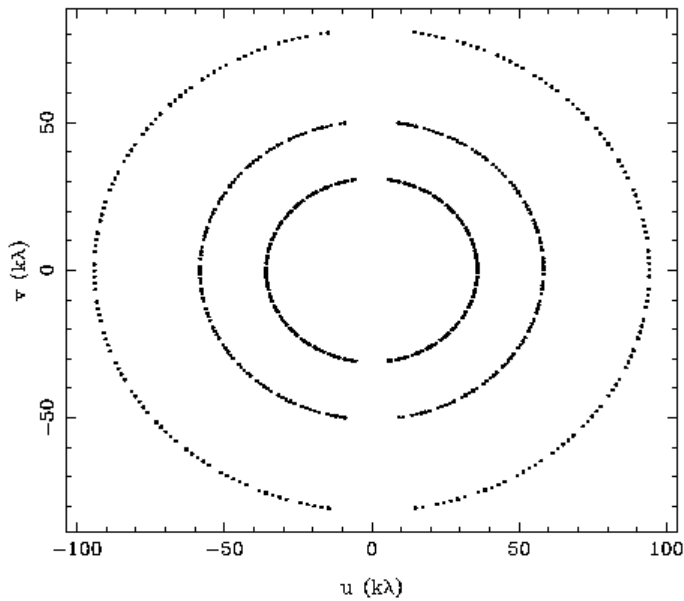


And the FT of the visibilities produces an image of the source:

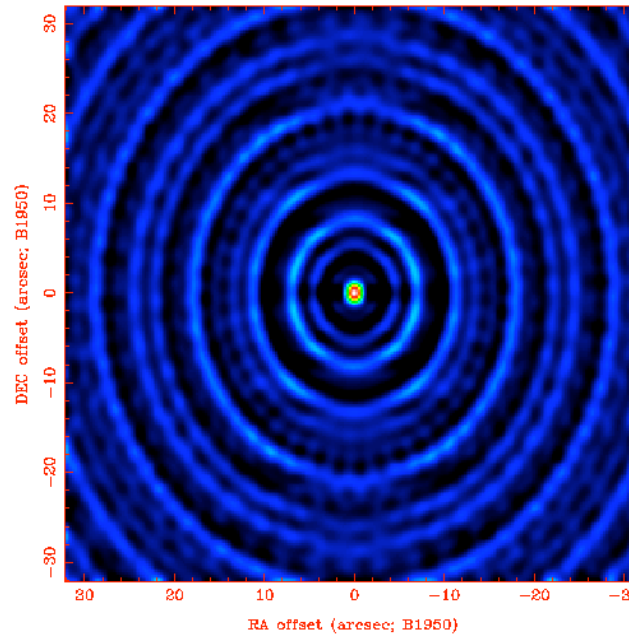


Real life is different - sampling of the uv -plane is often incomplete - we can use image reconstruction algorithms to help produce images of the source.

CLEAN algorithm



FT

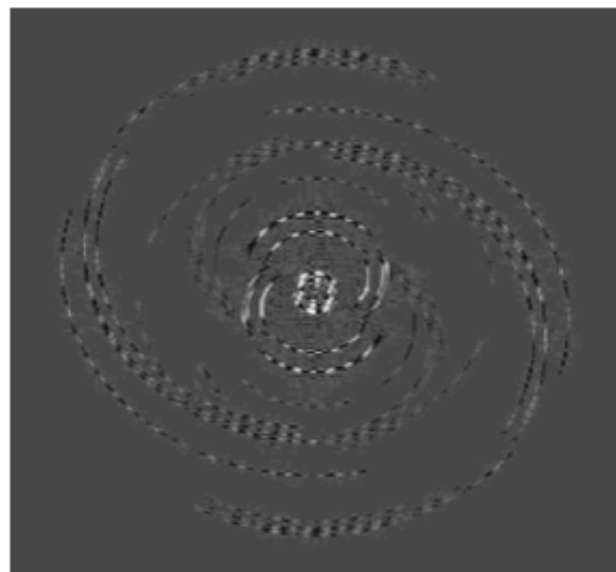


FT of the sampling function produces the Point Spread Function (PSF) usually referred to as the DIRTY BEAM in radio astronomy. Note (above) the high side-lobes that extend far from the central response.

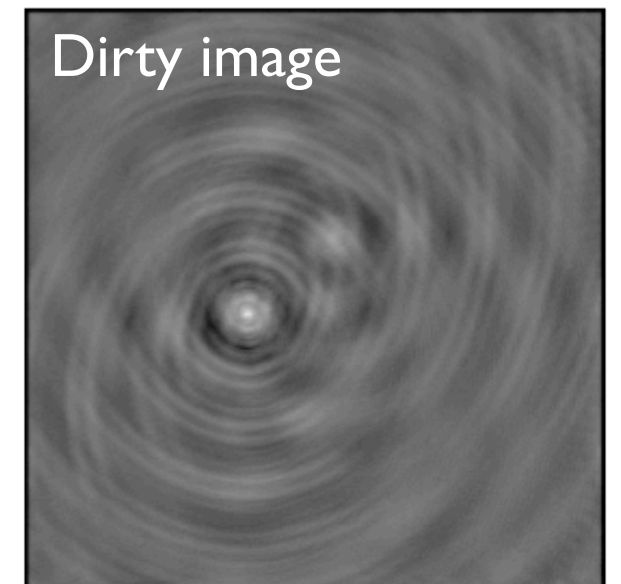
Above: sampling of the Visibility function in uv-plane is incomplete

In radio astronomy we know the PSF very well - its just the FT of the sampling function in the uv-plane. The sampling function has a value of “1” where we have measured data and “0” everywhere else.

We also have the concept of the “dirty image” (sometime also “dirty map”) - this is the fourier inversion of the Visibility function:



F.T.



We can write that the dirty image is the convolution of the true image with the dirty beam (sampling function):

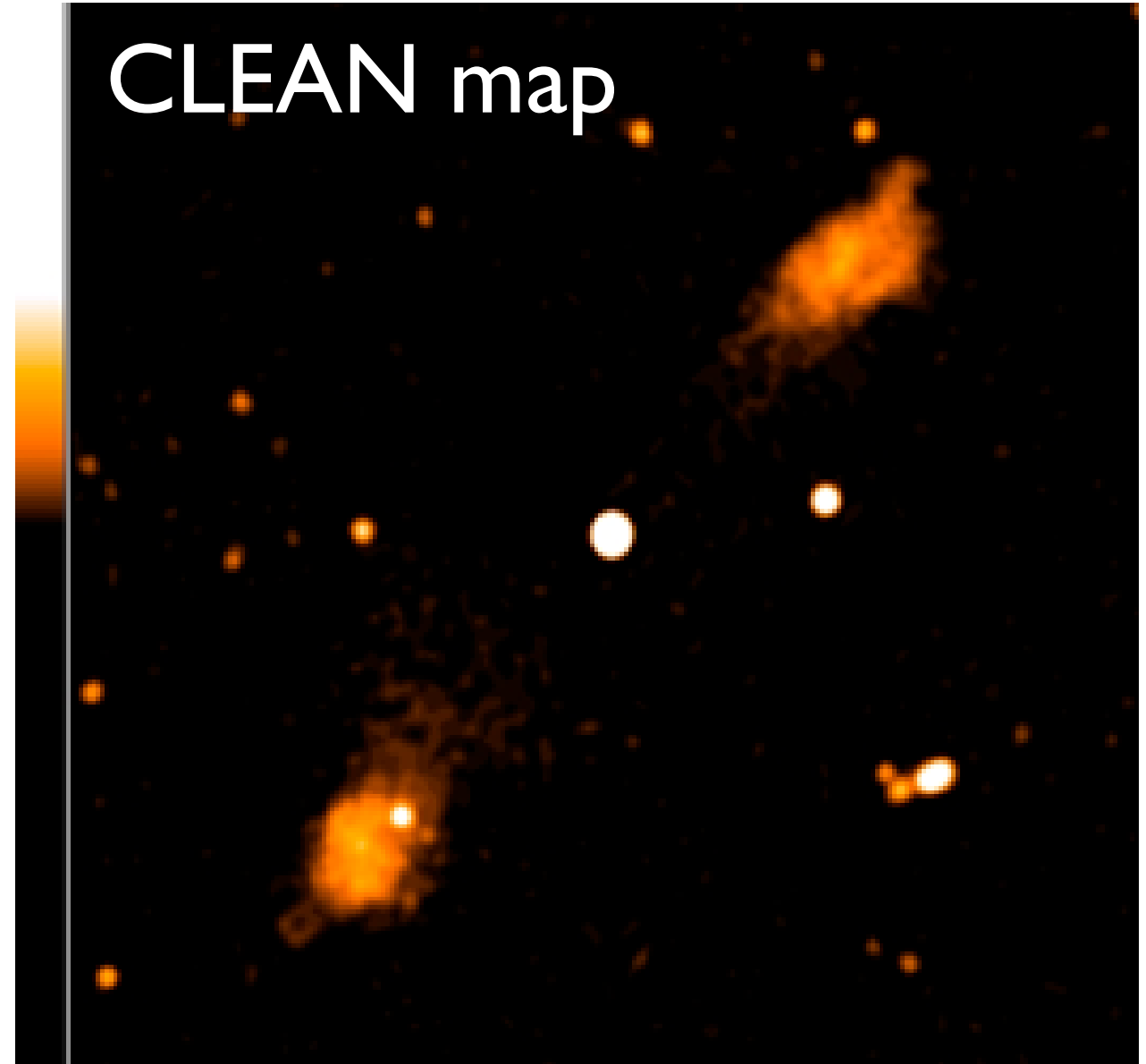
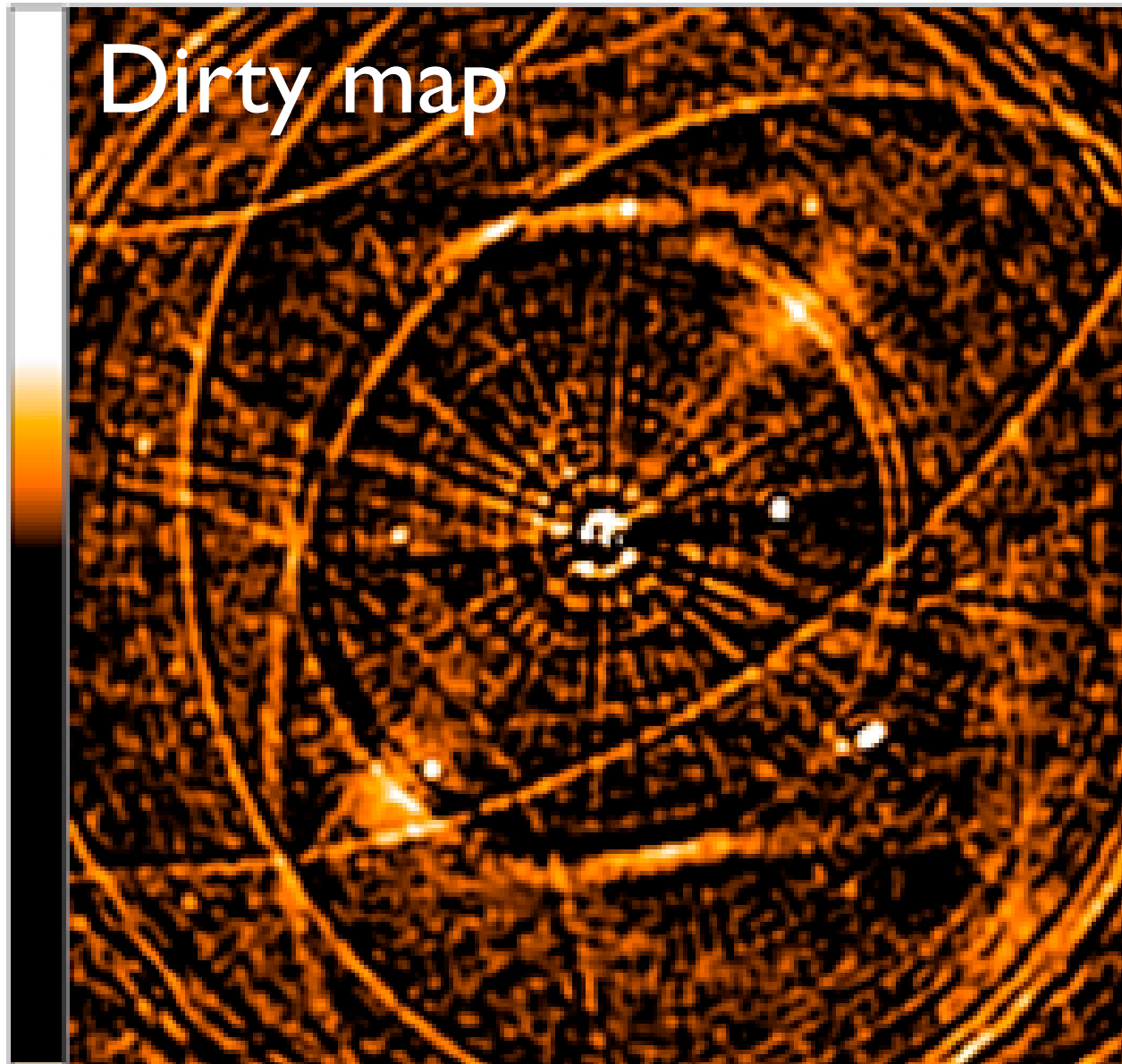
$$I^D(x,y) = I * B \quad \text{where } B \text{ is the dirty beam}$$

The CLEAN algorithm attempts to deconvolve the dirty beam from the dirty map.

In its simplest guise (Hogbom CLEAN) it works as follows:

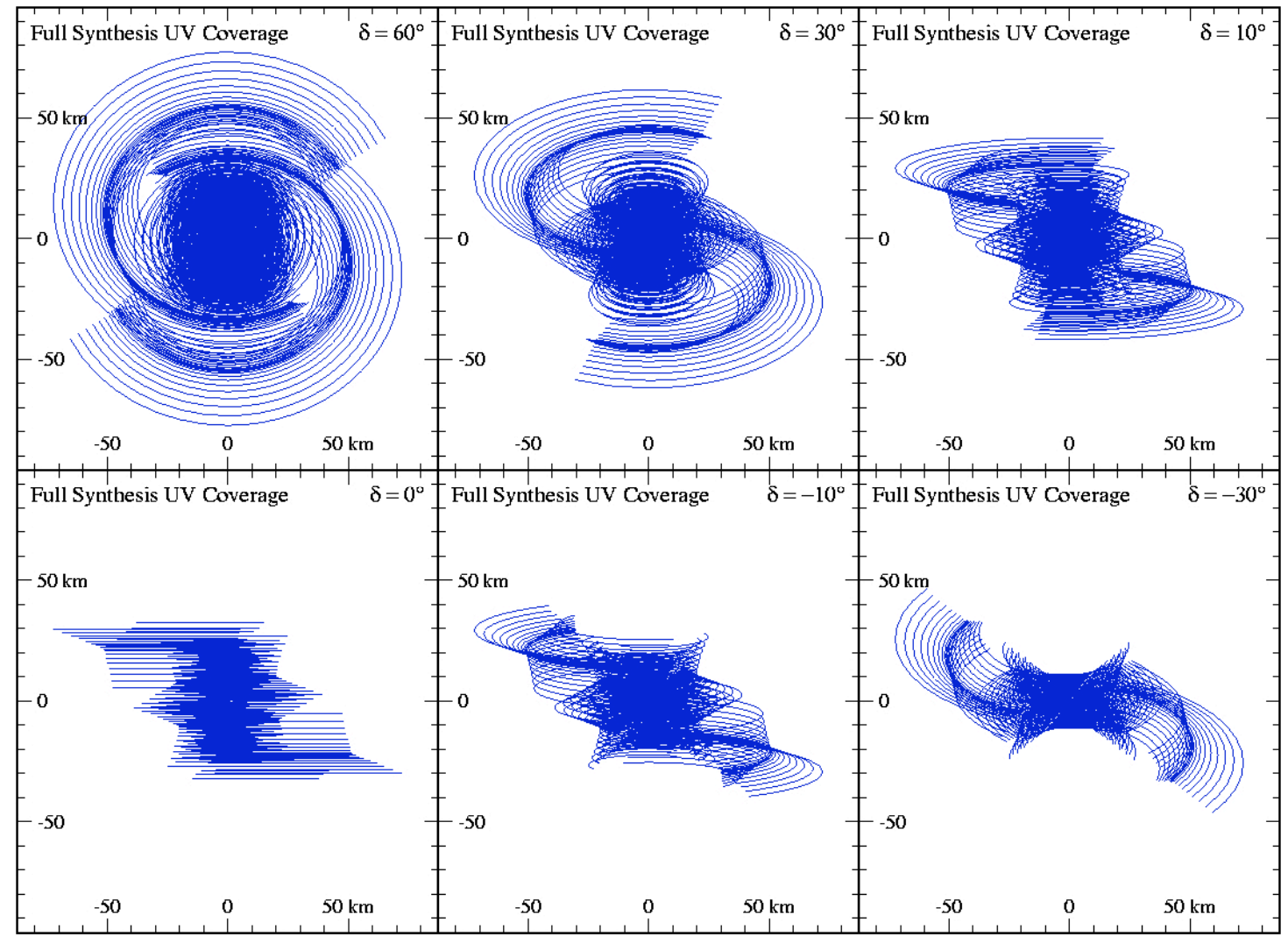
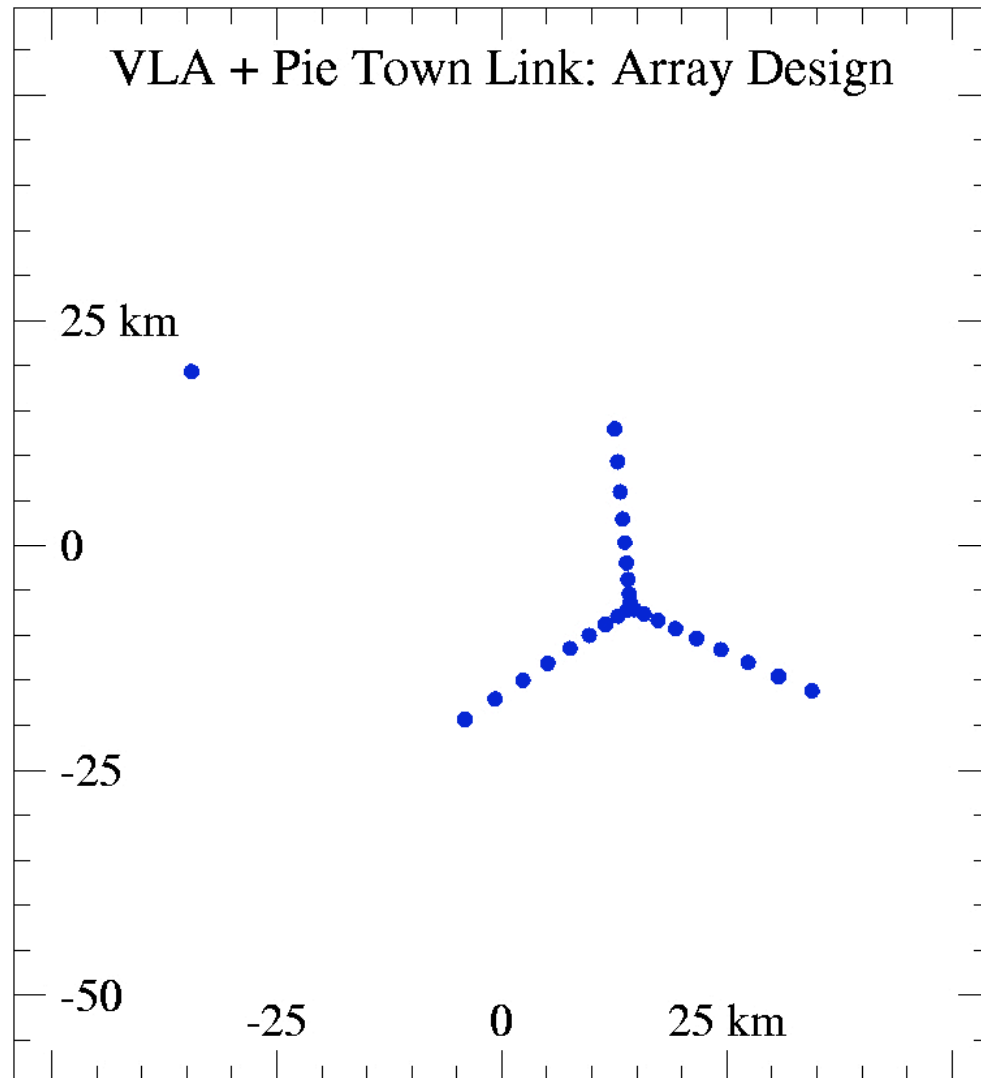
- (i) Assume the sky is +ve and that sources can be represented by a collection of point source delta functions.
- (ii) make the dirty map, and find the position and intensity of strongest source in map
- (iii) subtract some scaled fraction (e.g. 10%) of the dirty beam response at this position from the dirty map and store the position and intensity as a “CLEAN component” of the dirty map.
- (iv) find strongest source in the new dirty map, add this to the CLEAN component file and repeat the same process many times (e.g. 1000 iterations) until only noise is left in dirty map.
- (v) The final clean map is produced by taking all the CLEAN components, adding back the residual noise left in the dirty image (see iv), and then convolve this image with a Gaussian that was fitted to the central lobe of the dirty beam.

Below: VWSRT dirty map and CLEAN map. Note that the side-lobes seen in the Dirty map (which are artefacts associated with incomplete u-v plane coverage) are much reduced in the CLEAN map



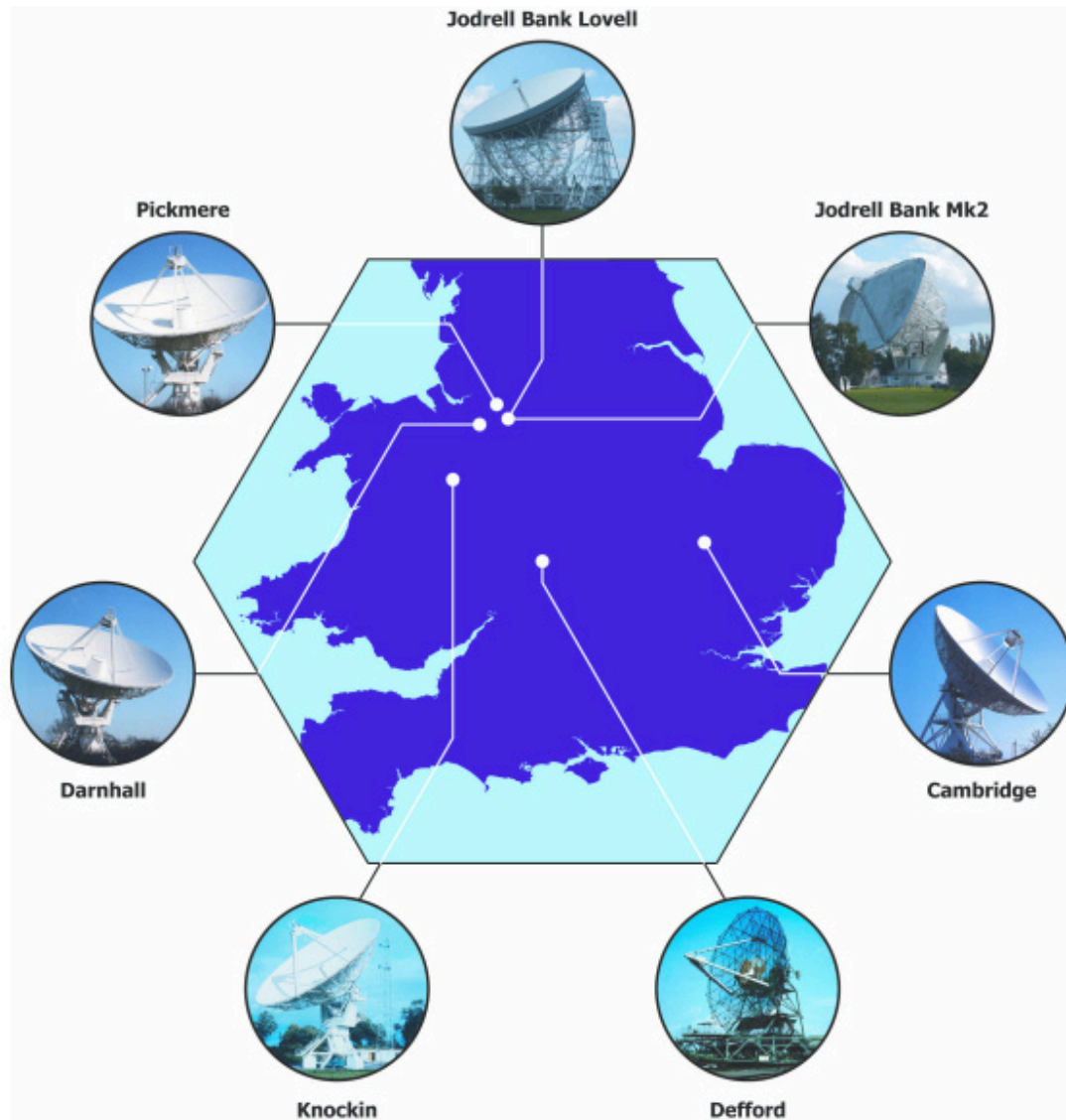
We will consider CLEAN in more detail later in this course - I introduce it now because you will play with it in the practical session.

The VLA can also observe with one of the VLBA antennas - “Pie Town”. This telescope increases the baseline length to 73km - improving the resolution of the array but also adding a large whole in the uv-coverage:

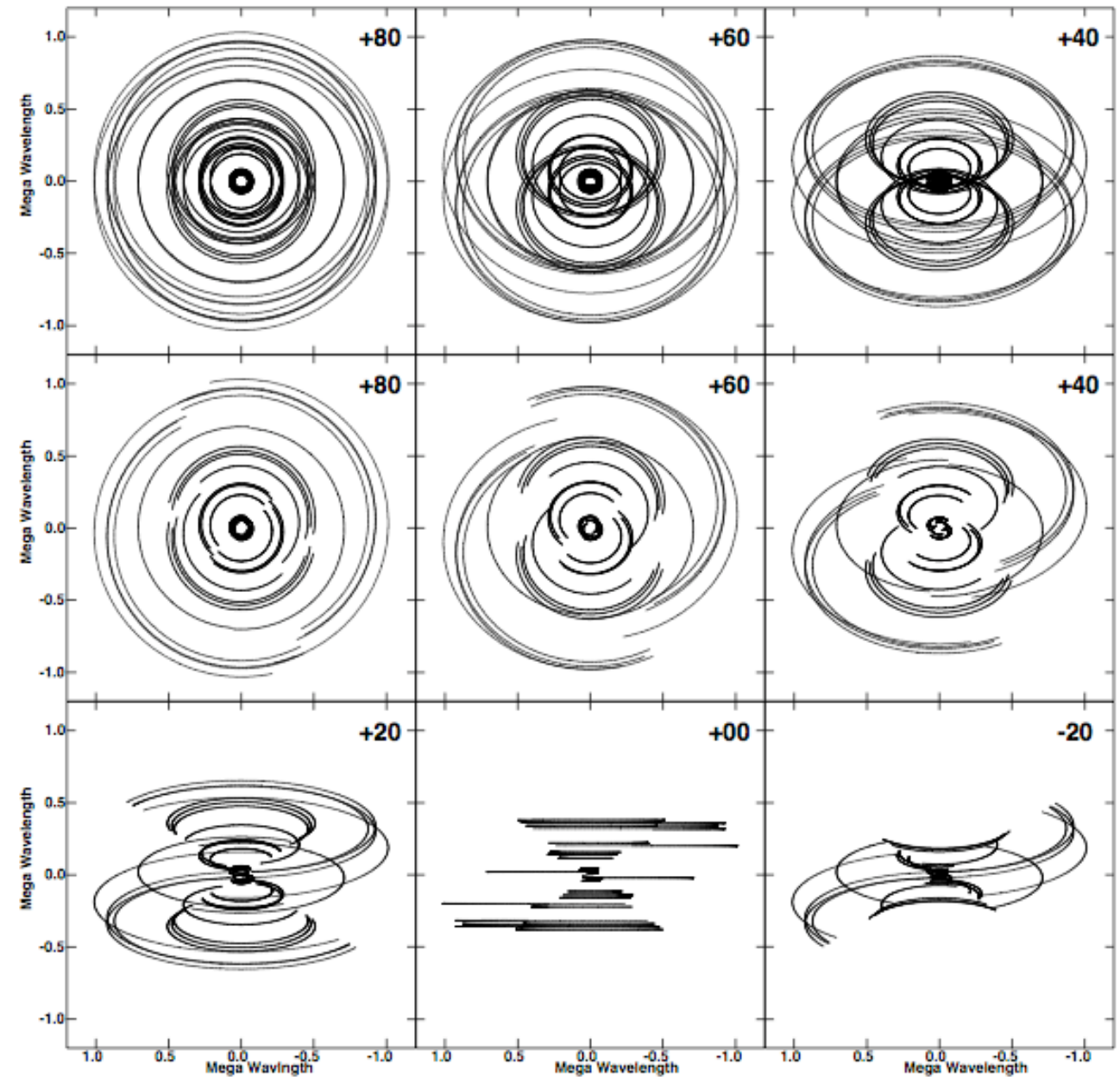


This extended array can still produce good images - especially for “full track” observations and for sources located at high declination.

The UK MERLIN array (6 telescopes spread across England) shows that even sparse arrays can produce good images from relatively poor uv-coverage:



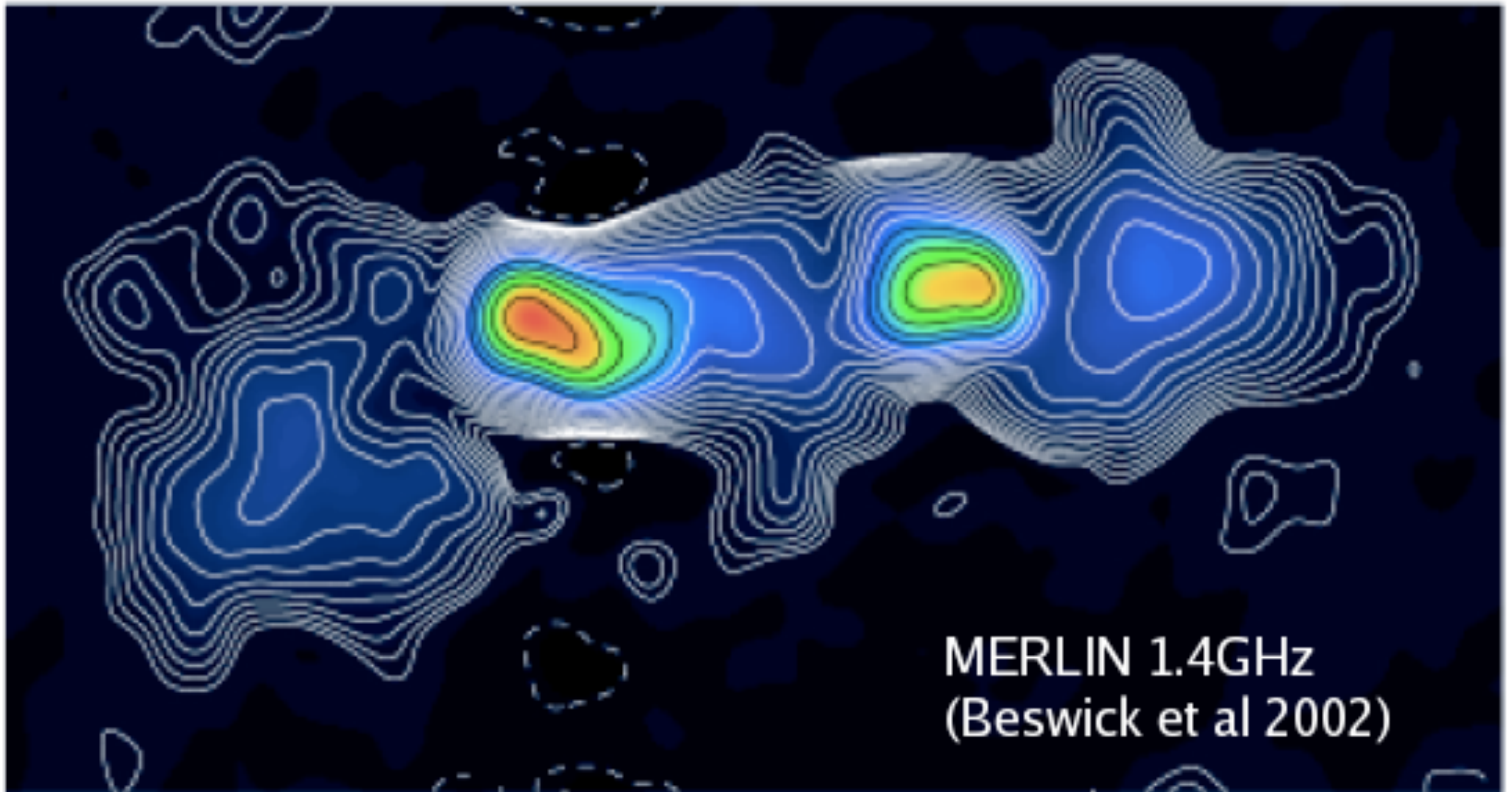
D.2 The UV coverage of MERLIN



MERLIN operated by the U of Manchester & STFC

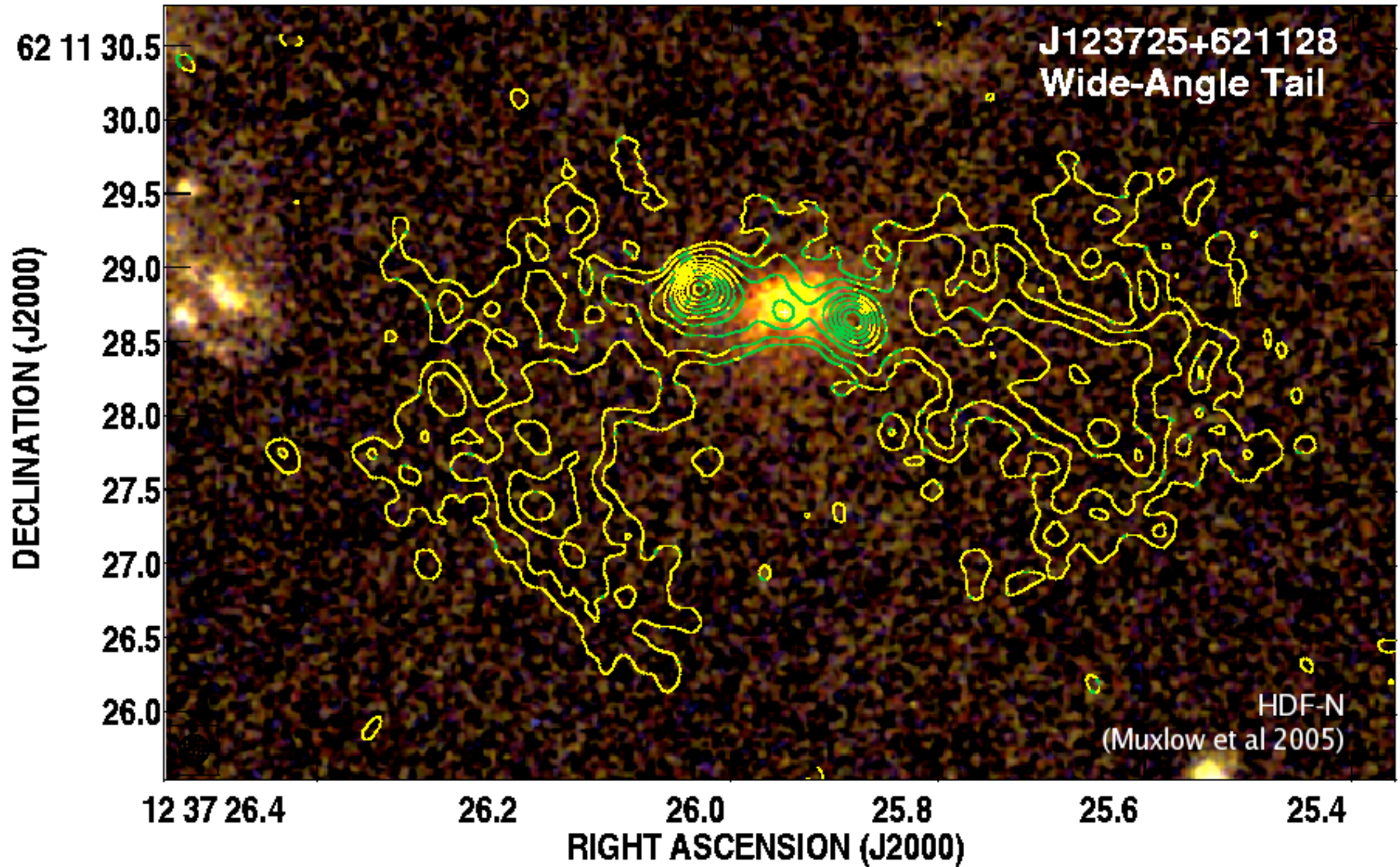
Figure D.4: (i) The uv coverage of MERLIN with 6 antennas.
Top row: Full Tracks (~ 24 hr) for circumpolar sources.
Middle row: 12 hour tracks for circumpolar sources.
Bottom row: Full tracks (≤ 12 hr) for low- δ sources.
 The uv axes are labelled in units of $10^6 \lambda$ for observations at 1.4 GHz; for observations at frequency ν GHz scale the units by $\nu/1.4$.

A MERLIN image of a nearby radio galaxy 3C293.



Not only can data from different configurations of the VLA be combined, but data can be combined from many different radio interferometers....

A very deep MERLIN+VLA image of a radio galaxy in the Hubble Deep Field North (HDF-N):



VLA and MERLIN data are often combined when sources present scales on MERLIN (subarcsecond) and VLA (arcsecond) scales at 1.4 GHz.

Very Long Baseline Interferometry (VLBI) is also a sparse array with many wholes in the uv-coverage. There are several VLBI arrays around the world:



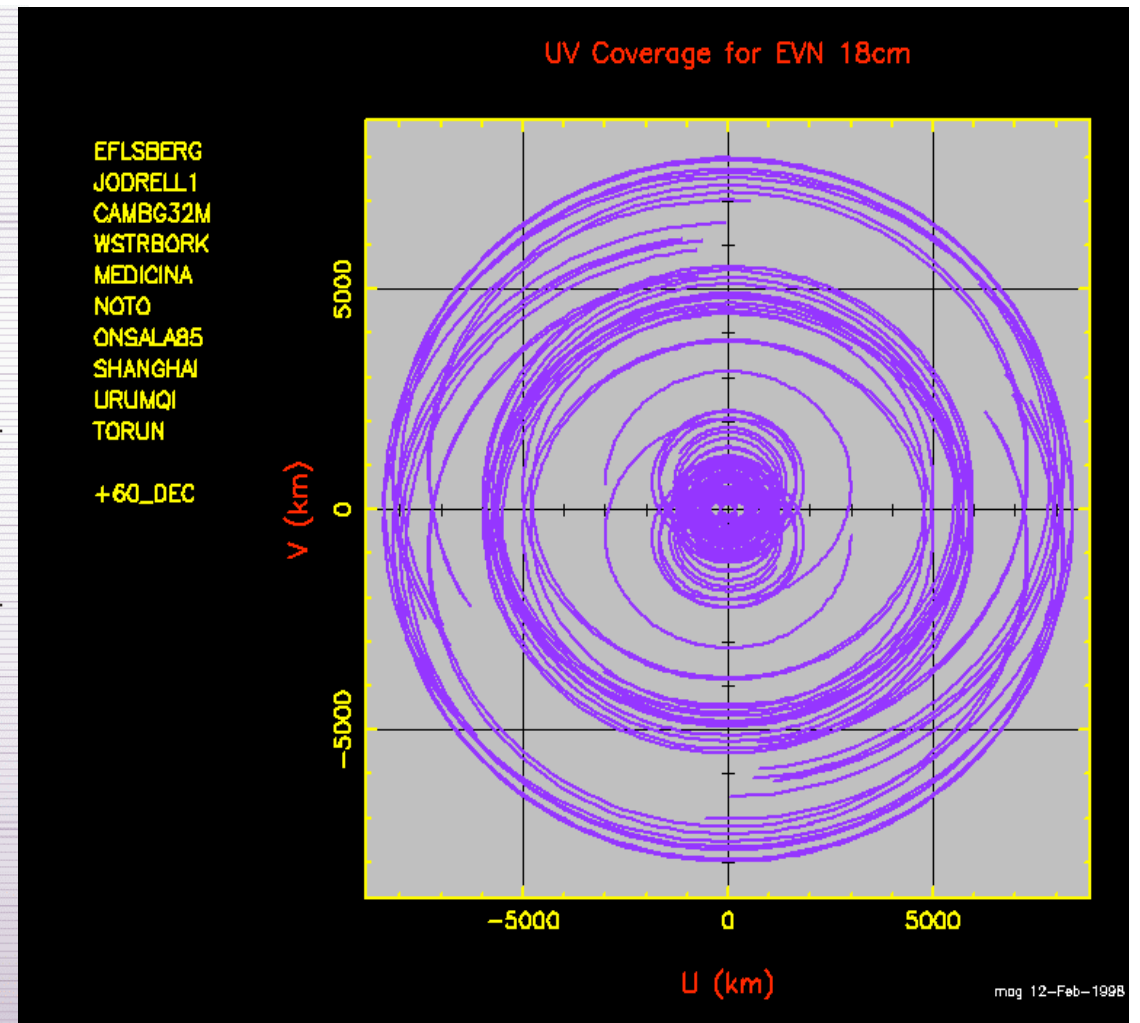
VLBA - Very Long Baseline Array: 10 VLA style antennas spread around the continental USA.

Max. Baseline 8000 km.

Antennas are *not* connected to a central correlator in real-time - telescopes are widely separated - real-time connection currently impractical.

Operates at cm and mm wavelengths (90 cm to 3 mm)

Milliarcsecond resolution achieved at cm wavelengths.



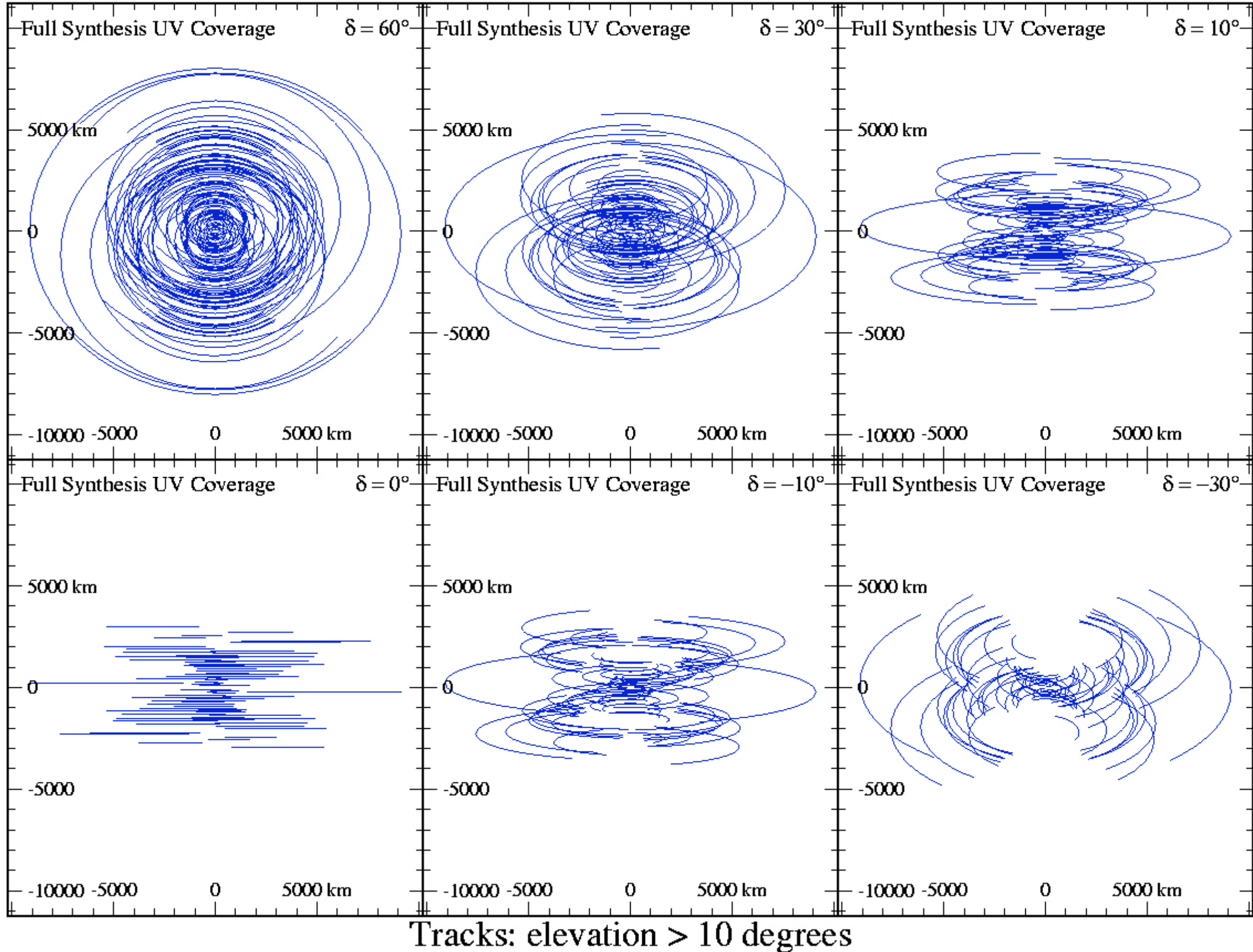
EVN - European VLBI Network.

~16 of the largest antennas in Europe, Asia and S.Africa. Part-time array (3 x 1 month per year). The EVN correlator is operated by JIVE (Joint Institute for VLBI in Europe), located in Dwingeloo, NL.

Max. Baseline 9000 km, shortest baseline 200km. Operates at cm and mm wavelengths (90cm to 7mm). Milliarcsecond resolution achieved at cm wavelengths.

Has a real-time capability (e-VLBI) in which the data are correlated in real-time by connecting the telescopes via optical fibre.

VLBI arrays, like the VLBA (see below) and EVN, naturally have large holes in their uv-coverage. Using advanced image processing algorithms, good images can still be made of compact objects.

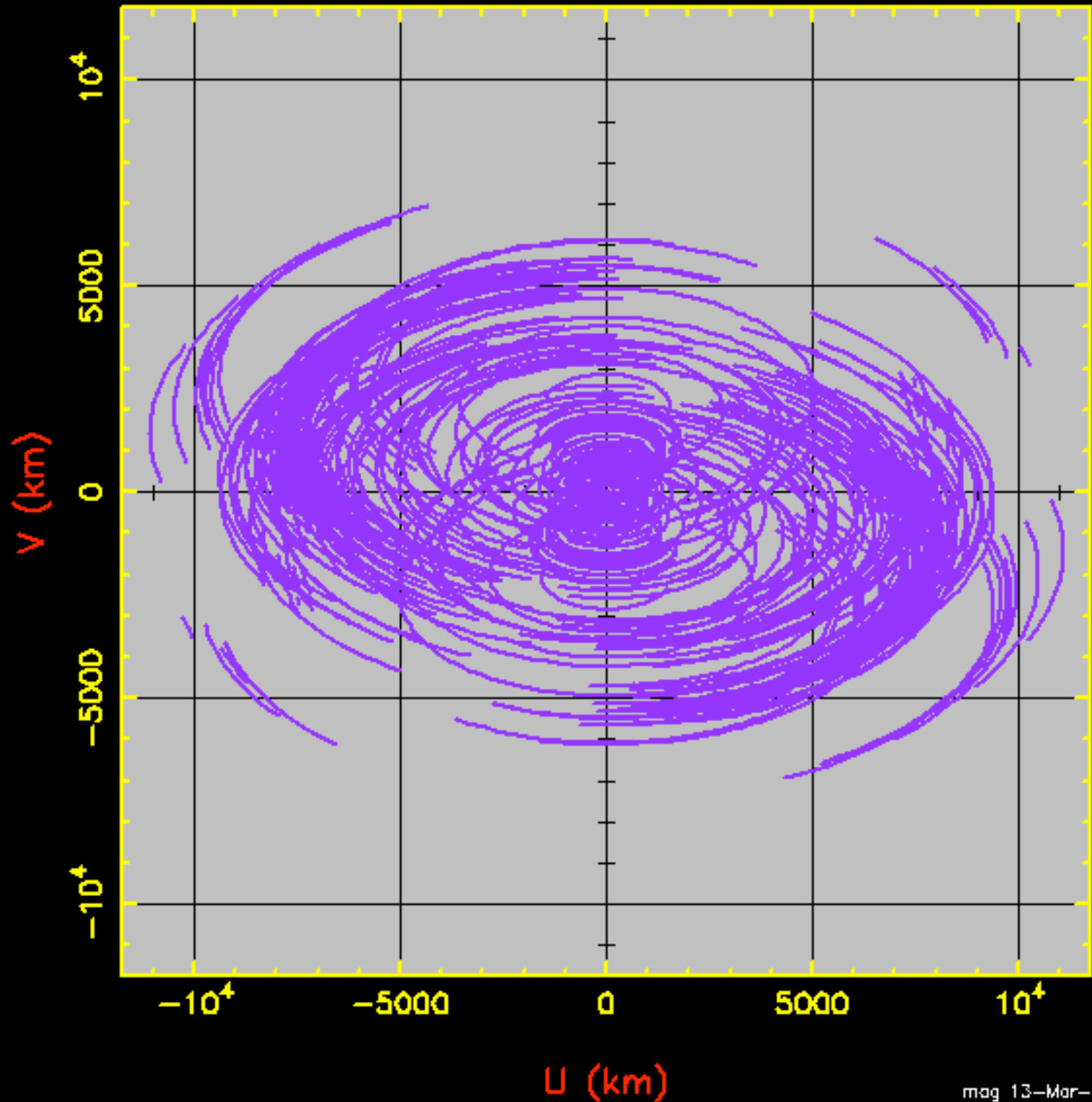


The EVN and VLBA often join together to form a Global VLBI Network:

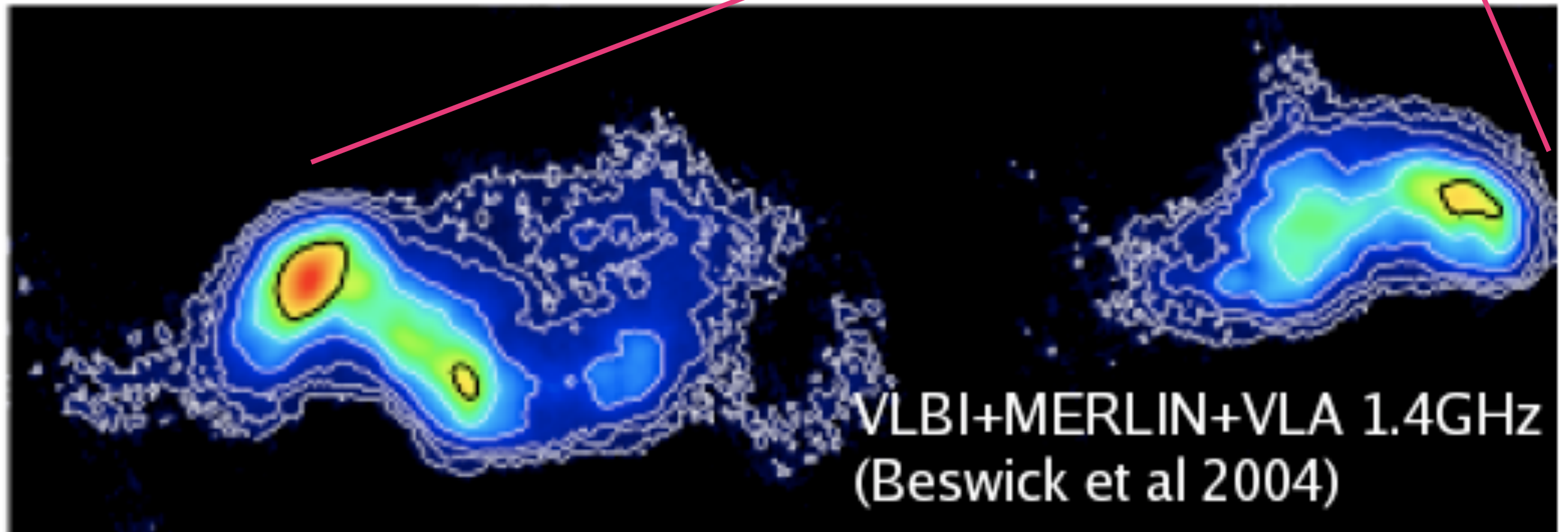
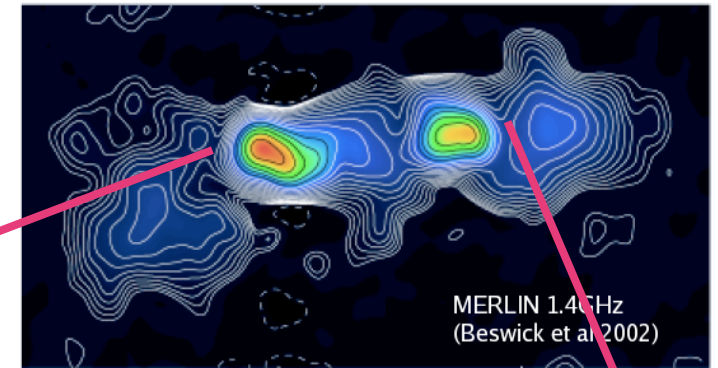
UV Coverage for EVN+VLBA

EFLSBERG
JODRELL1
CAMBG32M
WSTRBORK
MEDICINA
NOTO
ONSALA85
TORUN
VLBA_HN
VLBA_SC
VLBA_NL
VLBA_BR
VLBA_MK
VLBA_LA
VLBA_FD
VLBA_PT
VLBA_OV
VLBA_KP

+30_DEC



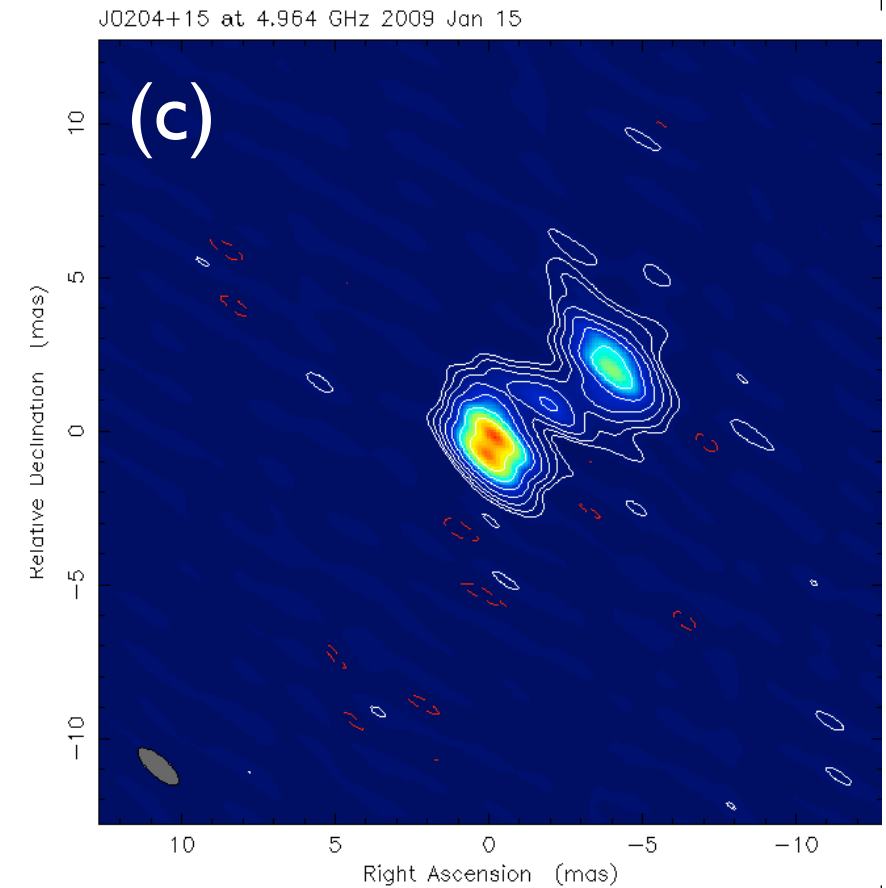
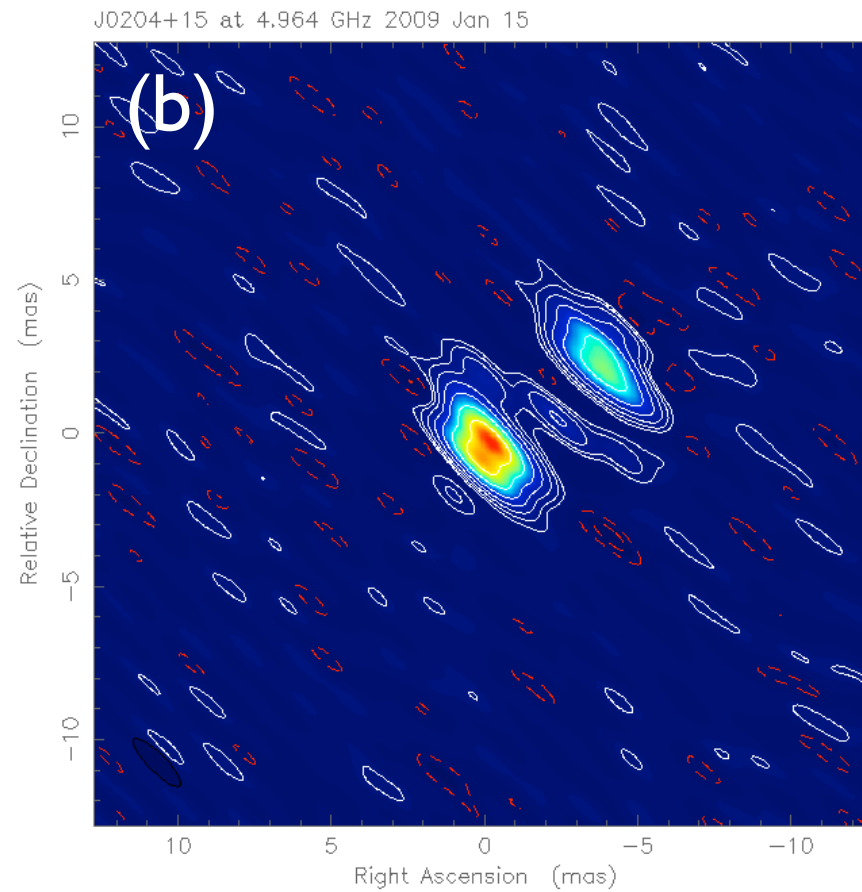
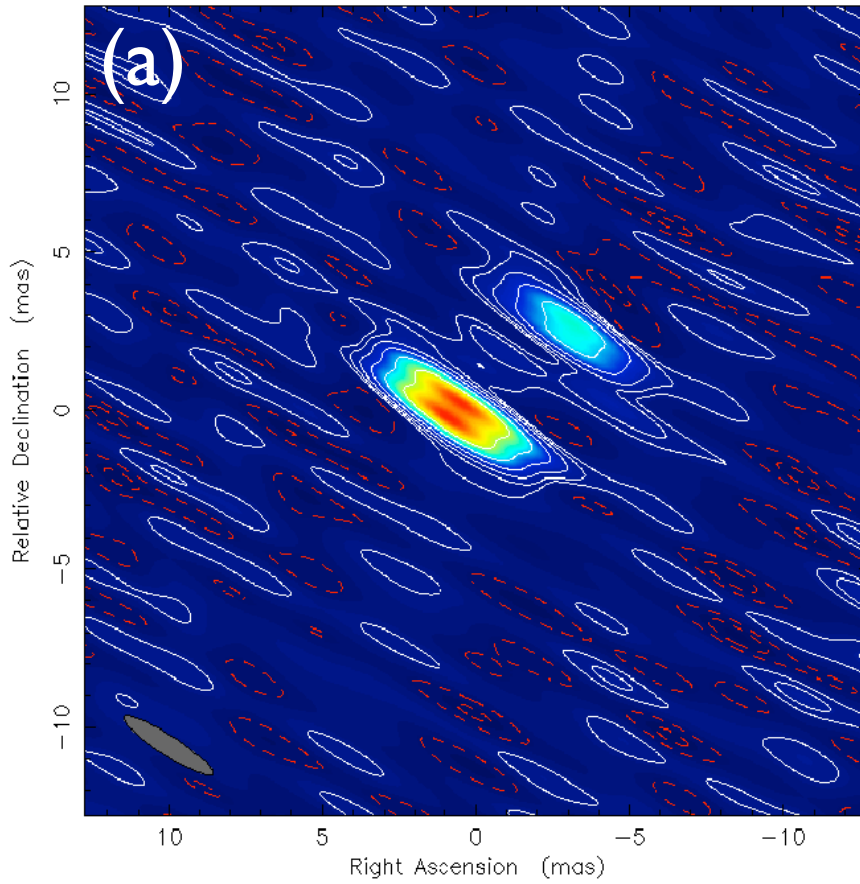
A higher resolution VLBI+MERLIN+VLA image of a nearby radio galaxy 3C293 (see previous slides):



N.B. the nature and resolution of the image changes, depending on how the data from each array are statistically weighted. We will return to the topic of data weighting in subsequent lectures.

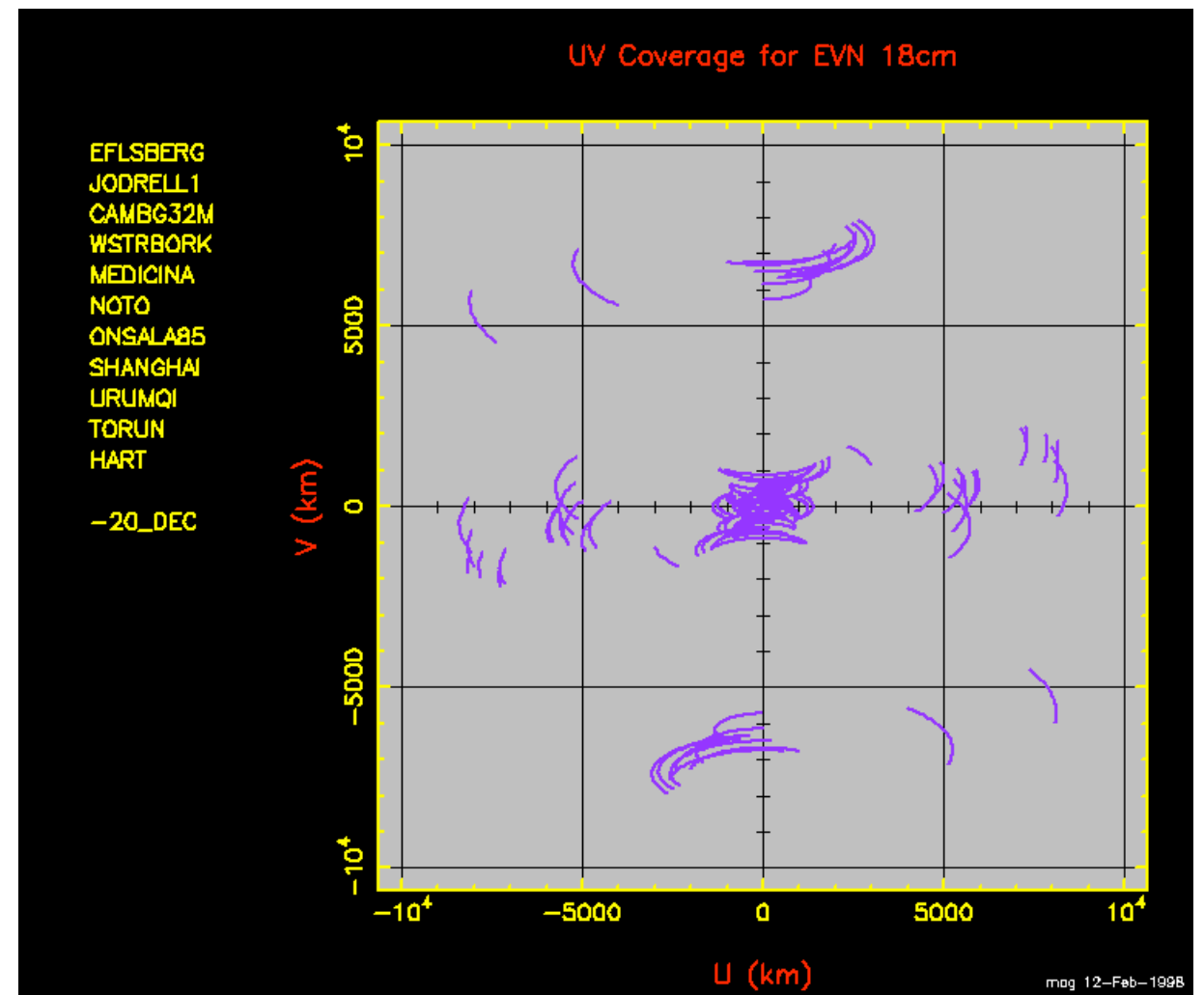
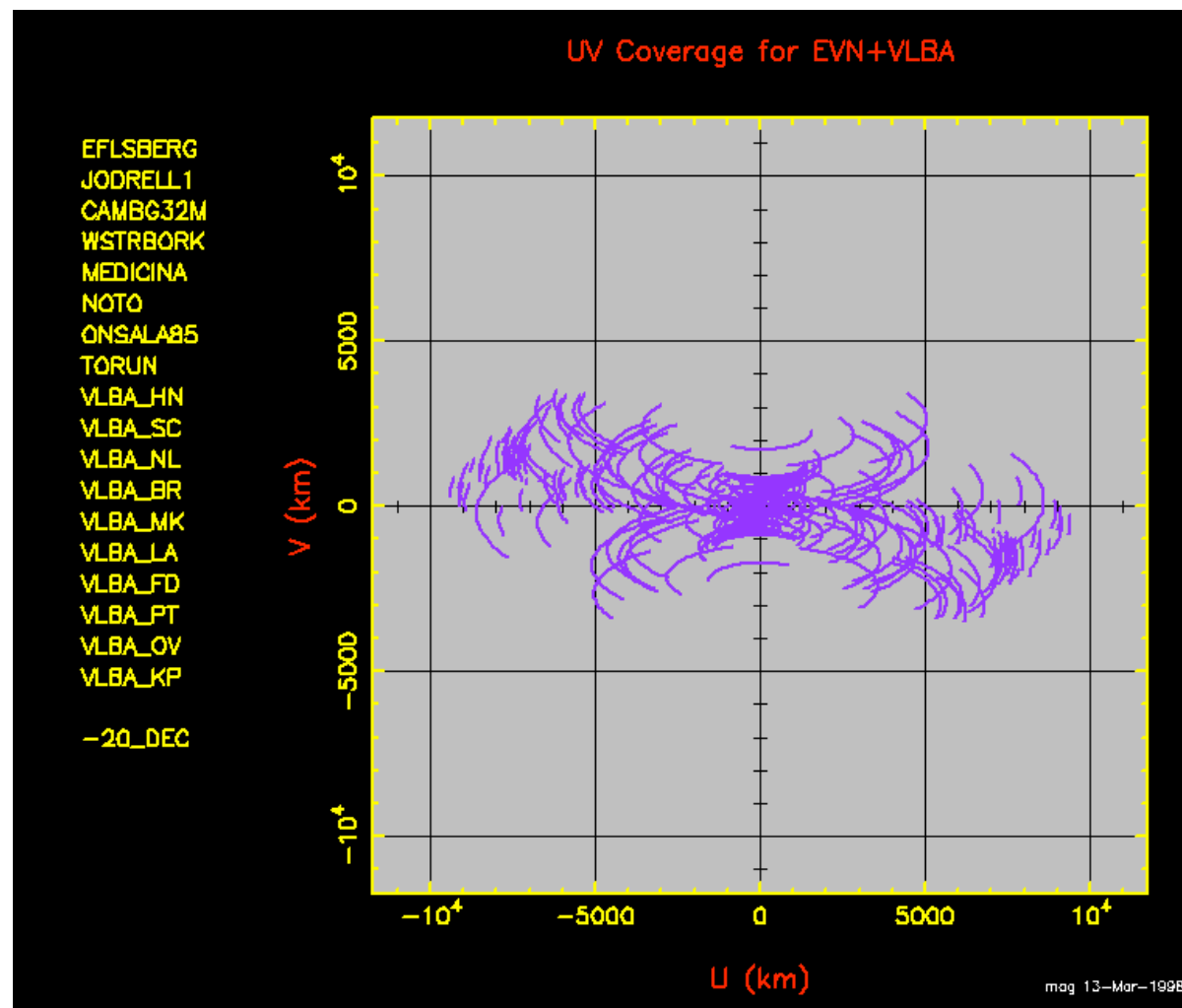
An e-VLBI image made with telescopes of the EVN and others around the world after observing for (a) 1.5 hr, (b) 2.5 hr and (c) 12 hr:

J0204+15 at 4.964 GHz 2009 Jan 15



Note that while the noise level improves, the real improvement in the quality of the image is the increasing coverage of the uv-plane as the observation is being made.

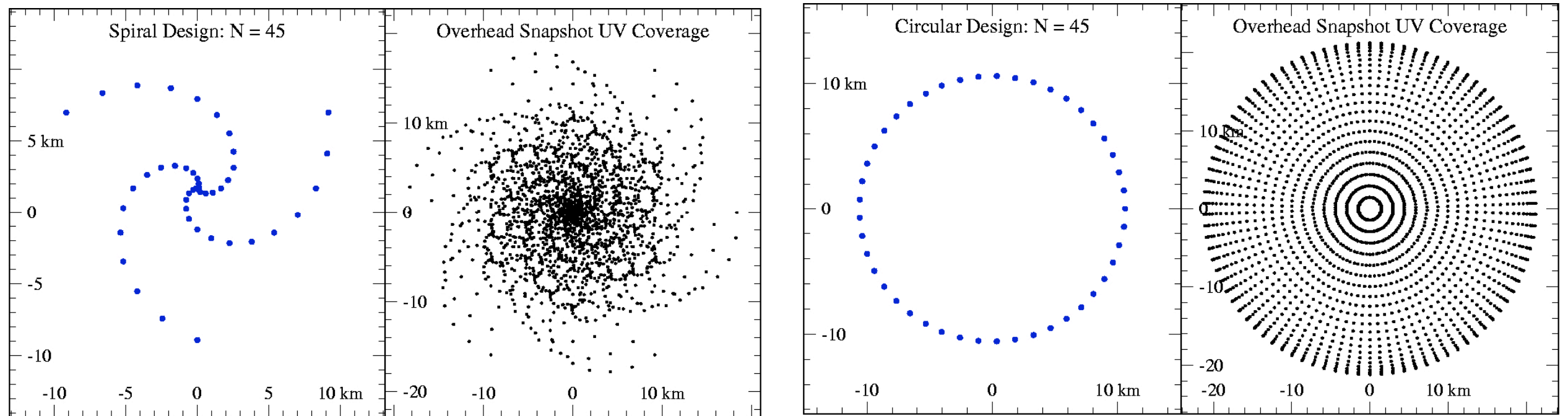
VLBI arrays like the EVN & VLBA have most of their telescopes located in the Northern hemisphere. The uv-coverage for sources in the southern sky (-ve declinations) is poor. The EVN can make use of telescopes located in the Southern hemisphere at European longitudes e.g. South africa:



At lower source declinations ($< +15$ degrees) the coverage of the EVN + VLBA array ("Global VLBI") becomes foreshortened (above left), resulting in an increasingly elongated beam and poorer uv-coverage. For the EVN this can be improved in the N-S direction by including Hartebeesthoek, in South Africa (above right).

uv-coverage - array optimisation

A good deal of attention has been given to the optimisation for new arrays (e.g. ALMA, LOFAR and SKA). Novel configurations have emerged e.g. circular arrays (maximised the number of long baselines) and spirals (has many short baselines).

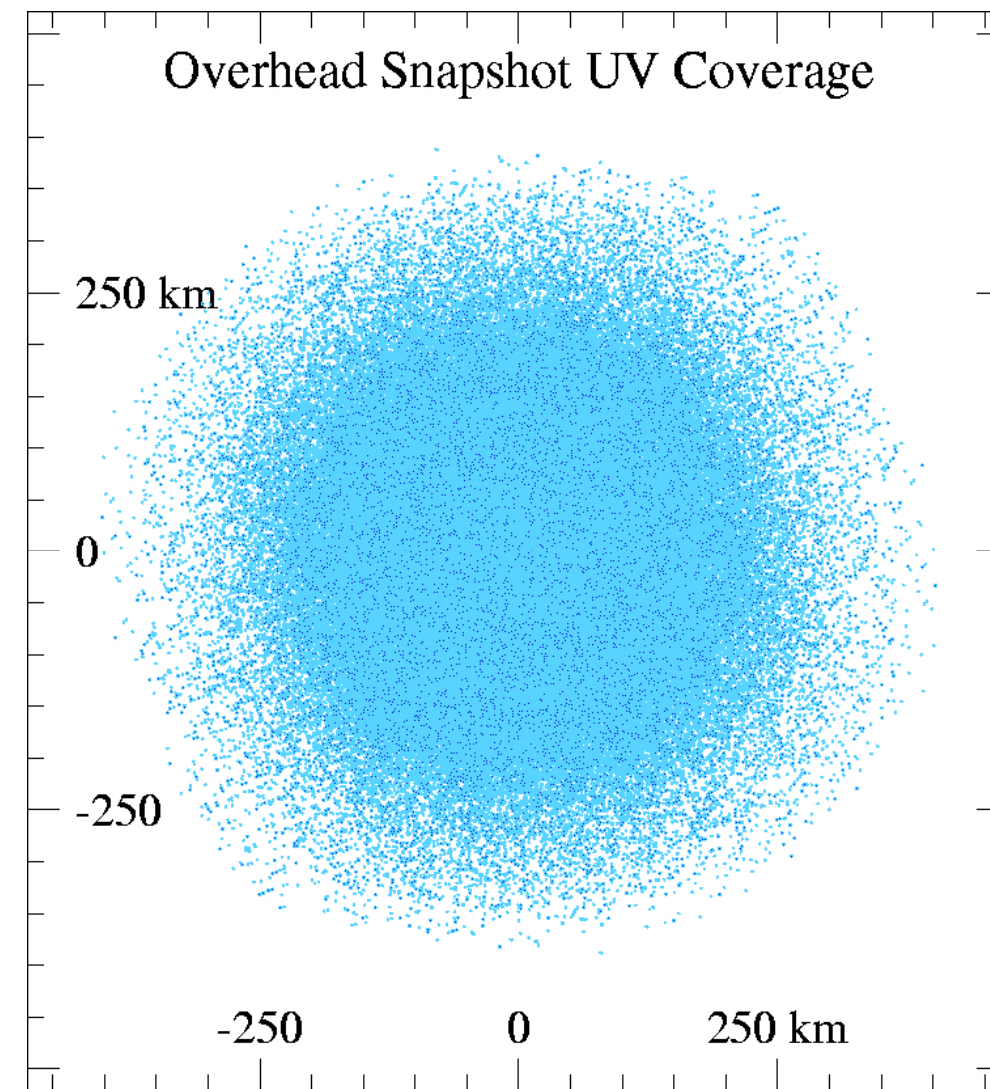
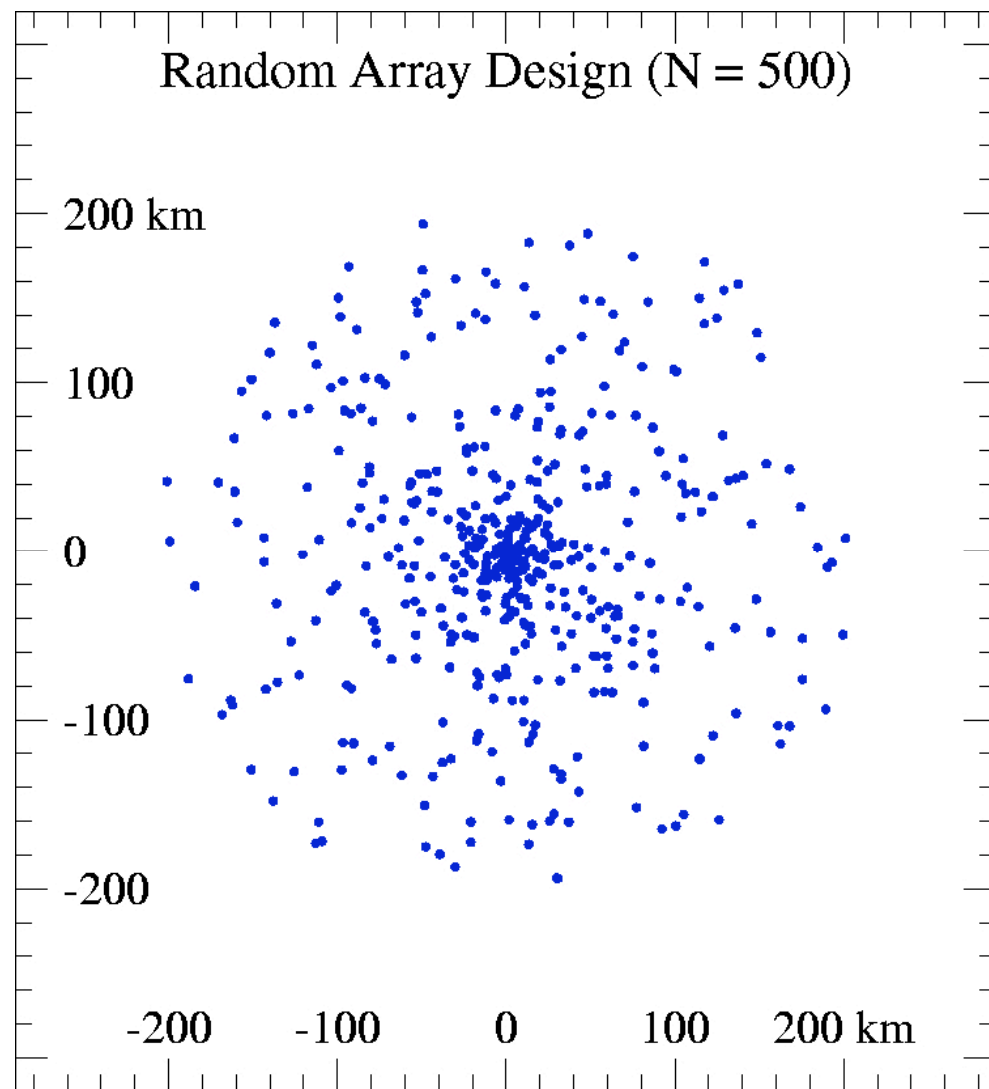


Spiral and ring configurations also make efficient use of infrastructure e.g. optical fibre.

Another idea that has emerged is the so-called “Large-N/Small-D” concept. Basically the idea is to use many small telescopes - this improves the uv-coverage and the antennas themselves can be manufactured using novel and cheap techniques/materials.

We’ll return to the topic of imaging and array design later in this course.

Random arrays (with some bias towards a compact core) also do surprisingly well in terms of uv-coverage:

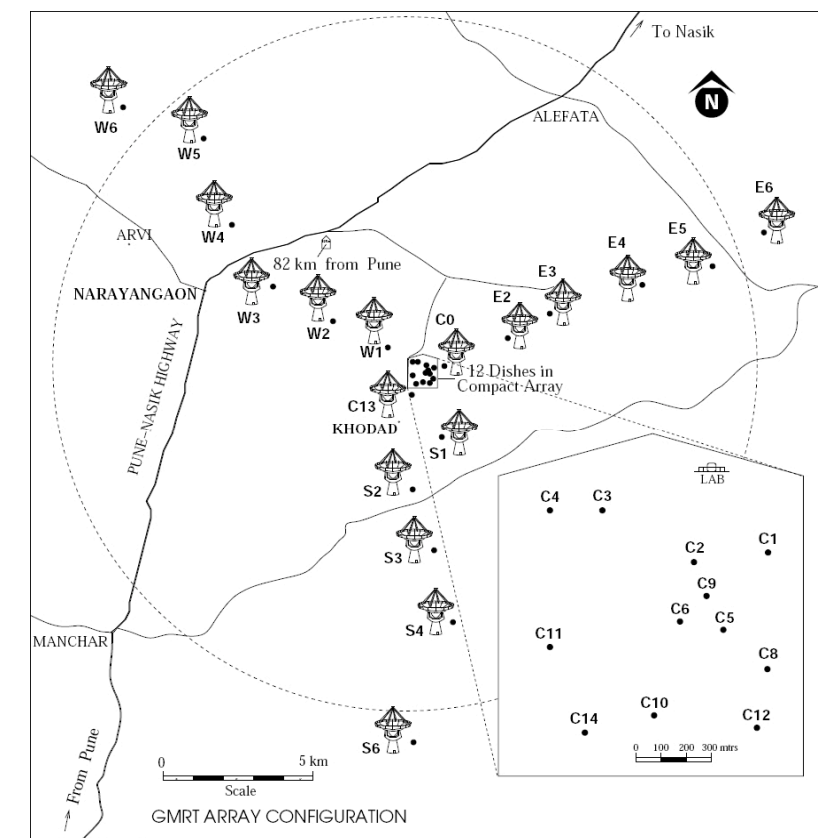
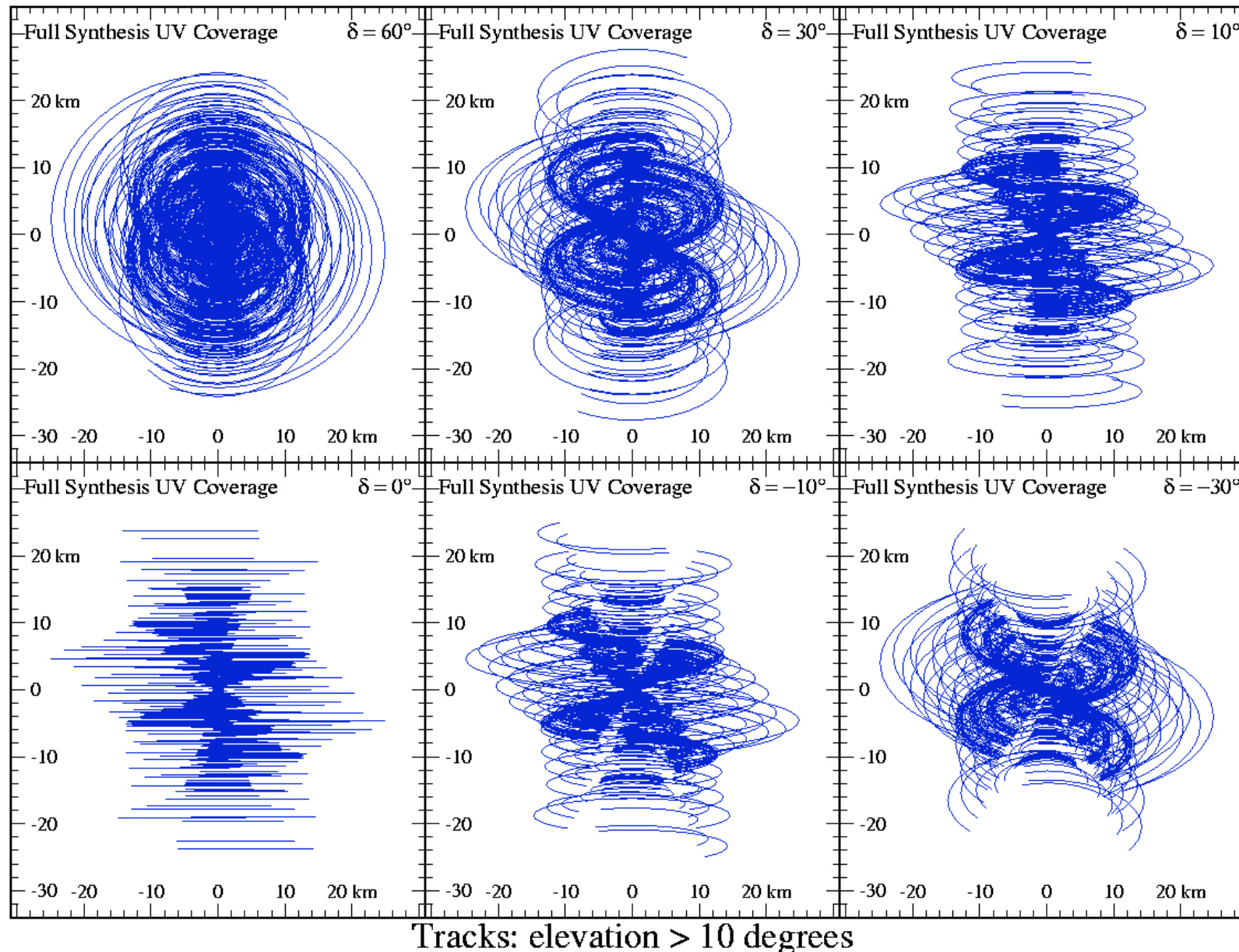


We'll return to the topic of imaging in radio astronomy and array design, later in this course.

Some (!) other cm interferometer arrays:

The GMRT (Giant Metre-wave Radio Telescope) - India works up to 1.4 GHz, has fixed antennas but has a dense central core.

In total there are 30 antennas, each 45-metre in diameter.



ATCA (Australian Telescope Compact Array) - The ATCA consists of six 22-m radio antennas. Freq range - 600 MHz to 90 GHz. Five of the six antennas are positioned at station posts along a three kilometre railway track oriented east-west. These five antennas can be positioned at any of 44 fixed stations. The sixth antenna is fixed on a station three kilometres to the west of the western end of the 3km railway track, thus allowing a maximum ATCA baseline of six kilometres. The shortest baseline is approximately 30m.



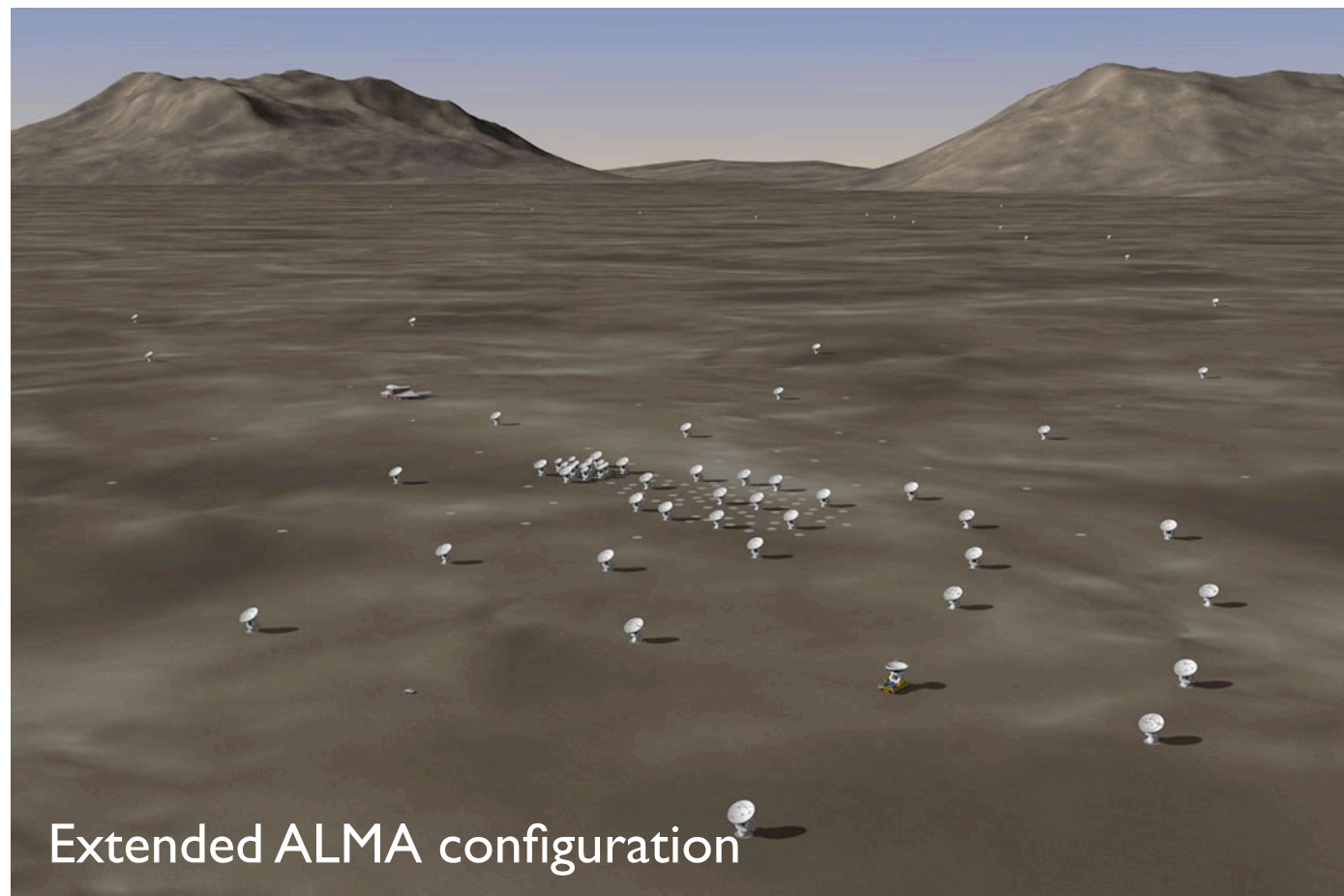
mm interferometer arrays:



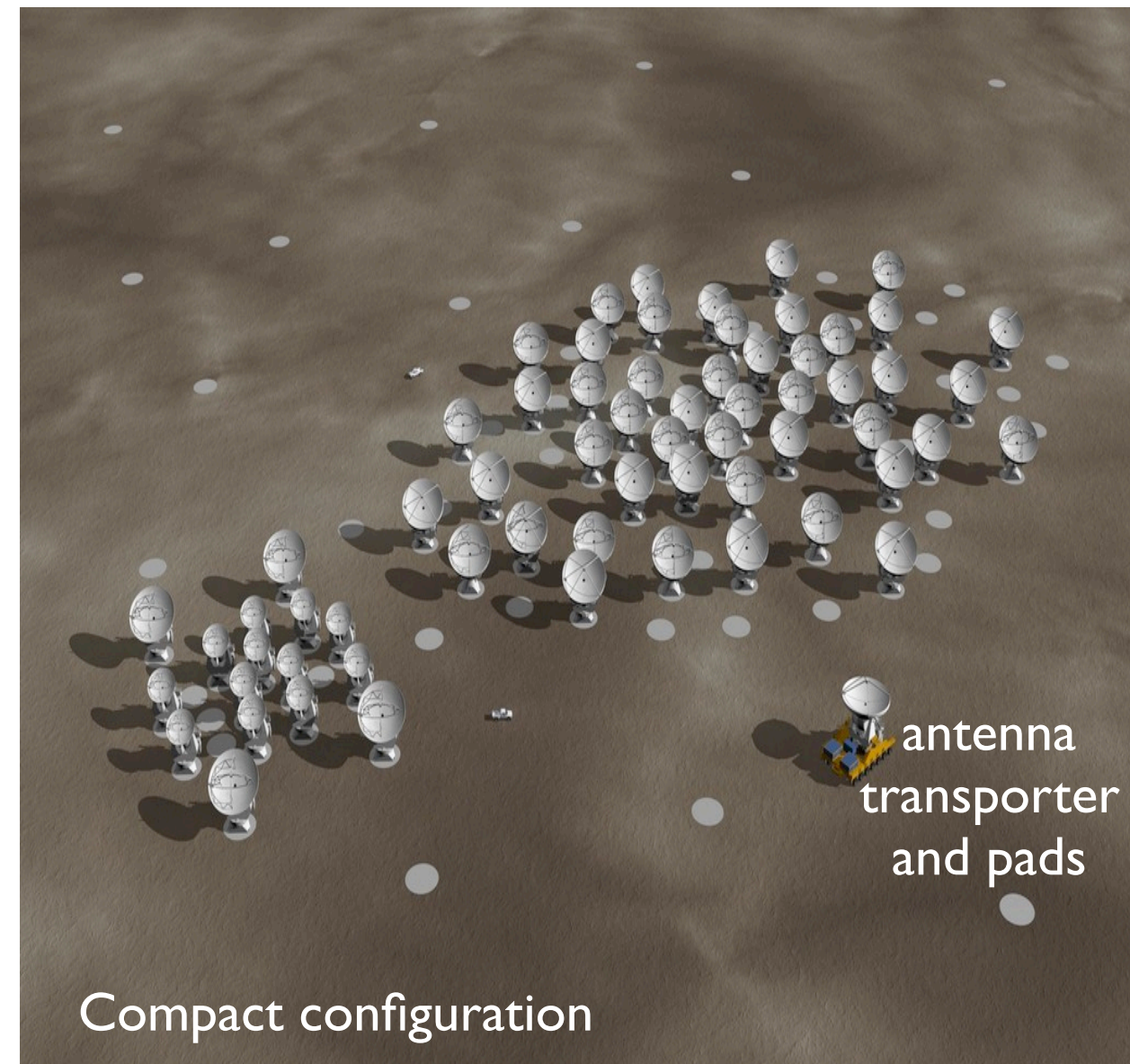
Moveable antennas(!) - array configurations scale from 150 metres to 15 km.

ALMA - Atacama Large Millimetre/Submillimetre Array - joint European/USA/Japanese project - currently under construction.

54 12-m antennas, 12 7-m antennas at 5000-m altitude! Freq coverage: 86-720 GHz



Extended ALMA configuration



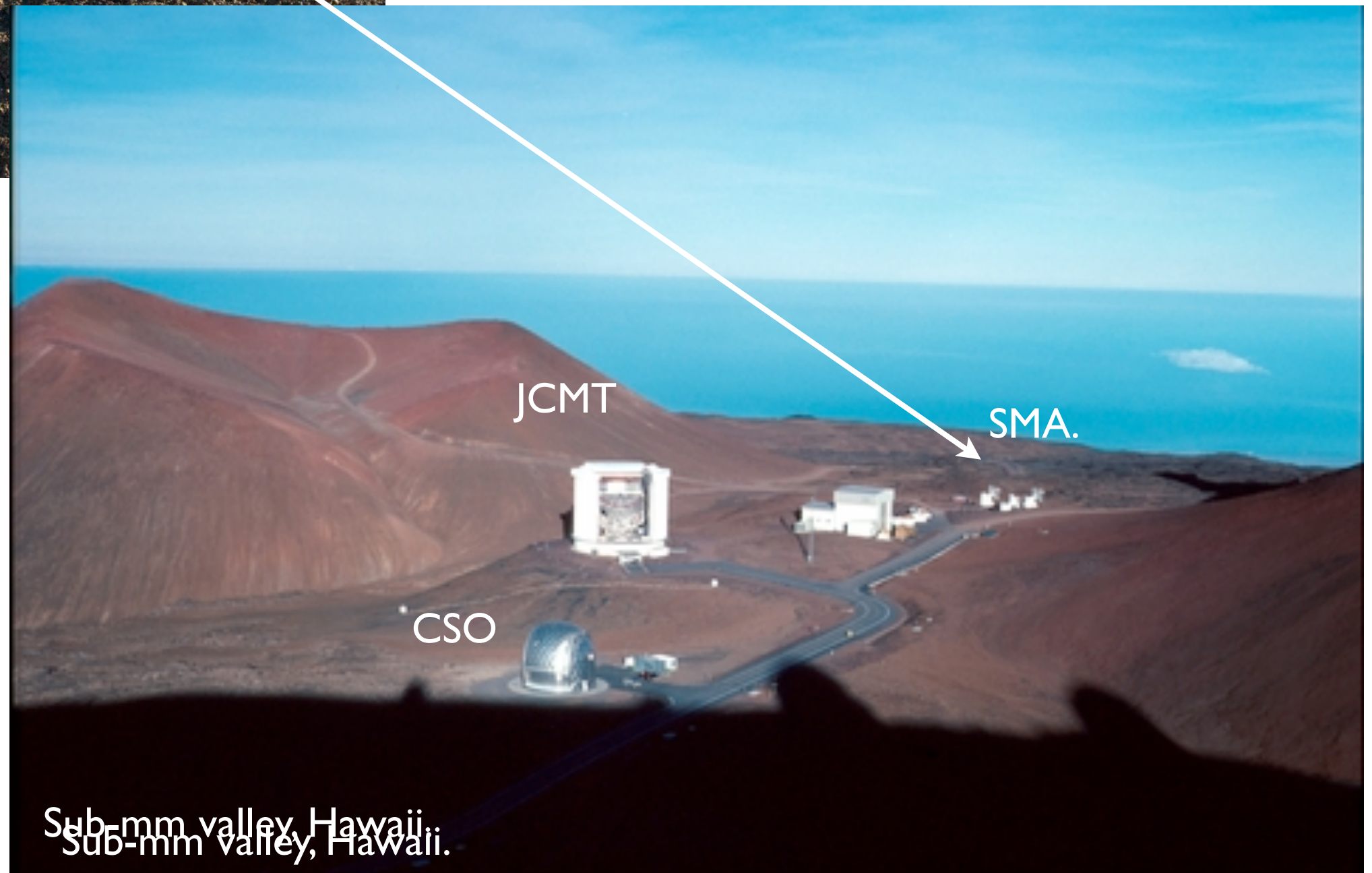
Compact configuration

antenna transporter and pads

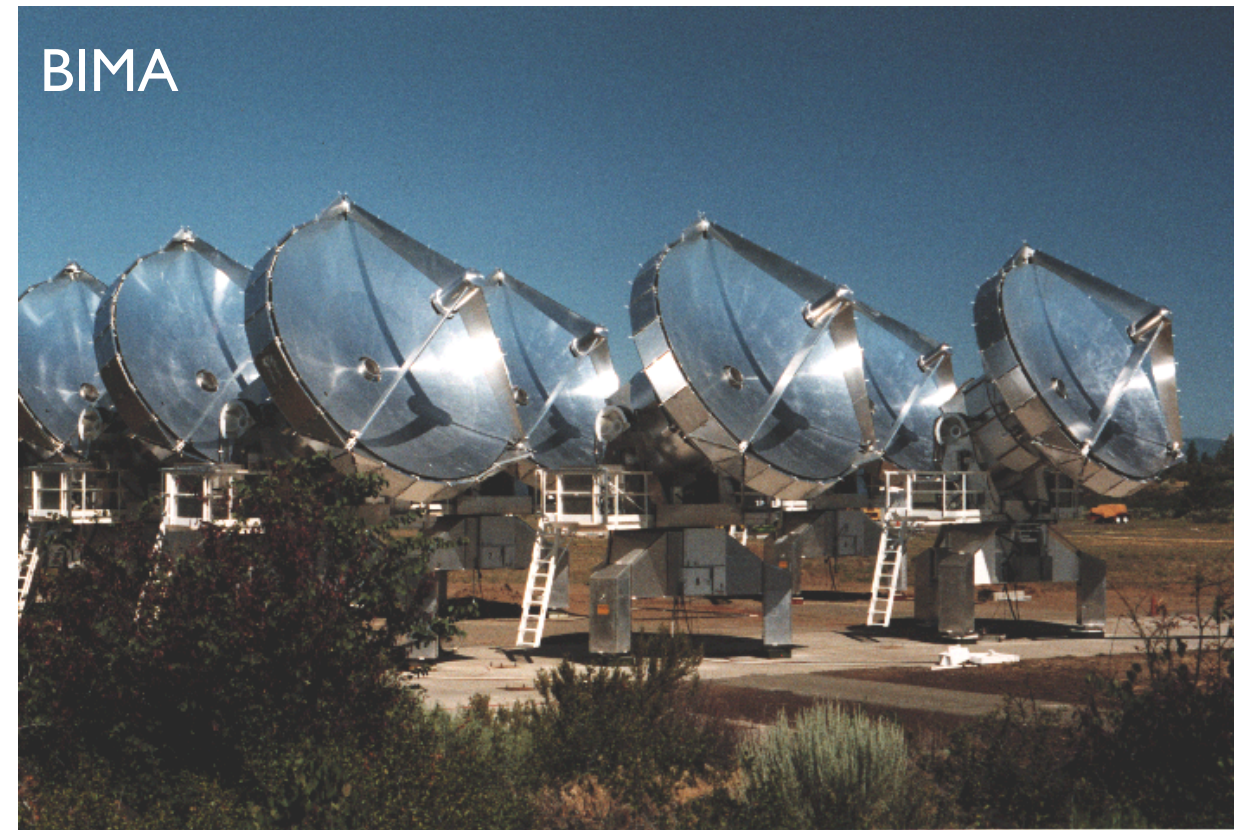
Existing mm interferometer arrays:



8 x 6-m antennas, also links up with 2 nearby sub-mm telescopes: JCMT and CSO operating at 345 GHz:

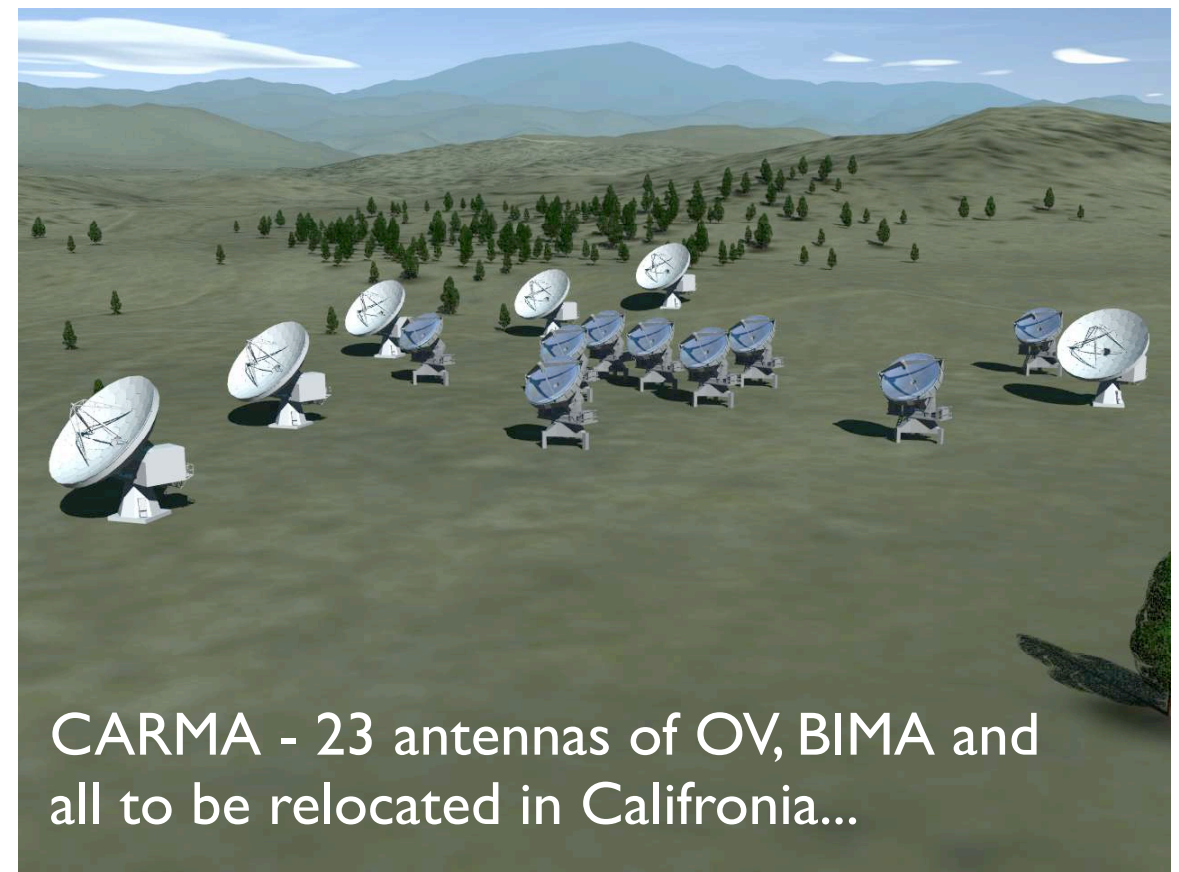


Max. baseline
~ 782m



+

=



CARMA - 23 antennas of OV, BIMA and all to be relocated in California...

Next week

Guest lecture from *Dr. Raffaella Morganti* - "Neutral hydrogen studies - emission and absorption"

